GEOLOGICA ULTRAIECTINA

Mededelingen van de
Faculteit Aardwetenschappen
Universiteit Utrecht

No. 127

GEODYNAMIC EVOLUTION AND MANTLE STRUCTURE

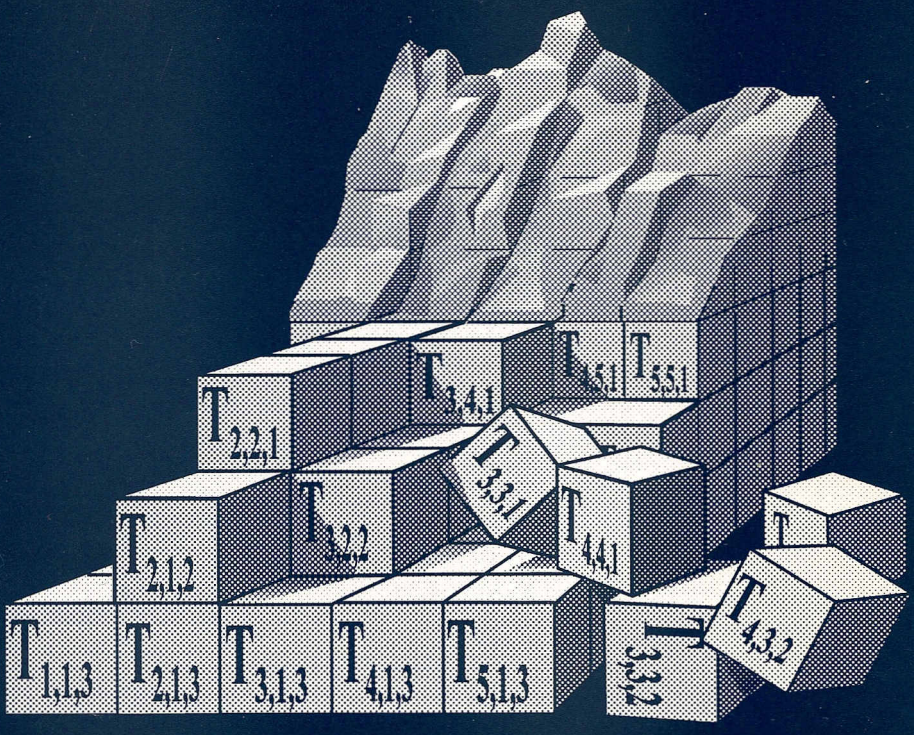

MARC DE JONGE

GEOLOGICA ULTRAIECTINA

Mededelingen van de
Faculteit Aardwetenschappen
Universiteit Utrecht

No. 127

GEODYNAMIC EVOLUTION AND MANTLE STRUCTURE

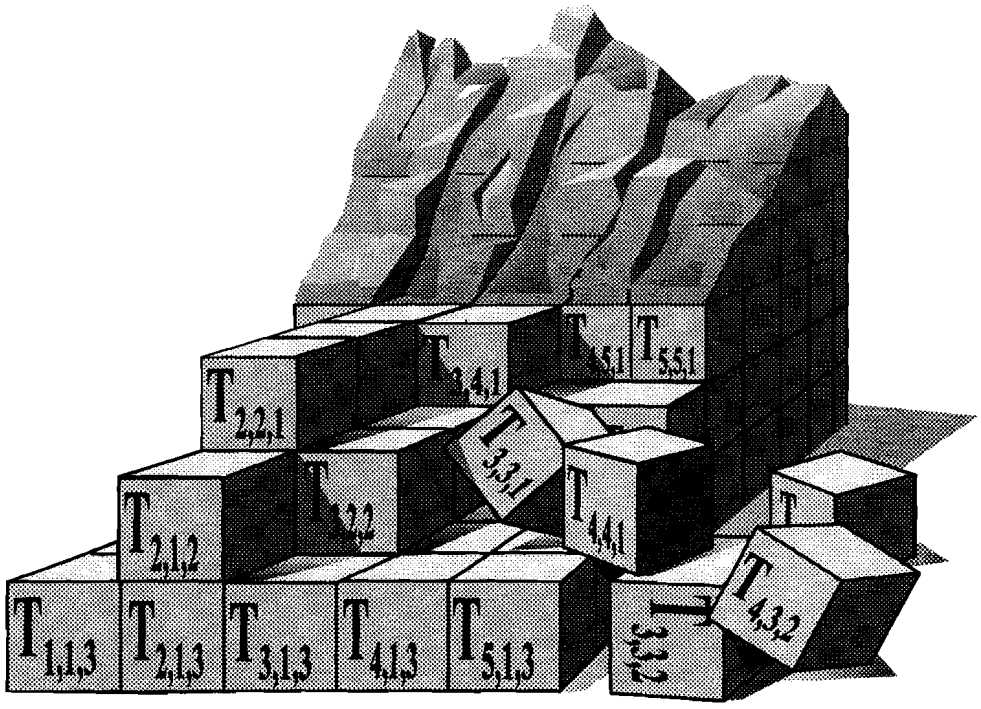

MARC DE JONGE

CIP-GEGEVENS KONINKLIJKE BIBLIOTHEEK, DEN HAAG

Jonge, Marc René de

Geodynamic evolution and mantle structure / Marc René de Jonge.
- Utrecht : Faculteit Aardwetenschappen, Universiteit Utrecht. - (Geologica Ultraiectina, ISSN 0072-1026 ; no. 127)
Proefschrift Universiteit Utrecht. - Met lit. opg. -
Met samenvatting in het Nederlands.
ISBN 90-71577-81-3
Trefw.: geodynamica ; Middellandse Zee-gebied / tomografie ; Middellandse Zee-gebied.

GEODYNAMIC EVOLUTION AND MANTLE STRUCTURE

Geodynamische ontwikkeling en mantelstructuur

(met een samenvatting in het Nederlands)

PROEFSCHRIFT

TER VERKRIJGING VAN DE GRAAD VAN DOCTOR
AAN DE UNIVERSITEIT UTRECHT,
OP GEZAG VAN DE RECTOR MAGNIFICUS
PROF. DR. J. A. VAN GINKEL, INGEVOLGE HET BESLUIT
VAN HET COLLEGE VAN DEKANEN IN HET OPENBAAR
TE VERDEDIGEN OP
WOENSDAG 13 SEPTEMBER 1995
OM HALF DRIE 'S MIDDAGS

DOOR

MARC RENÉ DE JONGE

GEBOREN OP 29 NOVEMBER 1961 TE TERNEUZEN

PROMOTOR: PROF. DR. M. J. R. WORTEL
COPROMOTOR: DR. W. SPAKMAN

The research in this study was carried out at the Department of Geophysics of the Institute of Earth Sciences, Utrecht University, Budapestlaan 4, 3584 DC Utrecht, The Netherlands.
It was funded by NWO/AWON (Netherlands Organisation for Scientific Research, Earth Sciences branch) as project 751-354-019.
The tomographic inversions described in chapter 4 were calculated at the NCF (National Computer Facilities) in Amsterdam and were funded with grant SC-245.

The following publications have resulted from this study:

M. R. de Jonge and M. J. R. Wortel, The thermal structure of the Mediterranean upper mantle; a forward modelling approach, *Terra Nova*, *2*, 609-616, 1990.

M. R. de Jonge, M. J. R. Wortel, and W. Spakman, From tectonic evolution to upper mantle model: an application to the Alpine-Mediterranean region, *Tectonophysics*, *223*, 53-65, 1993.

M. R. de Jonge, M. J. R. Wortel, and W. Spakman, Regional scale tectonic evolution and the seismic velocity structure of the lithosphere and upper mantle: the Mediterranean region, *J. Geophys. Res.*, *99*, 12091-12108, 1994. *(chapter 3)*

M. R. de Jonge, W. Spakman, and M. J. R. Wortel, Geodynamic evolution of the Alpine-Mediterranean region: a tomographic analysis, *J. Geophys. Res.*, <submitted>, 1995. *(chapter 4)*

After all, it is possible I may be mistaken; and it is but a little copper and glass, perhaps, that I take for gold and diamonds. I know how very liable we are to delusion in what relates to ourselves, and also how much the judgements of our friends are to be suspected when given in our favour. But I shall endeavour in this discourse to describe the paths I have followed...

René Descartes, Discourse on the method of rightly conducting the reason and seeking truth in the sciences, 1637

Voor Rian

Contents:

Introduction

We have now another object in our view; this is to investigate the operations of the globe, at the time that the foundation of this land was laying in the waters of the ocean, and to trace the existence and the nature of things, before the present land appeared above the surface of the waters.

James Hutton, Theory of the Earth, 1788

With the advent of plate tectonic theory a framework has become available in which many observed features of the structure of the Earth can be understood. The theory can explain the geological processes that have resulted in terranes as diverse as oceans, mid-oceanic ridges, mountain belts, and intra-continental basins. However, despite its explanatory power plate tectonic theory is rarely used for its predictive properties, which should after all be an important aim of any scientific theory. In this research I will address some implications of the plate tectonic concepts, by using plate tectonic theory, to predict thermal and elastic properties of the interior of the Earth which were not used to formulate the theory. This prediction is made by forward numerical modelling of lithosphere scale tectonic processes. The work will focus on the Alpine-Mediterranean region, but the method described is applicable to any part of the Earth where Mesozoic or later plate collision processes can be reconstructed with sufficient detail from geological observations.

In the past much effort has been placed in trying to understand the complicated tectonic structures found in the Alpine-Mediterranean system and the development of this region in terms of lithospheric processes. Whereas for most parts of the world the prime source of information for reconstructing lithosphere-scale processes is the pattern of magnetic reversals of the oceanic floor, this data set is of limited use within the Mediterranean region. This is a result of the fact that oceanic lithosphere in the region shows only very little consistent magnetic structure. It falls into two categories: very young, extending -formerly continental- regions, where no clear ridges and associated magnetic patterns have (yet) developed and old Cretaceous lithosphere (dated by stratigraphic means), which was formed in the long magnetically quiet interval. Reconstructions of plate tectonic processes within this realm are therefore poorly bounded by magnetic data.

Despite the virtual absence of the oceanic data inside the region, it is possible to reconstruct the large-scale motion of the Eurasian and African plates (bounding the region in the north and south) from the opening history of the Atlantic ocean [Savostin et al., 1986] and from the difference between polar wander curves of Africa and Eurasia [Westphal et al., 1986]. By combining the geometrical boundary conditions given by large scale motions with information of (micro-)plate rotations, stratigraphy and structural geology

some workers have succeeded in determining a geometrically consistent descriptions of plate motions and internal deformation throughout the development of the currently observed geological structure [Dercourt et al., 1986 and Dewey et al., 1989].

These reconstructions are known as paleogeographic reconstructions, when the attention is mainly focused on the distribution of continental and oceanic environments, or palinspastic reconstructions when basin sedimentology and geology is the prime subject. In either case an important feature included in the recent reconstructions is the general tectonic setting of the studied region during its evolution. For the sake of uniformity I will refer to all sufficiently detailed reconstructions of geological processes as tectonic reconstructions. These reconstructions are characterised by a substantial amount of geological interpretation as many instances of oceanic lithosphere formation, subduction, and intra-plate deformation are only recognizable in the form of narrow zones of anomalous lithology in old orogenic belts. It is for example virtually impossible to accurately quantify the size of the old basins that have become incorporated in the Alps and Carpathians. Furthermore, the motion of plates or plate-fragments is often only known with a large margin of error. An important aim of this study is to assess the quality of the tectonic reconstructions by studying their implications for the underlying mantle structure. In Chapter 1 I will present a brief outline of the currently available hypotheses concerning the development of the Mediterranean region and illustrate some of the problems encountered.

In chapter 2 the forward modelling approach designed to study the implications of the tectonic reconstructions is presented. In the forward models the information implicit in the tectonic reconstructions is used to determine an unperturbed (but not necessarily homogeneous) initial mantle structure and an accompanying material flow field. It is then possible to calculate the thermal effects of the tectonic development on the underlying mantle.

The first objective of this research is testing the quality of various interpretative reconstructions by modelling their implications for the present lithosphere and upper mantle structure. The modelling approach produces predictions (from the unperturbed past situation towards the present structure) that follow from the plate tectonic assumptions and the time dependent tectonic reconstructions. It is clear that a prediction of the mantle has only limited use if it cannot be checked against observations. There is however, a means to test the predicted structure because we can compare it with the detailed seismic velocity structure of the lithosphere and upper mantle that is obtained by delay-time tomography.

The second objective of this research stems from the lack of explanatory power that seismological studies of the structure of the mantle provide. When the first experiments with seismic delay-time tomography were performed it was already suggested that the imaged lateral P-wave velocity heterogeneities were indicative for the tectonic processes in the area. [Aki et al., 1977 and Dziewonski et al., 1977]. In these initial studies, however, no connection

between the tomographic results and the actual tectonic history could be given, either because of the small area covered or because of the low spatial resolution of the mantle images. Although the resolution and accuracy of global models improved in subsequent years [Clayton and Comer, 1984 and Dziewonski 1984], the correlation between imaged mantle P-wave velocity heterogeneities and the expected structure from plate tectonic theory remained poor.

This situation changed when results obtained by Spakman [1986] and Spakman et al. [1988] showed a clear P-velocity anomaly with a spatial extent that suggested it was directly related to a northward subduction of African lithosphere below Crete. One important observation in this study was that the maximum depth of subduction is substantially larger than that of seismic events in the region. This result indicates that P-wave velocity anomalies of the mantle can reflect a much longer portion of the subduction history than earthquake hypocentre locations. The image of the Mediterranean upper mantle in this work furthermore shows a number of zones of high P-velocity that roughly follow the orogenic belts found in the region, but that were not always associated with deep seismicity. The interpretation was made that these zones were also the result of past subduction processes. This study will go a step further in the interpretation of the presently observed seismic structure. When the forward models and the tomographic results show a good correlation (a problem that will be extensively addressed in Chapter 4) we have in the underlying tectonic reconstruction a true quantitative explanation for the current seismic velocity heterogeneities. The development of the mantle towards its present structure can then be understood in terms of tectonic processes that have also left their mark in the surface geology. In this way we quantitatively verify the tectonic processes that are responsible for the development of the complicated structure presently observed by seismological means.

A third use of the modelling approach exists from an epistemological viewpoint: especially a well established theory like plate tectonics needs to provide falsifiable predictions to be of scientific value [Popper, 1963]. It is of course beyond the scope of this research to reassess the validity of plate tectonics, but by comparing forward models and recently obtained tomographic results previously unaddressed implications of the theory can be confronted with observations. This somewhat philosophical consideration does play a role in the error discussion of chapters 3 and 4 where limitations of the modelled plate-like nature of subducted lithosphere may be part of the source of discrepancies between forward models and tomographic results. It is in those errors of the forward models that we encounter the limits of the simple plate-tectonic approximation of the dynamics of the Earth and we find new questions on the nature and properties of the Earth's mantle.

References:

Aki, K., E. Husebye, and A. Christofferson, Determination of the three-dimensional seismic structure of the lithosphere, *J. Geophys. Res., 82*, 277-296, 1977.

Clayton, R. W., and P. Comer, A tomographic analysis of mantle heterogeneities, *Terra Cognita, 4*, 282-283, 1984.

Dercourt, J., L. P. Zonenshain, L.-E. Ricou, V. G. Kazmin, X. Le Pichon, A. L. Knipper, C. Grandjacquet, I. M. Sbortshikov, J. Geyssant, C. Lepvrier, D. H. Perchersky, J. Boulin, J.-C. Sibuet, L. A. Savostin, O. Sorokhtin, M. Westphal, M. L. Bazhenov, J. P. Lauer, and B. Biju-Duval, Geological evolution of the Tethys from the Atlantic to the Pamirs since the Lias, in *Evolution of the Tethys*, edited by J. Auboin, X. Le Pichon, and A. S. Monin, *Tectonophysics, 123*, 241-315, 1986.

Dewey, J. F., M. L. Helman, E. Turco, D. H. W. Hutton, and S. D. Knott, Kinematics of the western Mediterranean, in *Alpine Tectonics*, edited by M. P. Coward, D. Dietrich, and R. G. Park, *Spec. Publ. Geol. Soc. London, 45*, 265-283, 1989.

Dziewonski, A. M., Mapping the lower mantle: determination of lateral heterogeneity in P velocity up to degree and order 6, *J. Geophys. Res., 89*, 5929-5952, 1984.

Dziewonski, A. M., B. H. Hager, and R. O'Connell, Large-scale heterogeneities in the lower mantle, *J. Geophys. Res., 82*, 239-255, 1977.

Popper, K. L., Conjectures and refutations, the growth of scientific knowledge, Routledge and Kegan Paul Ltd., London, 1963.

Spakman, W., Subduction beneath Eurasia in connection with the Mesozoic Tethys, *Geol. Mijnbouw, 65*, 145-153, 1986.

Spakman, W., M. J. R. Wortel, and N. J. Vlaar, The Hellenic subduction zone: a tomographic image and its geodynamic interpretation, *Geophys. Res. Lett., 15*, 60-63, 1988.

Savostin, L. A., J.-C. Sibuet, L. P. Zonenshain, X. Le Pichon, M.-J. Roulet, Kinematic evolution of the Tethys belt from the Atlantic ocean to the Pamirs since the Triassic, in *Evolution of the Tethys*, ed. by J. Auboin, X. Le Pichon, and A. S. Monin, *Tectonophysics, 123*, 1-35, 1986

Westphal, M., M. L. Bazhenov, J. P. Lauer, D. M. Pechersky, and J.-C. Sibuet, Paleomagnetic implications on the evolution of the Tethys belt from the Atlantic ocean to the Pamirs since the Triassic, in *Evolution of the Tethys*, ed. by J. Auboin, X. Le Pichon, and A. S. Monin, *Tectonophysics, 123*, 37-82, 1986.

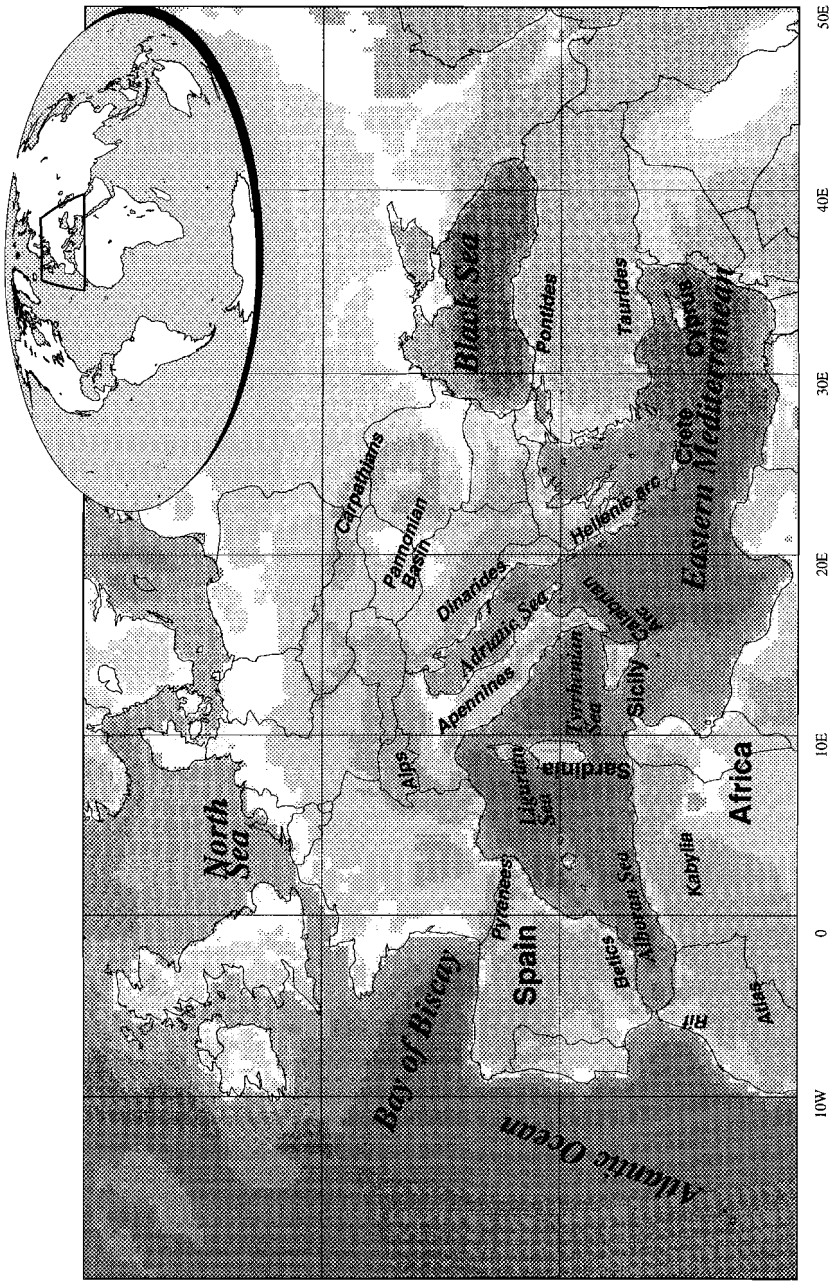

Figure 1. Location map of the study area..

Chapter 1

Mesozoic and Cenozoic tectonic evolution of the Alpine–Mediterranean region

Some think that even the ancients who lived long before the present generation, and first framed accounts of the gods, had a similar view of nature; for they made Ocean and Tethys the parents of creation, ...
Aristotle, Metaphysics, 350 B.C.

1.1 Introduction

The forward modelling of tectonic processes described in the next chapters is based on tectonic reconstructions of the Alpine-Mediterranean region. Both the model kinematics and the initial mantle and lithosphere structure are derived from these reconstructions. In this chapter I will therefore present a brief synthesis of the different reconstructions. I will discuss aspects of a number of models, based on work by Dercourt et al. [1986, 1990] and Dewey et al. [1989]. These reconstructions of the tectonic evolution are currently the most widely accepted, and provide sufficient information for the forward modelling. The modelling approach could be used to test other reconstructions but it is not the aim of this study to analyse every proposed history of the Mediterranean region. Instead, I will focus on the most recent hypotheses.

For orientation Figure 1 shows a map of the area addressed in this study. The tectonic processes in this region have resulted in a number of mountain belts and basins. Along the northern side the present terrane is dominated by the chains of the Pyrenees, the Alps, the Carpathians and the Pontides. These four chains delimit the northern side of the Mesozoic Tethys area. A common characteristic is the northward tectonic transport of Late-Mesozoic to Cenozoic sediments and Palaeozoic metamorphics over a presently continental basement belonging to the Eurasian mainland. A large strike-slip component of later motion on the delimiting faults is also often observed.

The southern edge of the region is dominated by the Mesozoic Atlas mountain belt of northern Africa, and by the island arcs of Sicily-Calabria, the Hellenides and Cyprus. A common characteristic of these regions is overthrusting over of various crustal fragments over the north-African and southern Tethys lithosphere. In a very condensed form the history of the Mediterranean could be summarized as the subsequent creation and destruction of the Tethys ocean that was located between these two zones of

orogenic belts. In the interior of the Alpine-Mediterranean region other mountain chains are also present: around the Adriatic Sea the Apennines and Dinarides and around the Alboran Sea the Betic, Rif, and Kabylia mountains. Furthermore, inside the region a number of basins are found: the oceanic remnant of the Mesozoic southern Tethys in the eastern Mediterranean, the newly formed oceanic basins of the Alboran, Ligurian and Tyrrhenian Sea, the Intra-continental Pannonian basin behind the Carpathians, and the strongly extended Sea of Crete behind the Hellenic arc.

1.2 Tectonic reconstructions

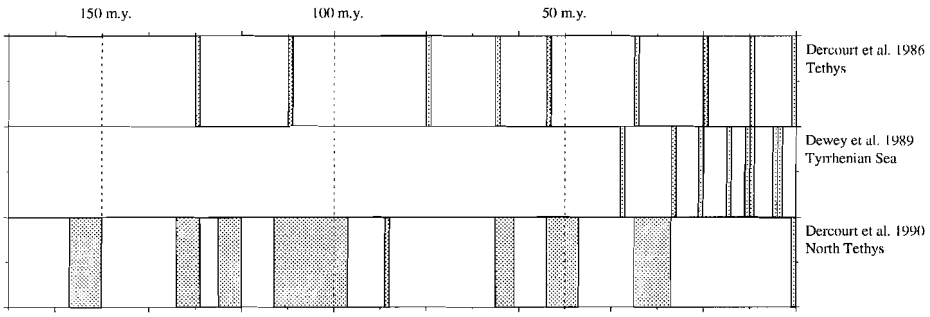

Figure 2. Time coverage of the tectonic reconstructions considered in this study. Grey bars show the periods where maps are available.

It is no simple undertaking to assemble all these different terranes into a single scenario for their development, yet it is precisely this that the tectonic reconstructions aim to do. In this section I will briefly describe the reconstructions used in this study. These reconstructions are made by Dercourt et al. [1986], Dewey et al. [1989], and Dercourt et al. [1990]. The tectonic information is represented as a number of maps for different times in the past (see Figure 2), featuring the main tectonic structures and geography. The large scale framework of these reconstructions is essentially the same, therefore the following section will focus on one, while differences between various hypotheses will be noted when applicable.

The history of the Alpine-Mediterranean region will be considered from the early Jurassic onwards, because before this time the mantle structure is determined by a stable configuration of continental lithosphere. The breaking up of the Pangean landmass is the initial setting for the modelling of the history of the region. By Early Jurassic time the African and European shelf regions are moving with a strike slip displacement. Eastward of the modelled region Asia and Africa have already become separated, with the Tethys ocean

in between [Savostin et al., 1986 Westphal et al., 1986], but this occurs outside the region of interest for this study.

Figure 3 (page 20) shows the paleogeography and main structural features and type of lithosphere taken from the Dercourt et al. [1986] reconstruction close to the Jurassic-Cretaceous boundary (130 m.y., in this study I will use absolute ages from Harland et al. [1982], but small differences in absolute timing of the processes will not be noticeable in the forward modelling results). The map inset is the alternative reconstruction for the Alpine region given by Dercourt et al. [1990]. The mentioned parameters are the ones I will use in the subsequent modelling. Figure 3 shows the onset of oceanic lithosphere formation in the Western (Neo-) Tethys and Valais Trough. It is this lithosphere that will become incorporated in subduction processes later in the development. The Adriatic promontory of the African plate and the adjoining Ionian, Gavrovo and Pindos regions are still and integral part of the African shelf region, although the Lago Negro basin is already starting to form. The first subduction in the region also begins during this time that will later develop into the Dinaride and Hellenide belts (see also Figure 1 for geographic names). The formation of oceanic lithosphere continues from this time onward to the end of the Cretaceous (65 m.y.) along different ridge systems. The tectonic development at this time however, is largely determined by extension and spreading processes. Note that the amount of oceanic lithosphere present in the Valais Trough is much larger in the map inset of Figure 3 (Dercourt et al. [1990] reconstruction). The total size of the oceanic basins in the Alpine-Mediterranean region is hard to assess, because subduction and oceanic lithosphere formation occur simultaneously. In this study I will use a minimum estimate for the oceanic basin surface area, but a larger amount of subducted lithosphere cannot be ruled out from the tectonic information. As a result the possibility should be taken into account that the forward models of the Alpine region show less high-velocity material than is actually present in the mantle.

Between 130 and 110 m.y. the reconstructions indicate a spreading ridge active between the Ionian Trough and North-Africa, thus separating the Hellenide-Adriatic region and the latter and producing the oceanic lithosphere that is presently found in the Eastern Mediterranean basin. Around 80 m.y. the Bay of Biscay is formed by south-eastward migration and rotation of the Iberian microplate. Already during this spreading phase of the Neo-Tethys, subduction processes are thought to start consuming lithosphere along the Valais trough, Carpathian Flysch basin and Pindos suture in the northern part of the region. During the Cretaceous ocean floor formation in the South and subduction in the North continue.

Figure 4 (page 21) shows a reconstruction of a more advanced stage of the development (65 m.y.). This time subduction and thrusting processes occur in the region of the Kabylia mountains, where oceanic lithosphere that was formed in the Cretaceous disappears below the Iberian microplate. Northward subduction is also interpreted in the Calabrian arc (still located far west of its present position). Along the entire northern Tethys margin (Alps, Carpathians

and Pontides) the Austro-Alpine and adjacent regions overrides the Eurasian foreland. From this time onward to the Oligocene also the thinned continental lithosphere of the Pindos and Gavrovo zones are thought to become involved in thrusting, and to disappear below Dinarides and Hellenides. In the forward modelling we have assumed that these thrusting processes represent subduction. Oceanic crust formation in the region has stalled. In a general sense the plate geometry has become simpler as a result of this: the kinematics are now dominated by a two-plate Africa-Eurasia convergence.

The next maps (Figure 5, page 22) show the paleogeography at 35 m.y.. For this period we have three possible reconstructions (the lower left inset shows the Dewey et al. [1989] interpretation). This time some thrusting is given around the Iberian plate: in the Pyrenees and Betic cordillera. Soon after, the Iberian microplate becomes an integral part of the European continent. The Valais Trough has been consumed below the Alpine front. In the western Mediterranean subduction of old oceanic lithosphere marks the beginning of the formation of the Apennines. Note that Dewey et al. [1989] suggest a different shape and position for this convergent boundary.

Tectonic activity in the Alps is present from the Oligocene until after the Tortonian (10 m.y.) as is illustrated in Figure 6 (page 23). In this period large nappes are overthrusting the French, Swiss and Austrian molasse basins. But the type of lithosphere present at the contact has changed to continental somewhere around the early Oligocene, when the oceanic basins have been completely consumed.

The Carpathians show a similar evolution to the Alps, only the amount of oceanic crust, formed in the Cretaceous, is larger and subsequently more material gets subducted in the later stages. A difference is the typical back-arc extension that occurs during the Oligocene and Miocene in the Pannonian basin, which is not found in the Western part of the Alps. After the Oligocene subduction in the Dinarides has ceased, but further south, convergence rate along the Hellenides has increased. Also thrusting in the Pontide region is thought to have ceased while to the South the Cyprus arc and Tauride zones are still active. During the Early Miocene new oceanic crust is formed in the Ligurian Sea, because of very strong extension between Sardinia and Spain, and in the Alboran Sea. These processes started with continental rifting during the Aquitanian (20 m.y.). The eastward migration of the Apennine thrust front is well underway (but note the different amounts of extension at this time implicit in the Dercourt et al. [1986] and the Dewey et al. [1989] reconstructions).

The final stage of the tectonic development is shown in Figure 7 (page 24). The Tyrrhenian Sea has been formed by late stage extension (in the Late Miocene to Pliocene depending on the reconstruction considered) of the overriding plate. Thrusting in Alpine-Carpathian chains has (almost) stopped. The fastest moving plate boundary is found in the Hellenic arc system, where extension of the Sea of Crete accommodates much of the relative displacement. At present this region appears to be the only active subduction zone in the

Alpine-Mediterranean, although the possibility exists that the Calabrian arc is also still active.

In the following chapters I will test what the effects of the above described processes on the present lithosphere and mantle the above described must be, and whether these processes can explain the current seismological observations. In order to do so, the next chapter will give a description of the modelling method used to translate the tectonic hypotheses into physical processes.

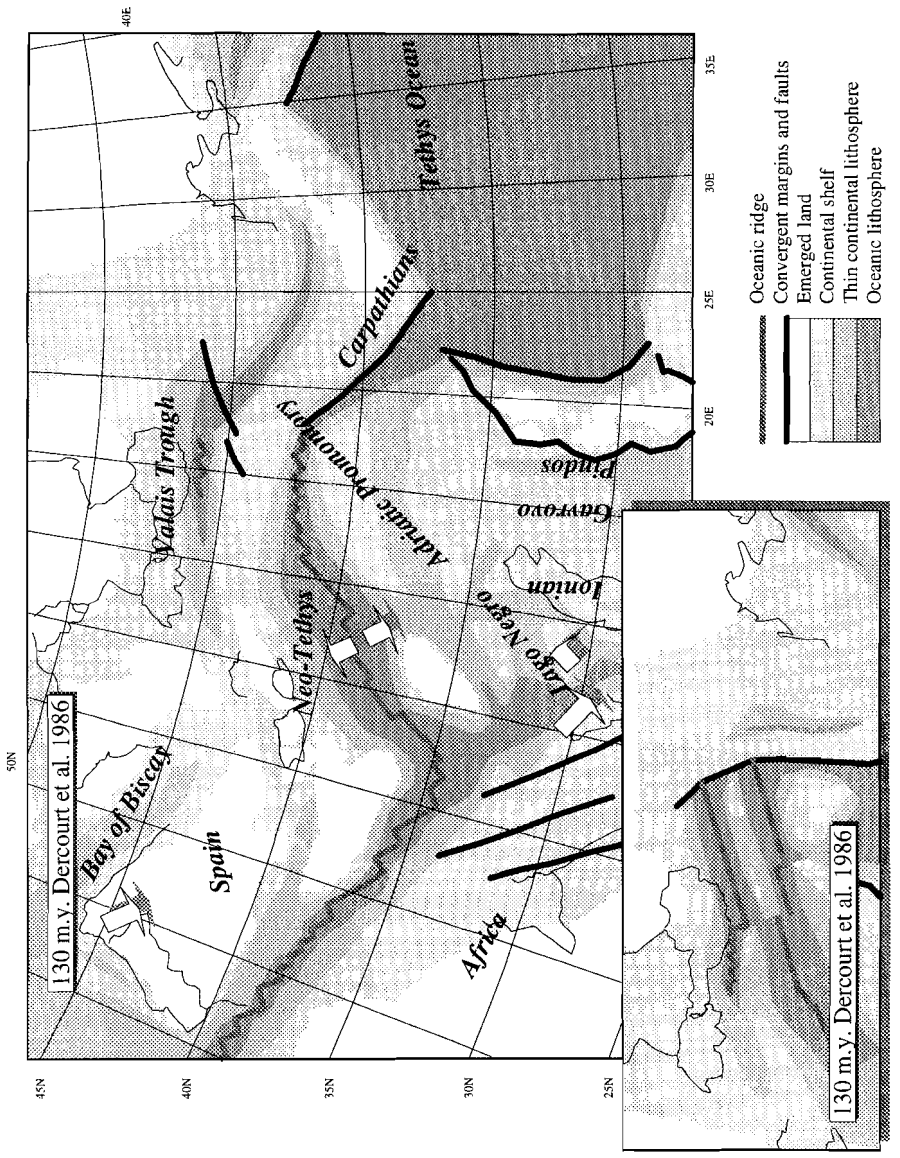

Figure 3. Paleogeography and main structures at 130 m.y., after Dercourt et al. [1986] and Dercourt et al. [1990].

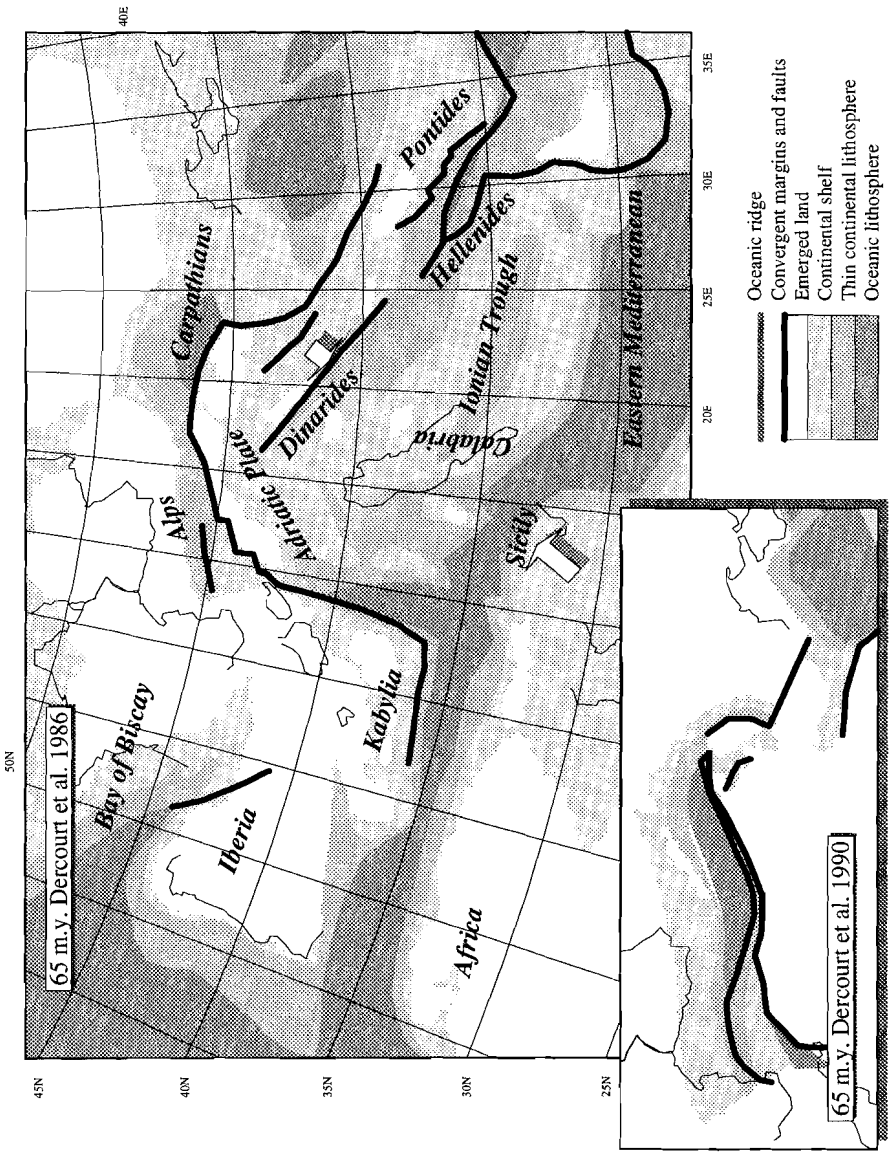

Figure 4. Paleogeography at 65 m.y., after Dercourt et al. [1986] and Dercourt et al. [1990].

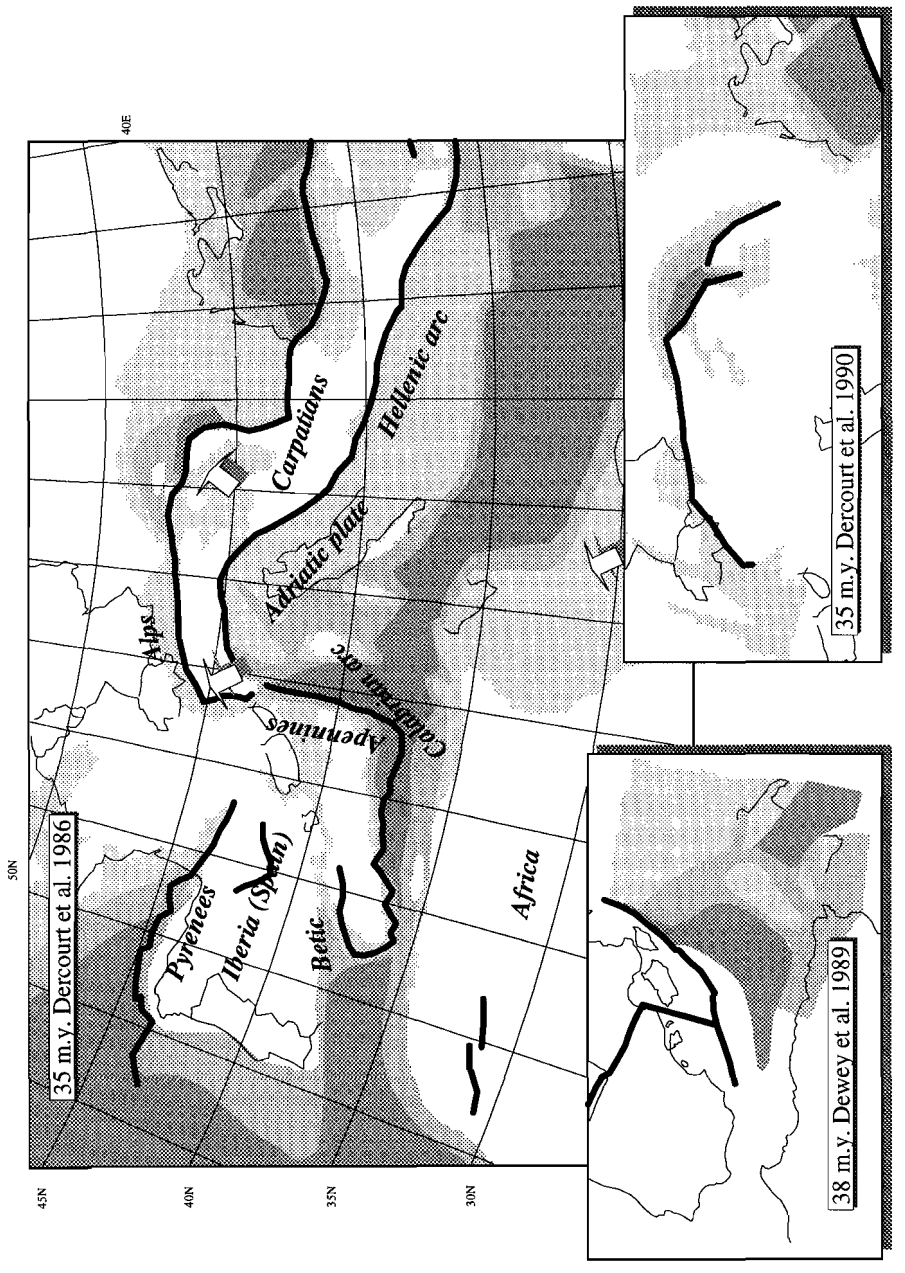

Figure 5. Paleogeography at 35 m.y., after Dercourt et al. [1986], Dewey et al. [1989], and Dercourt et al. [1990].

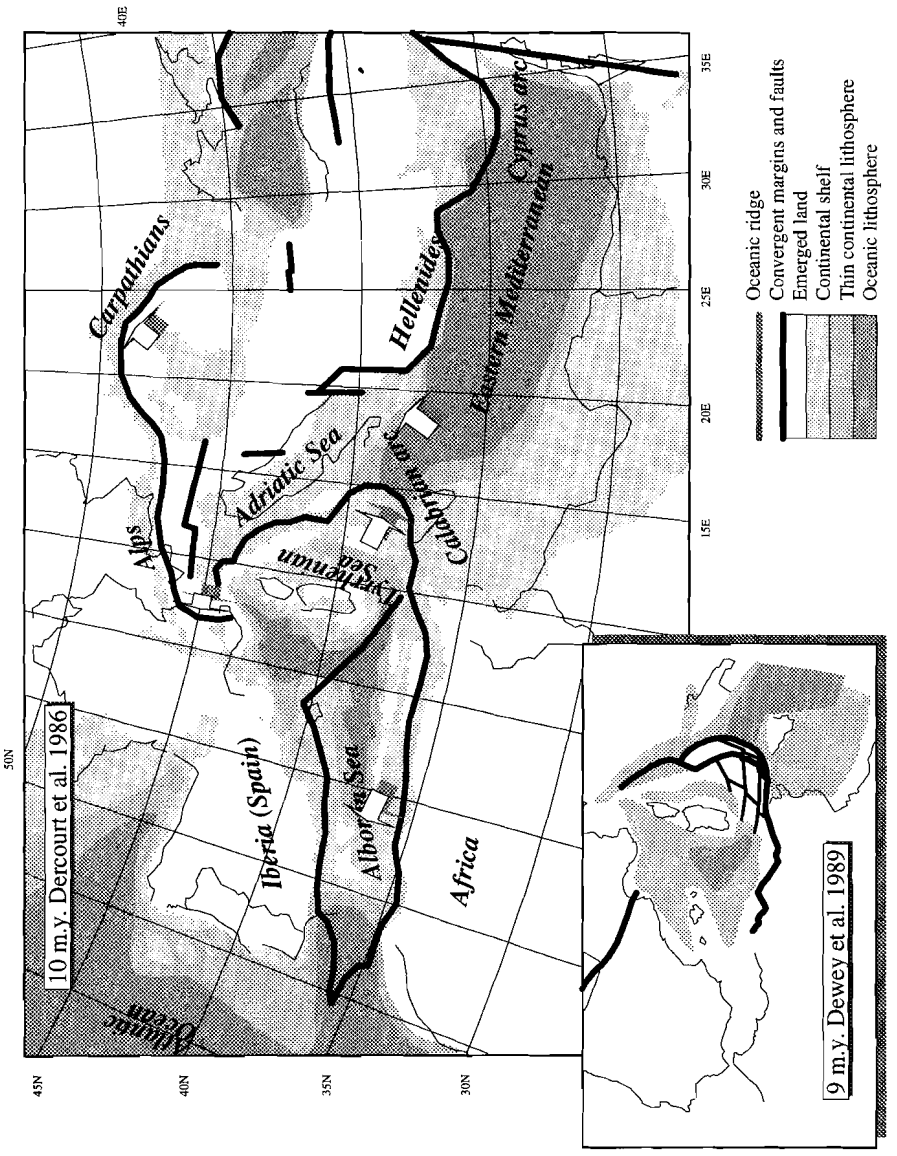

Figure 6. Paleogeography at 10 m.y., after Dercourt et al. [1986] and Dewey et al. [1989].

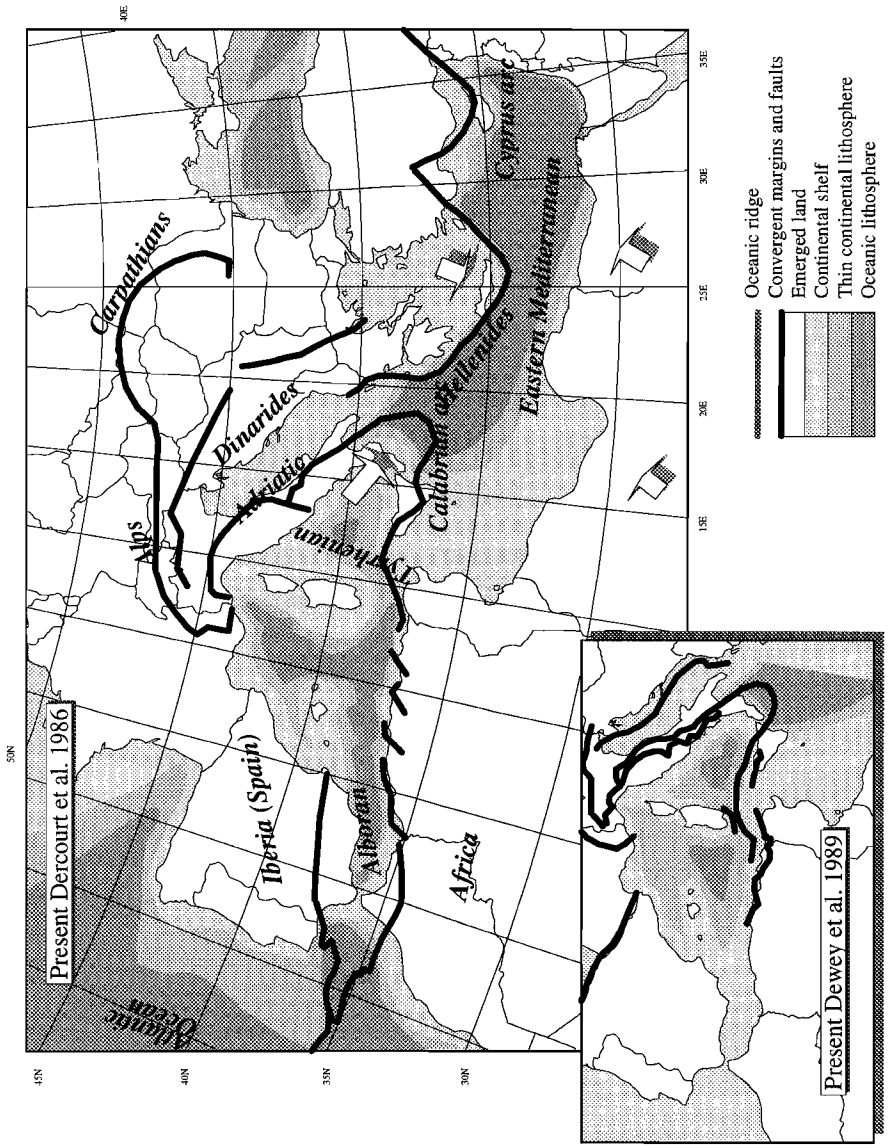

Figure 7. Present distribution of tectonic features and lithosphere types, after Dercourt et al. [1986] and Dewey et al. [1989].

References:

Dercourt, J., L. P. Zonenshain, L.-E. Ricou, V. G. Kazmin, X. Le Pichon, A. L. Knipper, C. Grandjacquet, I. M. Sbortshikov, J. Geyssant, C. Lepvrier, D. H. Perchersky, J. Boulin, J.-C. Sibuet, L. A. Savostin, O. Sorokhtin, M. Westphal, M. L. Bazhenov, J. P. Lauer, and B. Biju-Duval, Geological evolution of the Tethys from the Atlantic to the Pamirs since the Lias, in *Evolution of the Tethys*, edited by J. Auboin, X. Le Pichon, and A. S. Monin, *Tectonophysics, 123*, 241-315, 1986.

Dercourt, J., L.-E. Ricou, S. Adamia, G. Császár, H. Funk, J. Lefeld, M. Rakús, M. Săndalescu, A. Tollman, and P. Tchoumachenko, Anisian to Oligocene paleogeography of the European margin of Tethys (Geneva to Baku), in *Evolution of the Northern margin of the Tethys: The results of IGCP project 198*, edited by M. Rakús, J. Dercourt and A. E. M. Nairn, *Mém. Soc. Géol. Fr., 153(III)*, 159-190, 1990.

Dewey, J. F., M. L. Helman, E. Turco, D. H. W. Hutton, and S. D. Knott, Kinematics of the western Mediterranean, in *Alpine Tectonics*, edited by M. P. Coward, D. Dietrich, and R. G. Park, *Geol. Soc. Lond. Spec. Publ., 45*, 265-283, 1989.

Harland, W. B., A. V. Cox, P. G. Llewellyn, C. A. G. Pickton, A. G. Smith, and R. Walters, *A geologic time scale*, 131 pp., Cambridge Univ. press, Cambridge, 1982.

Savostin, L. A., J.-C. Sibuet, L. P. Zonenshain, X. Le Pichon, M.-J. Roulet, Kinematic evolution of the Tethys belt from the Atlantic ocean to the Pamirs since the Triassic, in *Evolution of the Tethys*, ed. by J. Auboin, X. Le Pichon, and A. S. Monin, *Tectonophysics, 123*, 1-35, 1986

Westphal, M., M. L. Bazhenov, J. P. Lauer, D. M. Pechersky, and J.-C. Sibuet, Paleomagnetic implications on the evolution of the Tethys belt from the Atlantic ocean to the Pamirs since the Triassic, in *Evolution of the Tethys*, ed. by J. Auboin, X. Le Pichon, and A. S. Monin, *Tectonophysics, 123*, 37-82, 1986.

Chapter 2

Thermal modelling of tectonic processes

The forms of bodies are infinitely varied; the distribution of the heat which penetrates them seems to be arbitrary and confused; but all the inequalities are rapidly cancelled and disappear as time passes on.
Joseph Fourier, The analytical theory of heat, 1878

The information contained in tectonic reconstructions consists of results of a large number of geological and geophysical studies. However, in the forward modelling method described in this study, these results are treated as input data. In the modelling approach the objective is to predict physical properties of the lower lithosphere and mantle from this 'data'. In this chapter I will describe the model assumptions and calculations that are used to predict mantle and lithosphere properties from tectonic reconstructions. The method is basically the same as the one described by De Jonge and Wortel [1990].

Important starting points of the modelling are the following two assumptions:

I) The structure of the lithosphere and underlying mantle are closely related. By this I mean that large scale tectonic processes, like those proposed in the tectonic reconstructions, are the surface expression of processes involving crustal, lithospheric and mantle levels of the earth. Horizontal motion of plates implies vertical displacement of material in the mantle.

II) A vertical component of motion affects the temperature distribution, because it can introduce cool lithospheric material into the mantle and it can bring hot material to the surface.

The first assumption is obvious from geometric considerations alone. When two lithospheric plates converge, the surface area destroyed is largely consumed in a subduction process. This means that surface motions of the tectonic reconstructions are associated with material flow that has a vertical component. For the same reason diverging and extending plates are accompanied by a vertical flow component. The second assumption is valid when the vertical motion takes place in a not purely adiabatic setting. Since the thermal gradient of the lithosphere is largely determined by conductive processes this condition is met when lithosphere is involved in the vertical motion (either as source or as destination of the flowing material).

A working hypothesis for this study is furthermore that the observable structure of lithosphere and mantle is strongly influenced by the temperature distribution. I consider the temperature effect as a prime cause for the observed mantle heterogeneity for a number of reasons. Firstly, subduction processes produce thermal anomalies that are associated with seismic velocity structure comparable in magnitude to seismic observations [Minear and

Toksöz, 1970; Sleep 1973], in other words: temperature differences suffice to explain the amplitude of the seismological structure. Secondly, the thermal effects of subduction and extension are better known and less dependent on the specific study area than compositional or anistropic features. Unlike these latter two features the temperature effect of subduction and extension is a minimum necessity (composition may or may not affect P-wave velocity in a certain region, anisotropy may or may not be present at a certain level, but thermal contraction or expansion is unavoidable when material moves). When I model the mantle structure as purely temperature determined the number of unknown parameters is therefore reduced to a minimum. The temperature dominance is not a required modelling assumption like the previous two, because its falsehood can be readily established by comparing model predictions and geophysical observations.

With these considerations the approach for the modelling becomes straightforward:

1 Determine an initial thermal state of the mantle (from the earliest stage of the reconstruction or from other considerations).
2 Determine the surface-displacement and deformation of lithosphere fragments through time.
3 Determine vertical flow associated with the horizontal motion.
4 Use both vertical (interpreted) and horizontal (directly from the tectonic reconstruction) material flow to displace the initial structure (stepwise through time in a numerical model).
5 Calculate diffusion of heat (after each step).
6 Calculate the effect of the present temperature structure (last step) on the required physical quantities.

In the following sections I will explain these modelling steps in more detail.

2.1 Initial thermal structure

In the tectonic reconstructions an indication is often given of the type of lithosphere present in different parts of the region (see for example Figure 2 of the previous chapter). When oceanic lithosphere is present at the time, it is possible to determine the initial thermal structure if the reconstruction specifies the time of formation of this lithosphere. This initial structure is derived from the cooling half-space approximation with average material properties (table 1). This model yields a conductive temperature distribution which has the following form (for a derivation see for example Carslaw and Jaeger [1959] or Turcotte and Schubert [1982]):

$$T(z,t)=T_0\ erf\left(\frac{z}{\sqrt{4\kappa t}}\right) \qquad 1)$$

In equation 1 T_0, denotes the mantle temperature at surface conditions (extrapolated along an adiabat), known as potential temperature [McKenzie, 1969; 1970], z is the depth coordinate, t is the time elapsed since the formation

of the lithosphere, and κ is the thermal diffusion parameter: $k/\rho c_p$. The cooling half-space approximation yields good predictions for basin depth and heat-flow of young oceanic lithosphere (less than 80 m.y. old), as shown by Sclater and Francheteau [1970], Sclater et al. [1971], and Tréhu [1975]. For older lithosphere it is expected to be less accurate because upward heat flow from below the conductive layer is for example ignored in this expression.

Note that old oceanic basins are not present in the studied region during the Early Jurassic (following the reconstructions rifting in the region started in the Triassic), and therefore these do not constitute an 'initial' condition. In the subsequent time-dependent thermal modelling a small net heat-low into the base of the model is included to allow for a heat contribution from the cooling core and slightly radiogenic lower mantle (both a few times 10^{12} W following Stacey [1992]), resulting in an upward heat flux of 10mW/m^2 at the base (1000 km depth) of the forward models. As a result the modelling for old oceanic lithosphere, starting from a young initial state provides a better prediction of heat-flow density and ocean floor topography than the half-space model at a large age (but not perfect, latent heat release from solidification is for example ignored).

Table 1:Physical properties for thermal modelling. Values from Turcotte and Schubert [1982], Toksöz et al. [1973].

		Unit	Oceanic crust and mantle (m)	Lower continental crust (2)	Upper continental crust (1)
specific heat	(c_p)	J/kg,K	1050	1050	1200
conductivity	(k)	W/m,K	3.34	3.3	3.0
expansion	(α)	1/K	$3.6\ 10^{-5}$	$1.6\ 10^{-5}$	$2.4\ 10^{-5}$
density	(ρ)	kg/m^3	3400	2900	2650
heat prod.	(H)	W/kg	0	10^{-11}	10^{-9}

Initial temperature structure in continental regions is calculated with a steady state approximation of a typical three layer continental model. Figure 1 shows the expressions used to determine the initial geotherm. The thermal parameters and symbols are shown in Table 1. The values for this modelling are average for a crust with an upper part of granitic and a lower part of an average diorite and amphibolite composition, comparable with values given by Rybach [1987]. The parameter that is required from the tectonic reconstructions is an estimate of the total thickness of the continental crust, which we obtain by combining the paleo-position of continental areas and indications of lithosphere type from the reconstructions with present crustal thickness information from Meissner et al. [1987] shown in Figure 2. Note that this present crustal thickness can only be used for terranes that have not been

changed by tectonic processes during the period we intend to model. In other cases the thickness is estimated from adjacent regions.

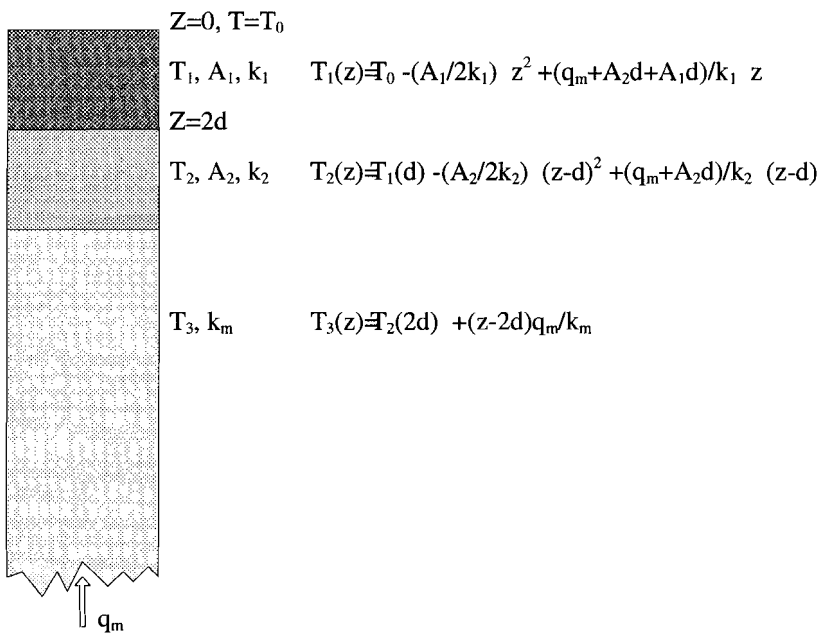

Figure 1. Schematic view and equation **2)** for a 1-dimensional steady-state continental model with two layers of constant radiogenic heat production.

The mantle contribution of heat flow for the initial continental models is kept at a fixed value of 21 mW/m^2, corresponding to the adiabatic gradient in the underlying asthenosphere [Anderson, 1981]. This is only the initial and steady state value, the heat flow, and subsequently the continental geotherm, are free to change in the modelling (although of course they will not do so if no material flow is occurring).

For both continental and oceanic regions the underlying mantle temperatures are calculated using an adiabatic temperature rise with depth (Equation 3). This expression yields the temperature at a given depth, from the potential temperature T_p [McKenzie, 1970]. $_pT$ is also the temperature determined with Equations 1 and 2 in the conductive part of the model, it is 1600K below the conductive part if no perturbations are present (e.g. Anderson [1981], Turcotte and Schubert [1982]).

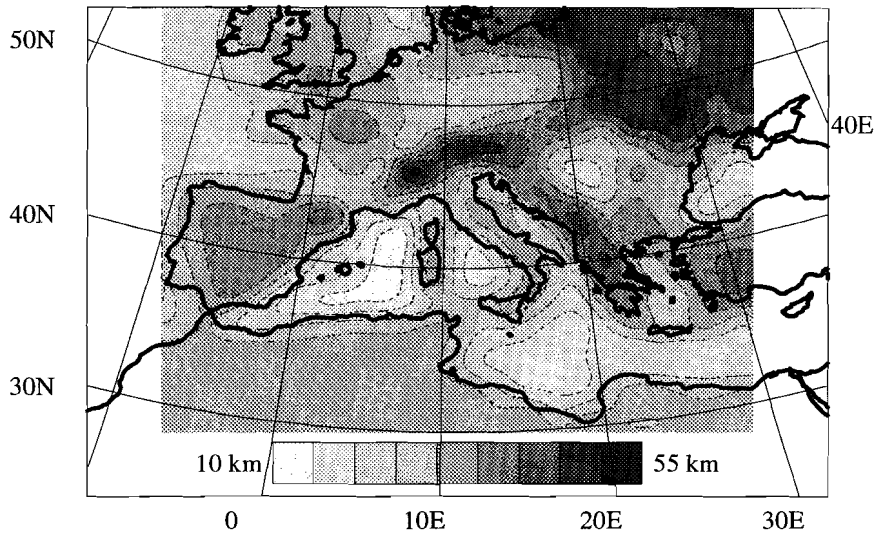

Figure 2. Thickness of crust (including sedimentary cover) after Meissner et al. (1978).

$$T(z)=T_p(z)e^{\frac{z\alpha g}{c_p}} \qquad 3)$$

In Equation 3, g is the gravitational acceleration, α the thermal expansion coefficient, C_p the specific heat, and T is expressed as absolute temperature.

The mantle temperatures are furthermore corrected with phase transition effects. A second order polynomial approximation for the depth of the 400km phase transition and a linear estimate for the depth of the 670km transition are used. These two corrections simulate phase transition effects by increasing the temperature with 150 K below both transitions at a depth that depends (mildly) on temperature. The parameters for these effects are shown in table 2. The depth and latent heat release of the 400 km discontinuity are fairly well established (see for example Anderson [1989] or Turcotte and Schubert [1982]). The value for the 670 km discontinuity is less well constrained. Estimates for the slope of the Clapeyron line for the transition from γ-spinel to silicate-perovskite plus magnesiowüstite are uncertain. In this study I will approximate this process with a simple linear estimate for the depth of this transition, based on seismological data. The depth of transition shown in table 2 is chosen so that a 1000K colder slab produces a depression in the phase boundary of 30 km [Barley et al., 1982; Richards and Wicks, 1990]. This may be a low estimate, as more recent work [Wicks and Richards, 1993] indicates a larger (46 to 80km) downward deflection for the comparably cold Izu-Bonin subduction zone. The entropy change for this transition is estimated to be

somewhat less than that of the 400 km transition [Navrotsky and Akaogi, 1984] but the ambient temperature at which the entropy change occurs is higher. Therefore I will assume that the latent heat released ($T\Delta S$) also increases the temperature by 150K ($T\Delta S/c_p$). Turcotte and Schubert [1982] arrive at a larger effect of 200K based on a different estimate for $T\Delta S$, but uncertainties in the thermodynamic properties are so large that this is can be regarded as essentially equivalent.

The modelling of phase transitions as abrupt temperature increases and the superposition of an adiabatic temperature rise on the geotherm implies that material is convecting freely in the model. The instantaneous temperature rise approximation in fact implies an isentropic flow [Turcotte and Schubert,1971]. This is valid for subduction zones, where material moves with a relatively high vertical velocity component. For the other parts of the mantle it is likely, given typical convection velocities, that the temperature rise occurs in a zone with a width of up to 50 km [Turcotte and Schubert, 1971]. Note that the uncertainties in these phase transitions is significant for the modelled temperature distribution, but for the seismic velocity anomalies, the quantity that will actually compared to observations, their contribution is much less important. The reason for this will become apparent in section 2.4, where the expression for the seismic velocity perturbation is discussed.

With the material properties and approximations mentioned, the thermal structure at the beginning of the tectonic reconstruction is determined. Figure 3 shows a combination of the possible initial structures found in the modelling. Here, the vertical temperature distribution is calculated with the above mentioned equations for oceanic and continental lithosphere. From these geotherms it is clear that especially the age of oceanic lithosphere will have an important impact on the thermal structure. The fact that continental lithosphere is present in a region is also important, but the actual thickness of the continental crust will have a much smaller effect on the thermal structure.

Table 2. Temperature effect and depth of phase transitions as a function of temperature.

Transition	ΔT	depth of transition
Olivine-spinel '400 km'	+150 K	$288+T*5.7\ 10^{-2}+T^2*1.67\ 10^{-5}$ km
Spinel-perovskite + magnesiowüstite '670 km'	+150 K	$700-T*1.5\ 10^{-2}$ km

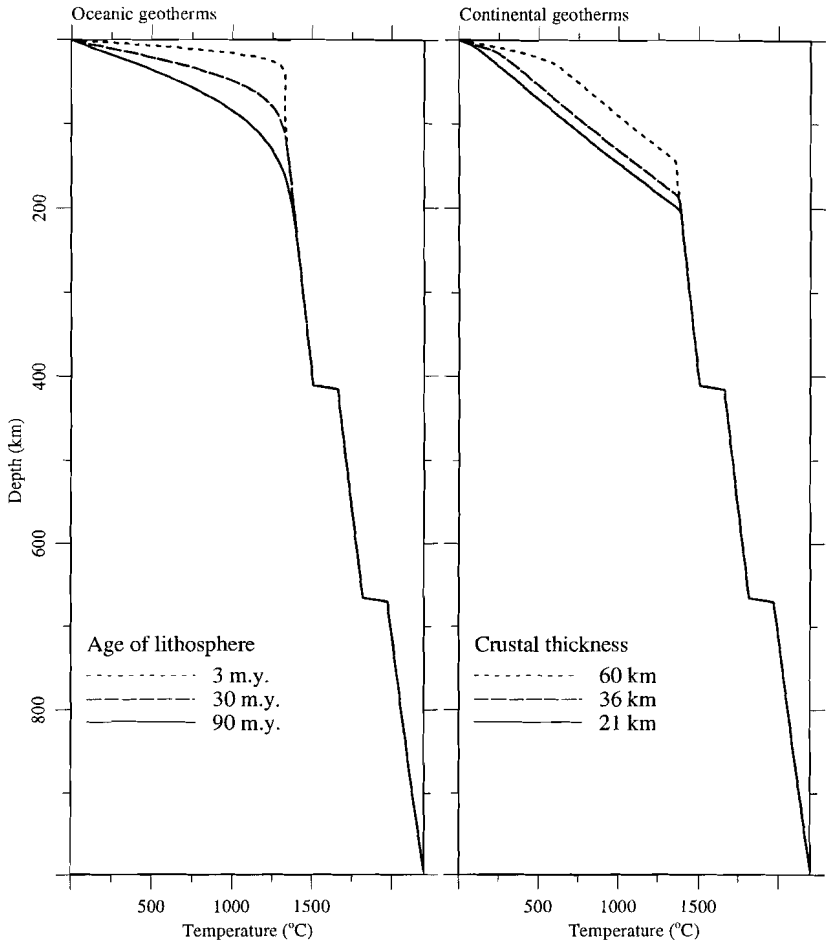

Figure 3. Initial geotherms for oceanic and continental lithosphere.

2.2 Determining a kinematic model from a tectonic reconstruction

The second step of the modelling requires information on the time-dependent displacement of material that is (implicitly) given in the tectonic reconstruction. I will discern two important categories of kinematic processes that influence the mantle and lithosphere structure: relative convergence between plates and intra-plate extension.

Convergent plate boundaries.

The relative motion occurring when two plates converge is considered to be accommodated at a subduction zone located at the (time-dependent) position taken from the tectonic reconstruction. As I will model the thermal effects of subduction in two-dimensional sections, the relevant parameters for this modelling are the component of the convergence rate parallel to the plane of the vertical section, and the angle under which the lithosphere is subducting in this section.

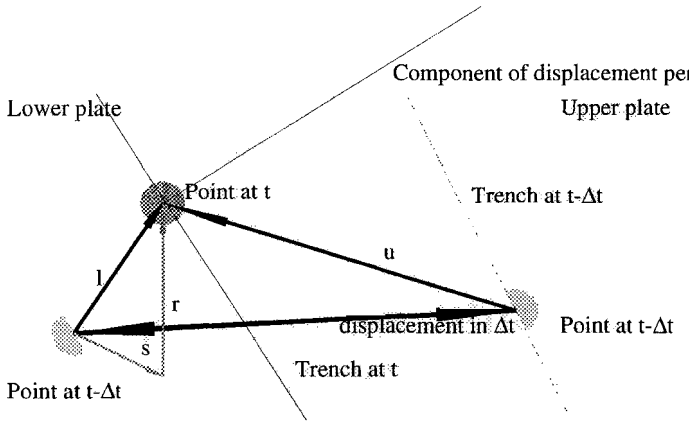

Figure 4. Determination of the convergence rate of a subduction zone from the tectonic reconstruction in the time interval t-Δt to t.

The convergence rate of subduction zones is determined from the reconstruction in the following manner: Rigid body motion of the subducting plate for a given point of the plate are given by the rotation of the lower plate as reconstructed from Paleomagnetic data. For the Dercourt et al. [1986] reconstruction, Savostin et al. [1986] specify Paleomagnetic rotation poles relative to Eurasia for the African, Adriatic, and Iberian plates. Similar data are available in the Dewey et al. [1989] reconstruction. The incremental -i.e. for a small time step- rotation of a point at the trench gives the lower plate motion vector relative to this point ($\bar{r}$). When the subducting plate shows an active oceanic ridge a vector ($\bar{s}$) representing the ocean floor spreading during the time step is added to this motion vector . These two contributions comprise the rigid body motion of the lower plate ($\bar{l}$) at the subduction zone (see Figure 4 for the symbols).

During the time step evaluated the upper plate may also have moved (either rigidly or as a result of intra-plate deformation). This motion ($\bar{u}$ in Figure 4) can be derived directly from the position of the trench indicated in the paleogeographic maps. The convergence velocity at the trench is now given by the difference between the upper and lower plate motion vectors and the

magnitude of the time step. The component of this motion perpendicular to the trench is the controlling rate of convergence used in the thermal modelling of the subduction zone, because it is this component that determines how much lithosphere must have been subducted in the time interval. Note that the vectors shown if Figure 4 are calculated for motions on a spherical earth, not as vectors in a flat plane. Furthermore, the time intervals used for the evaluation need not be equal to those of the tectonic reconstruction (like those shown in Chapter 1, Figure 2): in cases where the reconstruction shows large gaps the trench position has been interpolated (linearly between the known times). This is not quite the same as interpolating the resultant relative velocities derived from a large displacement and time step, as both the changing trench geometry and the plate rotation have complicated effects on the magnitude of the relative motion.

The convergence rate determined in this manner for different reconstructions of the studied area can vary strongly, both in space and in time. Figure 5 shows a few representative cases derived from the Dercourt et al. [1986] and the Dewey et al. [1989] reconstructions. In these figures the height of the bars denotes the perpendicular rate of convergence, while the horizontal position of the bar on the map gives the position of the subduction zone at the pertaining time. These figures show the convergence at the Tyrrhenian plate boundary, which is dominated by the outward migration of the Apennine-Calabrian system.

The second parameter controlling subduction processes is the angle under which the subducted lithosphere disappears into the mantle. In this study this angle is determined from the average type of lithosphere that has subducted. For the old oceanic basins (formed in or before the early Cretaceous, and only recently subducting) the angle was estimated to be 70°. Younger oceanic basins are modelled with smaller dip angles, down to 30° for subduction zones with an average age of the descending lithosphere of 20 m.y.. In those cases where the reconstruction implies the disappearance of substantial amounts of continental lithosphere an angle down to 30° is also used.

The determination of the dip angle from lithosphere properties has the disadvantage that the true dip of a subduction zone may not always be modelled correctly. However, the alternative -using the present dip angle from seismological data- would imply that seismological information is used in the forward models. I have deliberately avoided this circular reference because forward models will be compared to seismological results. Furthermore the present dip angle of Benioff zones is ill-constrained for many parts of the region. The primary quantities that will be addressed in this study are strongly controlled by the bulk amount of subducted lithosphere and the residence time of this material in the mantle. Neither of these properties is strongly dependent on small errors in the dip angle.

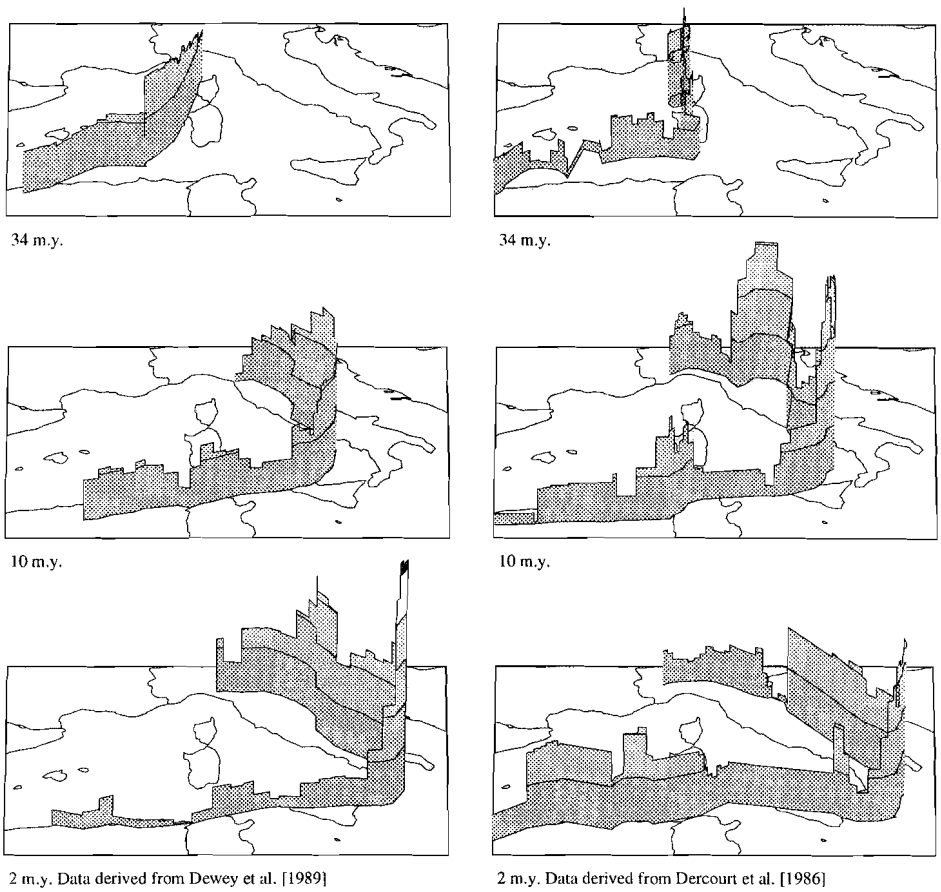

Figure 5. Perpendicular component of the relative convergence rate for three times and two tectonic reconstructions. Shading levels at 1 cm/yr intervals.

Intra-plate extension

The second process that will be evaluated in the forward modelling is extension of lithosphere. This process occurs in many parts of the Alpine-Mediterranean region, predominantly in the form of back-arc type regions on the overriding continental plate of subduction/convergence systems (eg. Western Mediterranean and Tyrrhenian region, Aegean Sea, and Pannonian basin). The material flow can be approximated with a pure shear type of deformation [eg.McKenzie, 1978].

Note that it is not my intention to claim that pure-shear is the actual mode of deformation in all modelled extensional regions. This approximation is chosen because the scale of features I intend to study is such that only average thermal effects on the scale of ten kilometres are needed, at that scale the effect of many smaller faults will be similar to that of the continuous pure

shear deformation. Furthermore, this approximation is computationally less intensive than simple shear models and it requires one less unconstrained assumption in the forward models (the nature of the extension fault).

The amount of extension is derived from the tectonic reconstruction by comparing the size of basins in the different stages of the development in the way shown in Figure 6. The modelling of extension is also done in a vertical section. The change in basin width in this section between two successive stages of the development determines the stretching factor (β). The vertical flow of material is determined by filling in the space created by lithospheric thinning with material from the asthenosphere below and on the sides of the basin.

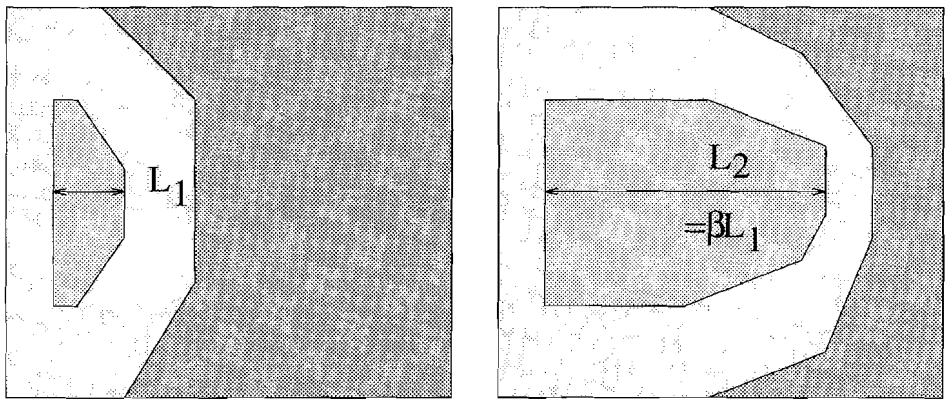

Figure 6. Modelling of (back-arc) extension process in time interval t-Δt to t.

With the initial structure derived from the tectonic reconstruction as in section 2.1 and the kinematics derived from the reconstruction derived as indicated in this section it is now possible to calculate the thermal effects of the lithosphere scale tectonic processes by numerical means.

2.3 Calculating the thermal development from the initial structure and the kinematic model

The thermal structure of a two-dimensional section of the study area is calculated in a way similar to the subduction zone modelling method published by Minear and Toksöz [1970] and Toksöz et al. [1971, 1973]. In this modelling the vertical section is subdivided in a large (400x200 in this study) number of cells. The initial temperature distribution is mapped to this grid. The motion of the subduction process is then modelled by shifting this temperature along a path determined by the dip angle of the slab, with a rate determined by the convergence rate of the subduction zone. Extension processes are modelled by shifting temperature (and material parameters of the crustal rocks) in

accordance with the (incremental) stretching factor (See Figure 7).

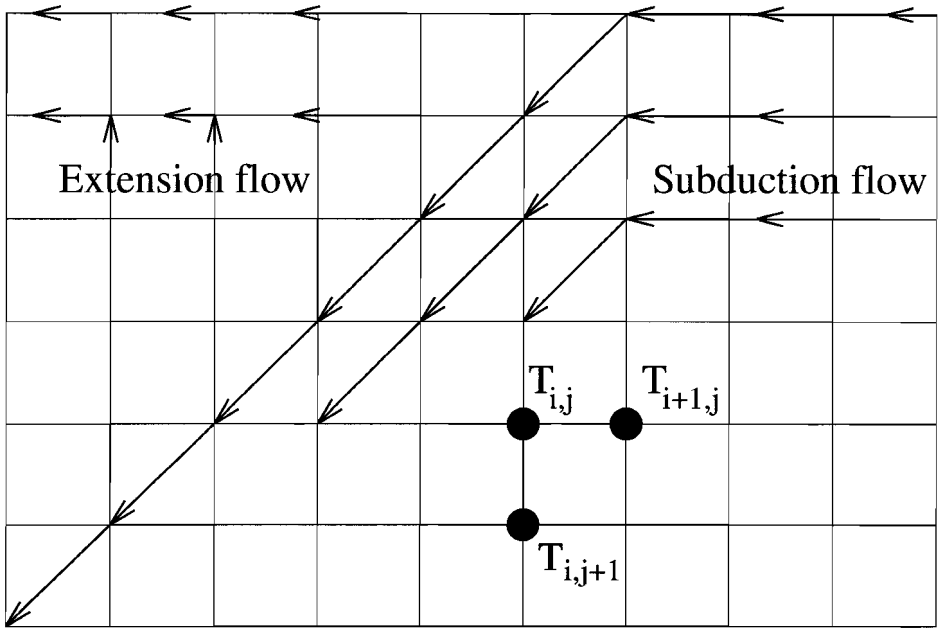

Figure 7. Material displacement derived from the tectonic reconstruction for a vertical section in the thermal modelling.

The thermal diffusion is calculated after each time step using a finite difference solution of the thermal problem (Equation 4).

$$\frac{\partial T}{\partial t} = \frac{k}{\rho c_p}\nabla^2 T + \frac{A}{c_p} \qquad 4)$$

In the current models A is only non zero for the crustal parts of continental models (radiogenic heat production is ignored for mantle material). Limited subduction of continental crust may have occurred in the Adriatic and Alpine region. In the modelling the contribution to the thermal structure is only evaluated for the upper 100km of the model, below this depth the properties of the mantle are considered identical for all cells. Boundary conditions for the thermal calculation consist of a fixed temperature of 0°C at the top, no heat flow through the left and right hand sides, and a constant heat flux at the bottom (to simulate the effect of a cooling core and lower mantle radiogenic heat production)

For computation this equation is discretized in a manner originally proposed by Douglas [1955], Peaceman and Rachford [1955], this method is known as the A(lternating) D(irection) I(mplicit) method, which has stability and convergence properties comparable to a two-dimensional Crank-Nicholson operator, but at a much reduced computational effort. To illustrate this I will briefly describe

the equations resulting from this discretization in the case of zero heat production and constant material properties. Equation 4 then reduces, after some rearranging to:

$$\nabla^2 T = \frac{1}{\kappa}\frac{\partial T}{\partial t} \quad (with\ \kappa = \frac{k}{\rho c_p})$$

With the A.D.I. discretization the ∇^2 and $\partial/\partial t$ operators are approximated with a two-step finite difference form, the two steps being:

$$\frac{1}{\kappa}\frac{T^{*n+1}_{i,j} - T^{n}_{i,j}}{\Delta t} = \frac{T^{*n+1}_{i-1,j} - 2T^{*n+1}_{i,j} + T^{*n+1}_{i+1,j}}{(\Delta x)^2} + \frac{T^{n}_{i,j-1} - 2T^{n}_{i,j} + T^{n}_{i,j+1}}{(\Delta y)^2}$$

and

$$\frac{1}{\kappa}\frac{T^{n+1}_{i,j} - T^{n}_{i,j}}{\Delta t} = \frac{T^{*n+1}_{i-1,j} - 2T^{*n+1}_{i,j} + T^{*n+1}_{i+1,j}}{(\Delta x)^2} + \frac{T^{n+1}_{i,j-1} - 2T^{n+1}_{i,j} + T^{n+1}_{i,j+1}}{(\Delta y)^2}$$

Rearranging and grouping κ, Δt, Δx, and Δy in the parameters λ and μ ($1+2\kappa\Delta t/\Delta x^2$ and $1+2\kappa\Delta t/\Delta y^2$ respectively) yields:

$$T^{*n+1}_{i-1,j} - \lambda T^{*n+1}_{i,j} + T^{*n+1}_{i+1,j} = T^{n}_{i,j-1} + \mu T^{n}_{i,j} + T^{n}_{i,j+1}$$

and

$$T^{n+1}_{i,j-1} - \mu T^{n+1}_{i,j} + T^{n+1}_{i,j+1} = T^{*n+1}_{i-1,j} - \lambda T^{*n+1}_{i,j} + T^{*n+1}_{i+1,j}$$

In these Equations the i,j indices denote the grid points of the modelling, the n-index is for the total time step ($=2\Delta t$), and T^* is an intermediate temperature solution (with no direct physical significance). Performing these two steps in succession is the identical to calculating one two-dimensional diffusion step. However, the advantage (over a standard 2D Crank-Nicholson operator) of the expressions above is that for the two half-steps the solution of both T^{*n+1} and T^{n+1} (from T^n and T^{*n+1} respectively) requires only the -computationally very efficient- inversion of tri-diagonal matrices. This means that an implicit solution for the forward stepping of a large number of high resolution sections becomes computationally well feasible. A minor disadvantage of the method is the necessity to maintain more storage space (T^{*n+1} needs to be kept available between steps).

The alternation of a displacement step (where the temperatures are shifted like in Figure 7) and a diffusion calculation in the above described manner results in a numerical estimate for the development of the temperatures in the

vertical section throughout the tectonic history. The final stages of the development of the vertical cross-sections are combined into a three dimensional model by mapping the calculated temperatures into a three dimensional cell model. Because the thermal modelling results will be compared to results from delay-time tomography obtained by Spakman [1993] and Remkes and Spakman [1994], the cells of the three-dimensional model are chosen so that they coincide with their tomographic models. In practice this means that a number of temperatures of the two-dimensional section are averaged, since the tomographic model uses larger cells (Figure 8). As a result the detail of the forward models is reduced to what the tomographic cell volume can contain.

Note that the mapping of thermal results to the coarser grid should only be done for comparison of P-wave velocities. Other temperature dependent parameters should be derived from the higher resolution thermal results directly. In Appendix 1 at the end of this chapter I will describe the resulting temperature model. This model is projected on a much finer grid (0.2X0.2 degrees) to illustrate the attainable resolution of the synthetic models

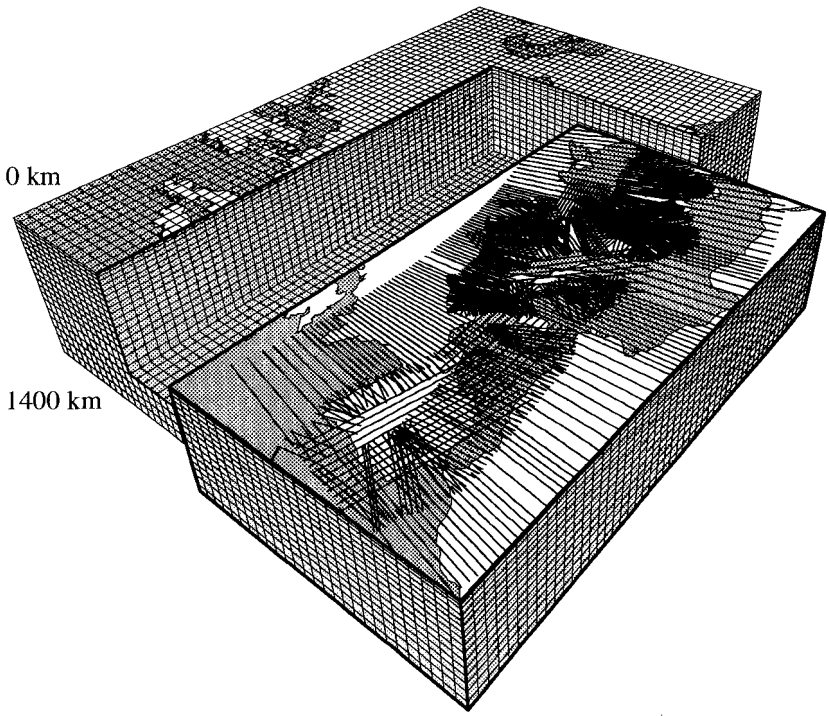

Figure 8. Three-dimensional cell model for the seismic velocity structure. Lines on the surface denote the traces of the vertical sections calculated in modelling the Dercourt et al. (1986) reconstruction (and that are combined into the 3D model).

2.4 Determining thermally controlled quantities

The calculated present thermal structure cannot be compared directly with observations of the lithosphere and mantle properties. Instead derived quantities are used to compare predictions with observations. In this study three quantities will be addressed in more detail:
- *Basement heat-flow density*: a prediction of the present shallow structure. This quantity is an almost direct translation of the temperature of the top layers of the model.
- *Subsidence of extensional basins*: a prediction of the time integrated shallow structure. This quantity requires some additional assumptions on material properties (density, expansion).
- *P-wave velocity structure*: a prediction of the -present- whole-volume structure. This quantity contains the most complete information on the mantle structure, but it also requires more 'post-processing' of the model temperatures than the previous two. In this study the focus of attention will be on the P-wave velocity structure because this quantity holds information on the whole mantle structure and its evolution, whereas the other two only give a constraint for the integrated properties of the shallow present-day structure.

Basement heat flow density

The temperature in the upper layers of the model follows from thermal calculations. In this study the surface heat-flow is free to change (the boundary condition for the top model layer is a fixed temperature of 0°C). Therefore it is possible to calculate the average heat-flow density from the temperature gradient and the crustal composition (Equation 5):

$$q = \left| k \frac{T(z+\Delta z) - T(z)}{\Delta z} \right| \qquad 5)$$

Heat-flow density is most strongly determined by late stages of extensional deformation, as these have a strong impact on the near surface temperature gradient. In Chapter 3 I will show the results of this approximation for two different reconstructions of the development of the Tyrrhenian sea. Physically, the modelled heat-flow density corresponds to the basement contribution in a sedimentary basin with an average granitic composition. A sedimentary cover is not included in the calculation. This is not a very important omission as, for sediments, a cover with a thickness d gives an maximum additional heat flow contribution of A.d W/m^2. A quick calculation shows that the neglected additional heat flow is of the order 1.5 mW/m^2 for every kilometre of average sediment in an old sedimentary basin (which is 2% of the typical total of 70mW/m^2). In fact, in the Mediterranean region it will often be much less (and sometimes even negative) as the thermal structure has not yet reached an equilibrium (a result of high sedimentation rates [Hutchinson et al., 1985].) Since the small-scale heterogeneity and uncertainty resulting from local fluid circulation and local geological structure in the observed heat flow is generally

much larger than the possible few percents error in the predicted heat flow, the sedimentary cover contribution can be ignored for regional scale modelling.

Basin topography

The second parameter than can be obtained from the temperature distribution is the subsidence of the basement as a result of stretching and subsequent temperature development. This parameter is derived from a simple local isostasy approximation. For the calculation of subsidence the following is assumed:

- Lithostatic pressure is constant (both laterally and through time) at a large depth.
- Elastic strength of interesting -i.e. strongly extending- regions is negligible (note that this is not the case if one wants to study basin edges, on- and offlap sequences or small-scale synthetic stratigraphy, but these phenomena are beyond the scope of this study).

Both these assumptions are of course only approximations of the real situation, but the main features of extensional basins should be predicted to the amount of detail present in the tectonic reconstruction.

The lithostatic pressure is found by numerically integrating the weight of a vertical column of material, down to a compensation depth of 200 km. If the pressure at this depth has changed from the previous time step, the amount of material added to or removed from the base of the column determines the subsidence in the way shown in Equation 6 and Figure 9:

$$\Delta H = \frac{P(t) - P(t-\Delta t)}{g(\rho_m - \rho_f)(1 - \alpha_m T_m)} \qquad \textbf{6)}$$

$$[with:\ P(t) = \sum_{j=0}^{m} g \Delta y_j \rho_j \left(1 - \alpha_j \frac{(T_j + T_{j+1})}{2}\right)\ ]$$

In Equation 6 the m-indices denote values at the compensation depth, the j grid index runs from the surface (0) down to this value. g is the average gravitational acceleration, ρ and α depend on the composition (like shown in table 1 of this chapter). Δy is the thickness of the layer for which the quantities hold. ΔH then equals the subsidence for a column with a basin infill with density ρ_f (in this study the density of water). The subsidence calculated in this way is a prediction of the back-stripped, water loaded, subsidence of the modelled basin (see for an example Sleep [1971] or

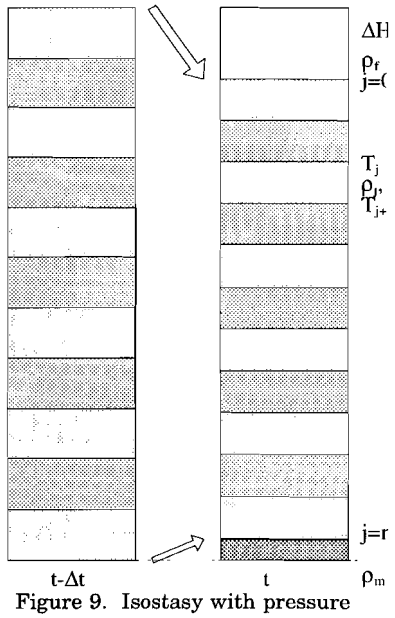

Figure 9. Isostasy with pressure balance.

Bond and Kominz [1984]). This time dependent quantity will not be addressed directly, but the bathymetry of the modelled basin follows from the cumulative subsidence, and this can be compared to the actual basin bathymetry. To obtain an absolute basin depth pressure at the compensation depth for a known thermal profile and topography is used as a reference, in this study this is done by imposing an ocean depth of 4km below sea level to 100 m.y. old oceanic lithosphere. From the initial equilibrium topography (which depends on the composition and thermal structure) the sum of the subsidence calculated for subsequent time-steps with Equation 6 gives the present water-loaded basin bathymetry.

P-wave velocity structure

The model result that reflects most of the lithosphere and mantle perturbations resulting from the tectonic development is the distribution of seismic velocities. In order to determine the seismic velocity heterogeneities the thermal structure has to be translated to a temperature-anomaly structure. This means the deviation of the model result from an average mantle temperature are calculated. A first order estimate of the temperature dependent P-wave velocity anomalies can than be calculated using:

$\Delta V_p \approx \Delta T \frac{\delta V_p}{\delta T} |_z$ or, for the relative anomaly $\approx \frac{\Delta T}{V_p(z)} \frac{\delta V_p}{\delta T} |_z$.

Since only ΔT, the difference between the temperature of the ambient mantle and the anomalous region, determines the velocity anomaly, the exact temperature of the mantle is not very critical. If at a certain depth temperature increases more as a result of phase transitions than in our modelling this will hold in a similar way for the anomaly (except for a narrow zone around the depth of the phase transition). This explains why the modelling of phase transitions described in section 2.1 can be done in an approximate way.

To calculate the depth-dependent temperature derivative of V_p the following approach is used.

The P-wave velocity in an isotropic elastic medium is:

$$V_p = \sqrt{\kappa + \frac{4\mu}{3}}$$

I will consider only the thermally determined lateral velocity structure. This means that only temperature dependent terms are considered and not the total differential expression:

$$\delta V_p = \frac{\partial V_p}{\partial T}\delta T + \frac{\partial V_p}{\partial P}\delta P + \frac{\partial V_p}{\partial X}\delta X \qquad 7)$$

The omission of pressure (P) dependent terms from Equation 7 is warranted, because the lateral pressure differences are negligible compared to the lithostatic pressure at the depth levels considered. The effect of composition (X) in equation 7, however, is definitely important in the crustal parts of the Earth. Since this study deals with lower lithosphere and mantle velocity structure only, the approximation that X is negligible is less problematic. This can be demonstrated with typical rheologies for the mantle, using composition and V_p values from Anderson [1989]. A typical mantle structure, that fits both observed average seismic properties and dominant xenolith composition consists of an olivine rich peridotite. This material has a typical P-wave velocity of 8.4 km/s. Suppose that the crustal part of an oceanic lithospheric slab has completely subducted and transformed to eclogite, with a typical P-wave velocity of 8.6 km/s. The expected compositional velocity anomaly is then 2.3% across a 4 km thick layer. On the grid size (see Figure 8) of the tomographic results this amounts to an average compositional cell-velocity anomaly of 0.1% (the tomographic cells have dimensions of 100km in the mantle). Similarly the effect of a thin garnet lherzolite layer (V_p=8.2 km/s) can be estimated to be -0.1% for a whole tomographic cell.

In contrast, the thermally induced lateral velocity anomaly associated with the slab will also be typically about 2.5%, but in this case throughout the 100 km thick layer (de Jonge and Wortel [1990]). The thermal effect of subduction is therefore, at the resolution of the tomographic results, at least an order of magnitude higher than compositional effects. Consequently, I will only consider the temperature derivative $\partial V_p / \partial T$ to determine the mantle velocity structure:

$$\frac{\partial V_p}{\partial T} = \frac{1}{2V_p\rho}\left[\frac{\partial K}{\partial T} + \frac{4}{3}\right] \qquad 8)$$

Where ρ= density, K= bulk modulus, μ=shear modulus, and the volume expansion coefficient is: $\alpha = -\frac{1}{\rho}\frac{\delta\rho}{\delta T}$.

Expression 8 can be evaluated numerically for different possible values of the elastic parameters of olivine (94% Fo) based on laboratory and seismological data (see the caption of Figure 9 for references). The resulting range of values for $\partial V_p/\partial T$ at different depths in the mantle is shown in Figure 9. In the left panel the shaded area denotes outcomes in a monte carlo analysis of the elastic parameters, the thick black line is the preferred average that will be employed in this study. As an illustration the right-hand side of this figure shows the effect of a 100°C low-temperature anomaly. it is clear that the importance of the temperature for the V_p structure diminishes strongly with depth. This means that the magnitude of seismic velocity anomalies modelled is expected to decrease with depth, not only as a result of thermal conduction, but also from the decreased sensitivity. Note that the effect of phase transitions on the

velocity structure is included in the form of abrupt changes in $\partial V_p/\partial T$.

An alternative measure for the mantle structure can be found in the distribution of S-wave velocities. In a similar manner as shown for V_p, $\partial V_s/\partial T$ can be evaluated. This results in the following expression:

$$\frac{\partial V_s}{\partial T} = \frac{1}{2V_s\rho}\left(\frac{\partial \mu}{\partial T} + \alpha\mu\right)$$

The corresponding depth dependence of $\partial V_s/\partial T$ is shown in Figure 10. I will not dwell on this model quantity since the resolution of comparison data in the form of S-wave studies is much less as shown in studies by for example Zielhuis [1992], and Panza [1984]. Furthermore the sensitivity of V_s for temperature alone appears to be less than that of V_p (compare Figures 10 and 11). An other effect that makes the S-wave velocity a less suitable quantity for comparing forward models and seismological results is the strong dependence on composition and partial melting. For the European region Zielhuis [1992] already noted that a significant part of the shallow V_s structure observed cannot be directly related to the temperature distribution.

Note that the equations for the seismic velocity and their temperature derivatives are based on the assumption that the material described is behaving like a normal elastic solid. When temperatures approach the solidus of olivine the estimates become less reliable. When the temperature anomaly is negative, like for subduction zones, temperatures move away from tthe solidus so this effect will not be very important, but in regions where the mantle is anomalously hot the modelled seismic velocity anomaly is an underestimation of the actual mantle velocity by an amount that depends on the partial melting (strongly for V_s, somewhat less for V_p because the effect of melting on the shear modulus is larger than that on bulk modulus).

A further complication is that the velocity structure is implicitly determined with an average pressure and temperature (through the fixed $\partial V_{s,p}/\partial T$ for a given depth) and assumed to be linearly dependent on both this and on the temperature perturbation, even for very large anomalies. The assumptions are only approximations of the actual situation, but the uncertainty range shown in Figures 10 and 11 hardly warrants a more exact determination of these parameters. With these conversions from temperature to physical properties the forward modelling is complete; the predicted parameters are of the same form as independent test criteria provided by geological and geophysical research. In the following chapter I will apply the above described modelling approach to the reconstructions of the tectonic evolution of the Alpine-Mediterranean region described in chapter 1.

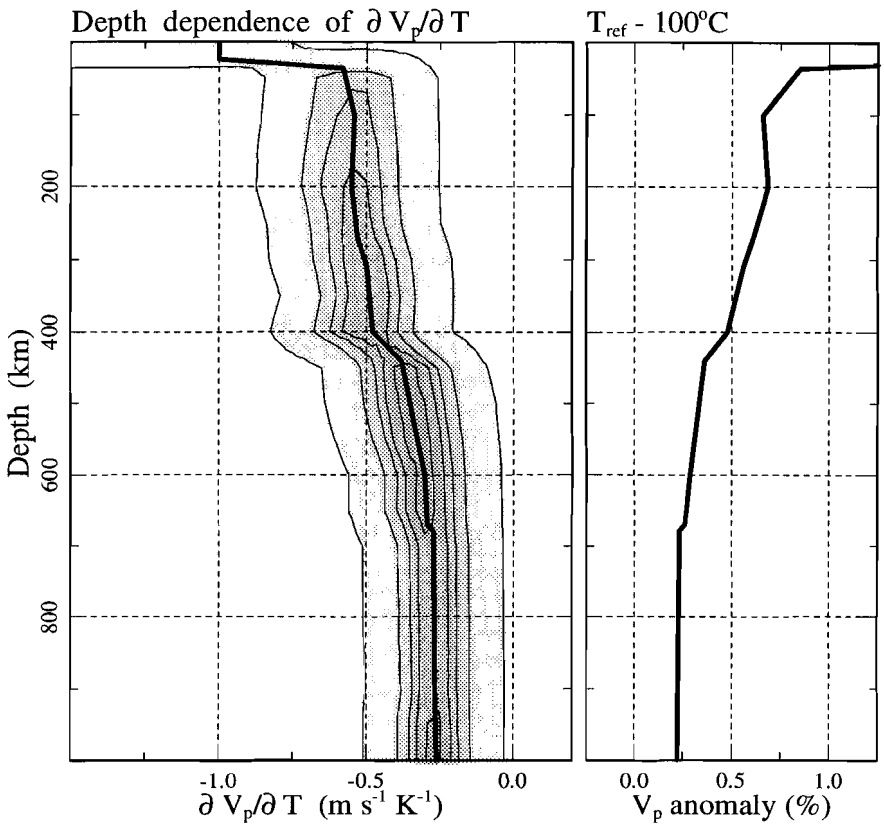

Figure 10. Left panel: depth dependence of P-velocity sensitivity to temperature, the grey area denotes the range, thick line the values used. Results obtained by a Monte Carlo evaluation of (extrapolated laboratory) results from Graham and Barsch [1969], Mizutani et al. [1970], Chung [1971], Anderson et al. [1972], Wang and Simmons [1972], Suzuki [1975], Sumino et al. [1977, 1983], Dziewonski and Anderson [1981], Suzuki et al. [1981, 1983], Turcotte and Schubert [1982], Sawamoto et al. [1984], Weidner et al. [1984], Bina and Wood [1987], Isaak et al. [1989], and Gwanmesia et al. [1990]. The right panel shows how the velocity anomaly that would result from a 100°C lower temperature decreases with depth (in % of the ambient P-velocity).

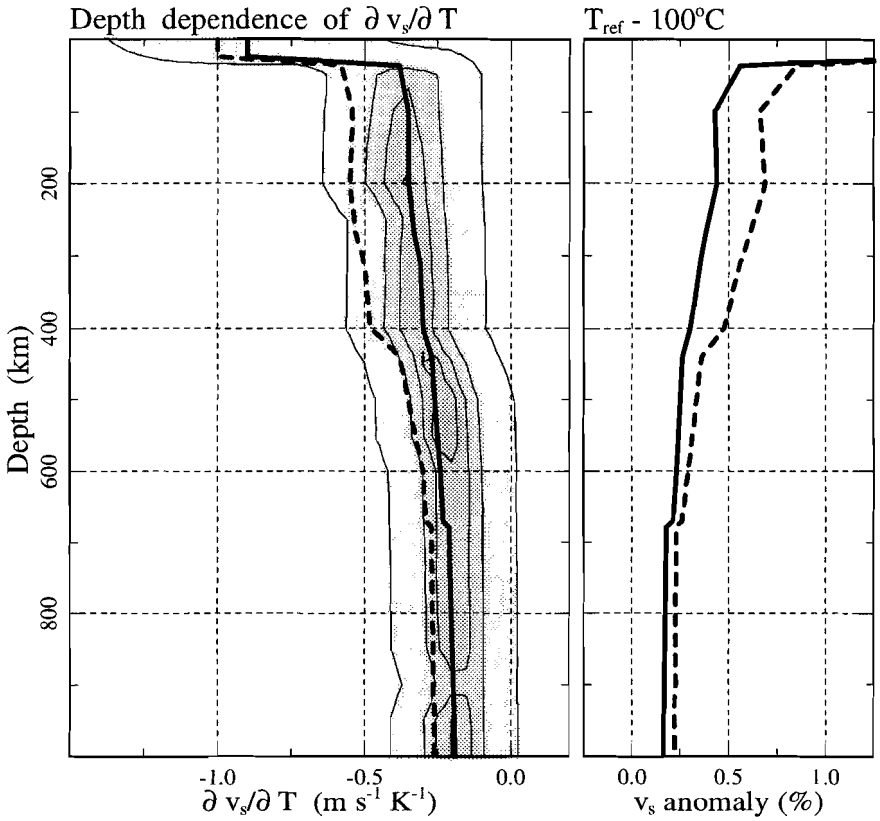

Figure 11. A similar plot as Figure 10, but now for the S-wave velocity. P-wave data shown for comparison as a dashed line in the left panel.

References:

Anderson, D. L., *Theory of the Earth*, 366 pp., Blackwell, Oxford, 1989.

Anderson, D. L., C. Sammis, and T. Jordan, Composition of the mantle and core, in *The Nature of the Solid Earth*, edited by E. C. Robertson, J. F. Hays, and L. Knopoff, pp. 41-66, McGraw-Hill, New York, 1972.

Anderson, O. L., Temperature profiles in the Earth, in *Evolution of the Earth*, edited by R. J. O'Connell and W. S. Fyfe, Geodynamics series, *5*, A.G.U. and Geol. Soc. Am., Washington, Boulder, 19-27, 1981.

Barley, B. J., J. A. Hudson, and A. Douglas, S to P scattering at the 650 km discontinuity, *Geophys. J. R. Astron. Soc., 69*, 159-159, 1982.

Bina, C. R., and B. J. Wood, Olivine-spinel transitions: Experimental and thermodynamic constraints and implications for the nature of the 400-km seismic discontinuity, *J. Geophys. Res., 92*, 4853-4866, 1987.

Bond, G. C., and M. A. Kominz, Construction of tectonic subsidence curves for the early Paleozoic miogeosyncline in the southern Canadian Rocky Mountains: implications for subsidence mechanisms, age of break-up, and crustal thinning, *Geol. Soc. Am. Bull., 95*, 155-173, 1984.

Carslaw, H. S., and J. C. Jaeger, *Conduction of heat in solids*, 510 pp., Oxford Univ. Press, Oxford, 1959.

Chung, D. H., Elasticity and equations of state of olivines in the Mg_2SiO_4-Fe_2SiO_4 system, *Geophys. J. R. Astr. Soc., 25*, 511-538, 1971.

De Jonge, M. R., and M. J. R. Wortel, The thermal structure of the Mediterranean upper mantle: A forward modelling approach, *Terra Nova, 2*, 609-616, 1990.

Dercourt, J., L. P. Zonenshain, L.-E. Ricou, V. G. Kazmin, X. Le Pichon, A. L. Knipper, C. Grandjacquet, I. M. Sbortshikov, J. Geyssant, C. Lepvrier, D. H. Perchersky, J. Boulin, J.-C. Sibuet, L. A. Savostin, O. Sorokhtin, M. Westphal, M. L. Bazhenov, J. P. Lauer, and B. Biju-Duval, Geological evolution of the Tethys from the Atlantic to the Pamirs since the Lias, in *Evolution of the Tethys*, edited by J. Auboin, X. Le Pichon, and A. S. Monin, *Tectonophysics, 123*, 241-315, 1986.

Dewey, J. F., M. L. Helman, E. Turco, D. H. W. Hutton, and S. D. Knott, Kinematics of the western Mediterranean, in *Alpine Tectonics*, edited by M. P. Coward, D. Dietrich, and R. G. Park, *Geol. Soc. Lond. Spec. Publ., 45*, 265-283, 1989.

Douglas, J., On the numerical integration of $\partial^2u/\partial x^2+\partial^2u/\partial y^2=\partial u/\partial t$ by implicit methods, *J. Soc. Ind. Appl. Math., 3*, 1955.

Dziewonsky, A. M., and D. L. Anderson, Preliminary reference Earth model, *Phys. Earth and Plan. Int., 25*, 297-356, 1981.

Graham, E. K., and G. R. Barsch, Elastic constants of single-crystal forsterite as a function of temperature and pressure, *J. Geophys. Res., 74*, 5949-5972, 1969.

Gwanmesia, G. D., S. Rigden, I. Jackson, and R. C. Liebermann, Pressure dependence of elastic wave velocity for β-Mg_2SiO_4 and the composition of the earth's mantle, *Science, 250*, 794-797, 1990.

Hutchinson, I. , R. P. von Herzen, K. E. Louden, J. G. Sclater, and J. Jemsek, Heat flow in the Balearic and Tyrrhenian Basins, western Mediterranean, *J. Geoph. Res., 90*, 685-701, 1985.

Isaak, D. G., O. L. Anderson, T. Goto and, I. Suzuki, Elasticity of single-crystal forsterite measured to 1700K, *J. Geophys. Res., 94*, 5895-5906, 1989.

McKenzie, D. P., Speculations on the consequences and causes of plate motions, *Geophys. J. R. Astr. Soc., 18*, 1-32, 1969.

McKenzie, D. P., Temperature and potential temperature beneath island arcs, *Tectonophysics, 10*, 357-366, 1970.

McKenzie, D. P., Some remarks on the development of sedimentary basins, *Earth and Plan. Sci. Lett., 40*, 25-32, 1978.

Meissner, R., Th. Wever, and E. R. Flüh, The moho in Europe - implications for crustal

development, *Ann. Geophys., 5B*, 357-364, 1987.
Minear, J. W., and M. N. Toksöz, Thermal regime of a downgoing slab and new global tectonics, *J. Geophys. Res., 75*, 1397-1419, 1970.
Mizutani, H., Y. Hamano, Y. Ida, and S. Akimoto, Compressional wave velocities of fayalite, Fe_2SiO_4 spinel and coesite, *J. Geophys. Res., 75*, 2741-2747, 1970.
Navrotsky, A., and M. Akaogi, The α, β, γ phase relations in Fe_2SiO_4-Mg_2SiO_4 and Co_2SiO_4-Mg_2SiO_4: Calculation from thermochemical data and geophysical applications, *J. Geophys. Res., 89*, 10135-10140, 1984.
Panza, G. F., The deep structure of the Mediterranean-Alpine region and large shallow earthquakes, *Mem. Soc. Geol. It., 29*, 5-13, 1984.
Peaceman, D. W., and H. Rachford, The numerical solution of parabolic and elliptic differential equations, *J. Soc. Ind. Appl. Math., 3*, 28-41, 1955.
Platt, J. P., and R. L. M. Vissers, Extensional collapse of thickened continental lithosphere: a working hypothesis for the Alboran Sea and the Gibraltar arc, *Geology, 17*, 540-543, 1989.
Richards, M. A., and C. W. Wicks, S-P conversion from the transition zone beneath Tonga and the nature of the 670 km discontinuity, *Geophys. J. Int., 101*, 1-35, 1990.
Remkes, M., and W. Spakman, Joint inversion of seismic delay times and regional geoid for the European mantle structure, *Terra Abstracts EUG, 5*, 124-125, 1993.
Rybach, L., A petrological model of the lower continental crust, derived from seismic velocities and from radioactive heat production, *Ann. Geoph., 5B*, 403-408, 1987.
Sawamoto, H., D. J. Weidner, S. Sasaki, and M. Kumazawa, Single-crystal elastic properties of the modified spinel (beta) phase of magnesium orthosilicate, *Science, 224*, 749-751, 1984.
Sclater, J. G. and J. Francheteau, The implications of terrestrial heat flow observations on current tectonic and geochemical models of the crust and upper mantle of the Earth, *Geophys. J. R. Astron. Soc., 20*, 509-542, 1970.
Sclater, J. G., R. N. Anderson, and M. L. Bell, Elevation of ridges and evolution of the central Eastern Pacific, *J. Geophys. Res., 76*, 7888-7915, 1971.
Sleep, N. H., Thermal effects of the formation of Atlantic continental margins by continental break-up, *Geoph. J. R. Astron. Soc., 24*, 325-350, 1971.
Sleep, N. H., Teleseismic P-wave transmission through slabs, *Bull. Seismol. Soc. Am., 63*, 1349-1373, 1973.
Spakman, W., S. van der Lee, R. D. van der Hilst, Travel-time tomography of the European-Mediterranean mantle down to 1400 km, *Phys. Earth Plan. Int., 79*, 3-74, 1993.
Sumino, Y., O. L. Anderson and I. Suzuki, Temperature coefficients of elastic constants of single crystal MgO between 80 and 1300 K, *Phys. Chem. Min., 9*, 38-47, 1983.
Sumino, Y., O. Nishizawa, T. Goto, I. Ohno and M. Ozima, Temperature variation of elastic constants of single-crystal forsterite between -190° and 400°C, *J. Phys. Earth, 25*, 377-392, 1977.
Suzuki, I., Thermal expansion of periclase and olivine and their anharmonic properties, *J. Phys. Earth, 23*, 145-159, 1975.
Suzuki, I., O. L. Anderson, and Y. Sumino, Elastic properties of single-crystal forsterite Mg_2SiO_4 up to 1200 K, *Phys. Chem. Min., 10*, 38-46, 1983.
Suzuki, I., K. Seya, H. Takei, and Y. Sumino, Thermal expansion of fayalite, Fe_2SiO_4, *Phys. Chem. Min., 7*, 60-63, 1981.
Toksöz, M. N., J. W. Minear, and B. R. Julian, Temperature field of a downgoing slab, *J. Geophys. Res., 76*, 1113-1139, 1971.
Toksöz, M. N., N. H. Sleep, and A. T. Smith, Evolution of the downgoing lithosphere and the mechanisms of deep focus earthquakes, *Geophys. J. R. Astr. Soc., 35*, 285-310, 1973.
Tréhu, A. M., Depth versus $(age)^{1/2}$: a perspective on mid-ocean rises, *Earth Plan. Sci.*

Lett., 27, 287-304, 1975.
Turcotte, D. L., and G. Schubert, Structure of the olivine-spinel phase boundary in the descending lithosphere, *J. Geophys. Res., 76*, 7980-7987, 1971.
Turcotte, D. L., and G. Schubert, *Geodynamics: Applications of Continuum Physics to Geological Problems*, 450 pp., Wiley, New York, 1982.
Wang, H., and G. Simmons, Elasticity of some mantle crystal structures 1. Pleonaste and hercynite spinel, *J. Geophys. Res., 77*, 4379-4392, 1972.
Weidner, D. J., H. Sawamoto, and S. Sasaki, single-crystal elastic properties of the spinel phase of Mg_2SiO_4, *J. Geophys. Res., 89*, 7852-7860, 1984.
Wicks, C. W., and M. A. Richards, A detailed map of the 660-kilometer discontinuity beneath the Izu-Bonin subduction zone, *Science, 261*, 1424-1427, 1993.
Zielhuis, A., S-wave velocity below Europe from delay-time and waveform inversions, Ph.D thesis, 148 pp., Utrecht University, Utrecht, 1992.

Appendix 1

The temperature distribution of the upper mantle

Although the calculated temperatures that follow from the forward modelling cannot be compared directly to observation, model temperatures can give useful information for mantle chemistry, rheology and related quantities. As an illustration the following figure (1) shows the present temperatures at different depths in of the upper mantle, calculated from the tectonic development proposed by Dercourt et al. [1990, 1986]. For this illustration temperatures are not mapped on the tomographic cell volume, but on a grid of 0.2° by 0.2 by 15 km. When the forward model values are presented this way they cannot be compared to tomographic results. The values shown are however closer to the actual model results. Therefore, in the determination of mantle properties that are not based on the tomographic inversion the temperatures shown in this Figure should be used.

In Figure 2 the data of Figure 1 are displayed again, in this figure absolute temperatures that are below 75% of those of the ambient mantle, are denoted with grey shading. The seismic events around (±30km) the depth level, taken from the ISC catalogue, are also plotted. The seismic events are almost exclusively restricted to the predicted cold areas. This observation illustrates how the forward mantle models of the temperatures can be employed for the prediction of other mantle properties than the ones that are explicitly addressed in this study. Note that if the temperatures were averaged over the tomographic cell model this type of information would have been lost. Since the relation between temperature and seismicity is a matter of strong controversy, it is hard to assess the significance of the correlation shown in Figure 2. For many properties similar problems are present, it is at present often impossible to use the high-resolution thermal models directly for verification of the modelling method and the underlying tectonic reconstructions. I will therefore not deal with the direct temperature model results in the following chapters.

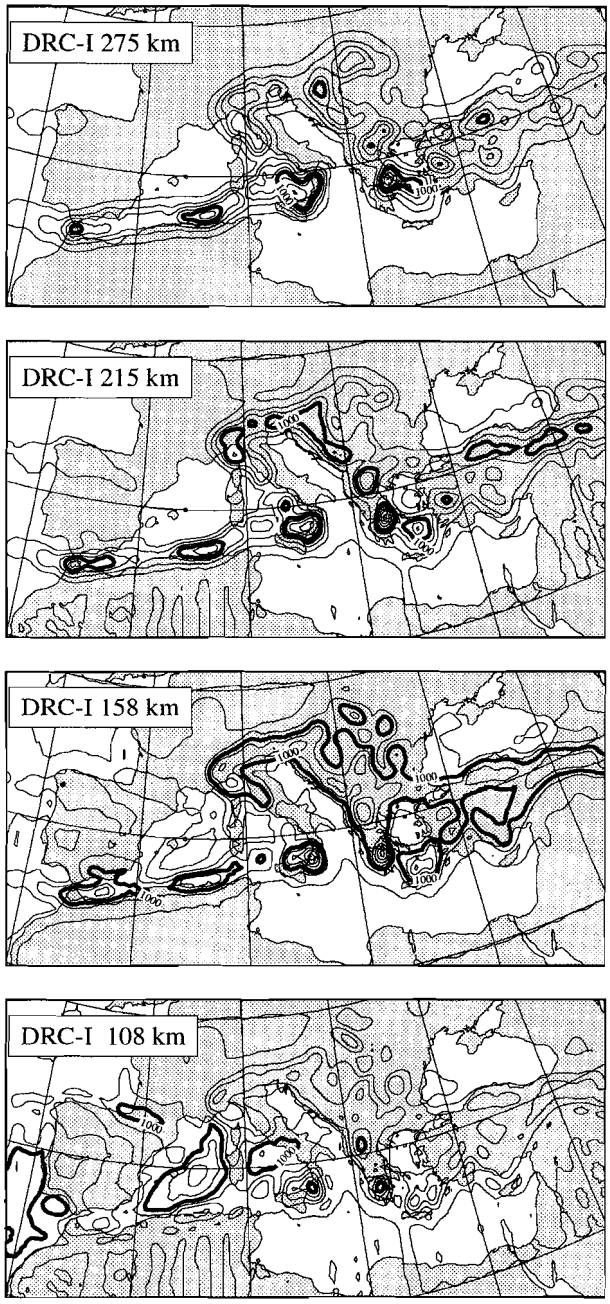

Figure 1. Present modelled temperature distribution of the upper mantle, based on the Dercourt et al. (1986,1990) reconstructions. Contour lines at 100°C (thin) and 500°C (thick).

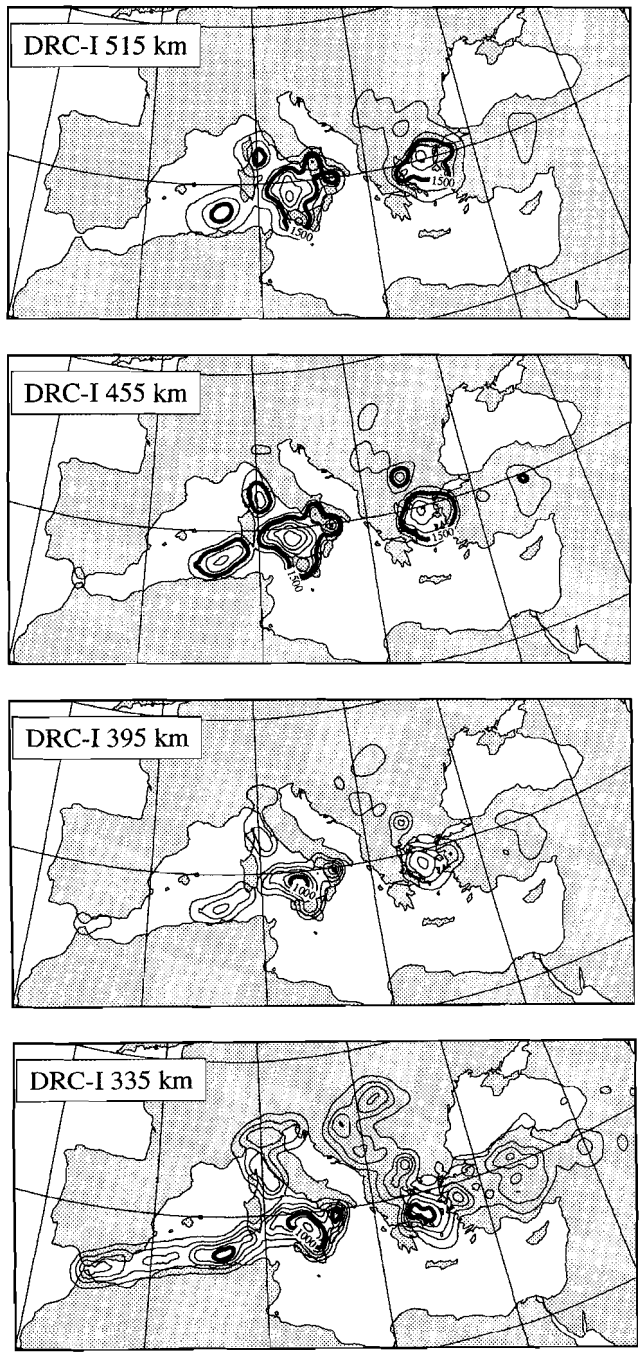

Figure 1. Continued from previous page.

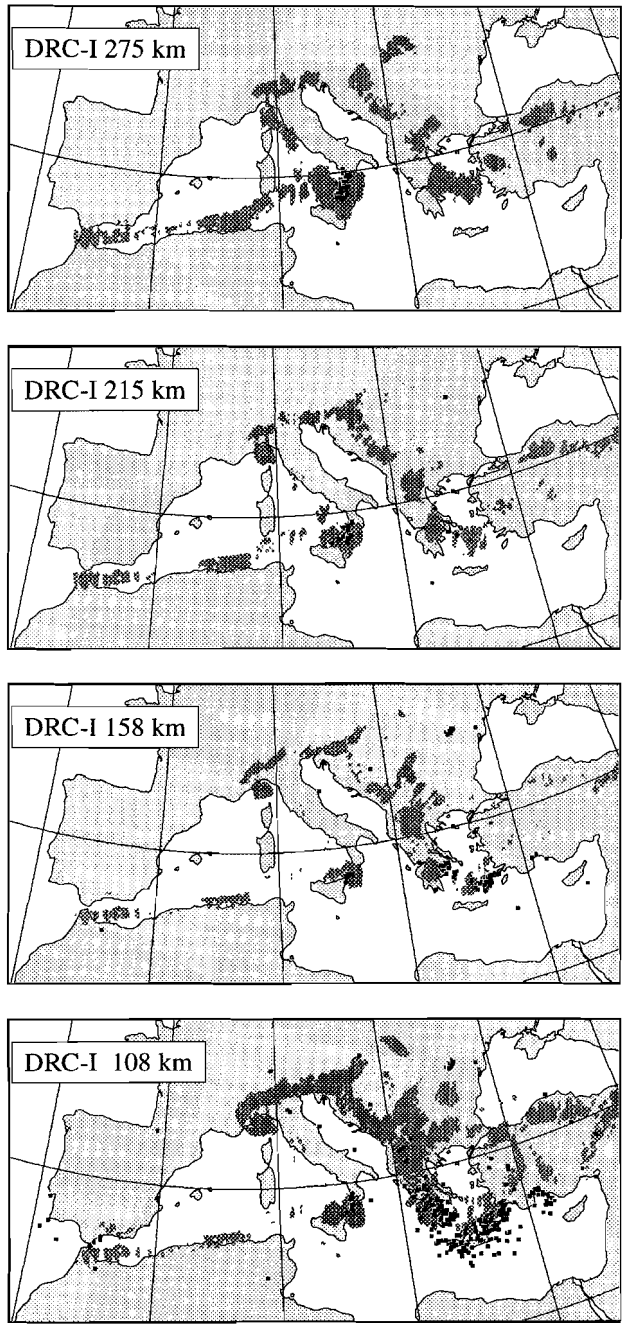

Figure 2. Present modelled temperature: grey shading below 75% of the ambient mantle (or below 750°C). Black squares denote seismic events from the ISC-catalogue.

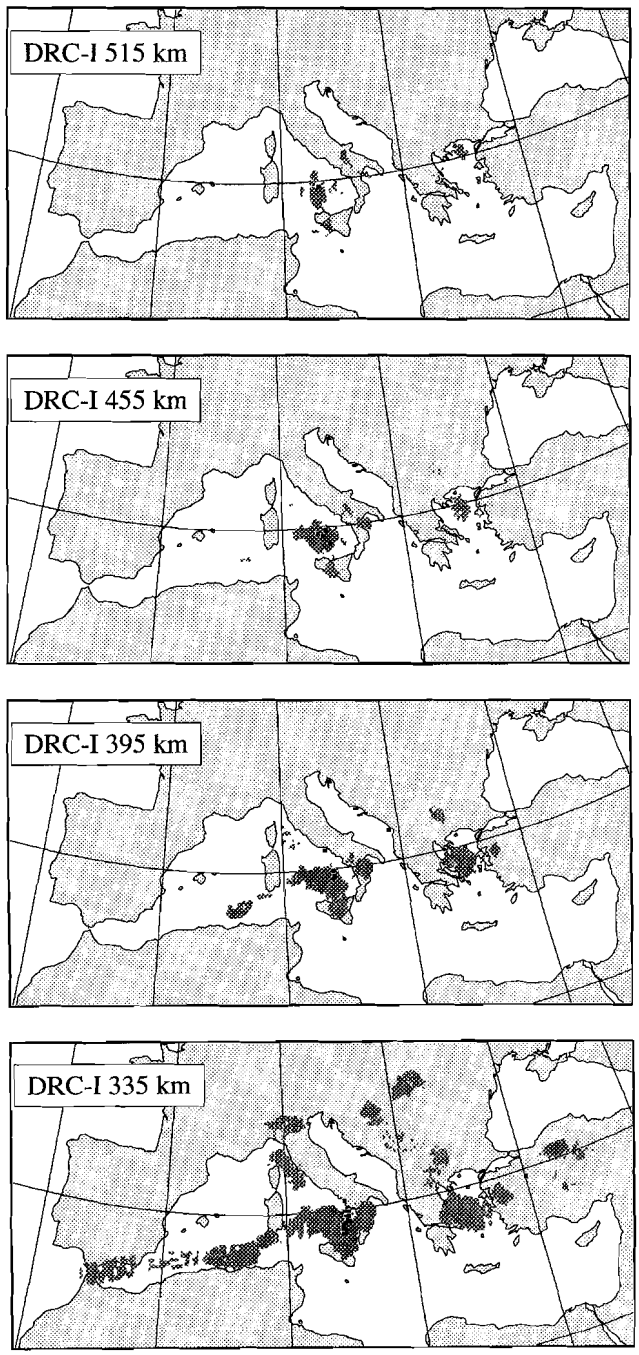

Figure 2. Continued from previous page.

References:

Dercourt, J., L. P. Zonenshain, L.-E. Ricou, V. G. Kazmin, X. Le Pichon, A. L. Knipper, C. Grandjacquet, I. M. Sbortshikov, J. Geyssant, C. Lepvrier, D. H. Perchersky, J. Boulin, J.-C. Sibuet, L. A. Savostin, O. Sorokhtin, M. Westphal, M. L. Bazhenov, J. P. Lauer, and B. Biju-Duval, Geological evolution of the Tethys from the Atlantic to the Pamirs since the Lias, in *Evolution of the Tethys*, edited by J. Auboin, X. Le Pichon, and A. S. Monin, *Tectonophysics, 123*, 241-315, 1986.

Dercourt, J., L.-E. Ricou, S. Adamia, G. Császár, H. Funk, J. Lefeld, M. Rakús, M. Săndalescu, A. Tollman, and P. Tchoumachenko, Anisian to Oligocene paleogeography of the European margin of Tethys (Geneva to Baku), in *Evolution of the Northern margin of the Tethys: The results of IGCP project 198*, edited by M. Rakús, J. Dercourt and A. E. M. Nairn, *Mém. Soc. Géol. Fr., 153(III)*, 159-190, 1990.

Chapter 3

Forward models for the seismic velocity structure of the Alpine-Mediterranean region†

But as for certain truth, no man has known it,
Nor will he know it ; neither of the gods,
Nor yet of all the things of which I speak.
And even if by chance he were to utter
The final truth, he would himself not know it;
For all is but a woven web of guesses.
Xenophanes, Frag. 34, ca. 500 B.C.

Abstract. We present a numerical modelling approach, designed for the verification of tectonic reconstructions and for a quantitative analysis of the seismic velocity structure of the lower lithosphere and upper mantle. In this forward modelling procedure we use published reconstructions of the tectonic evolution of a region to predict the thermal structure, from which we calculate physical quantities like *P* wave velocity, basin subsidence and basement heat flow. We show an application of this approach to two reconstructions of the late Mesozoic and Cenozoic evolution of the Mediterranean region. The resulting synthetic velocity models are tested against seismological models of the mantle structure, obtained independently by delay time tomography. Subsidence and heat flow predictions are compared with actual observations to further constrain the geological assumptions underlying the forward models. The mantle models predicted from reconstructions of the evolution of the Mediterranean region correlate with major features in the tomographic images. From our model results we conclude that the present distribution of seismic velocities in the Mediterranean region is largely determined by the tectonic evolution during at least the last 40 m.y. This means we can verify processes represented in different tectonic scenarios with the seismologically determined velocity structure. Seen from a different perspective, the model results contribute to understanding the causes of the velocity structure imaged by delay time tomography by showing how the tectonic evolution results in this structure.

---

† This chapter has been published without the footnotes as: M. R. de Jonge, M. J. R. Wortel, and W. Spakman, Regional Scale Tectonic Evolution and the Seismic Velocity Structure of the Lithosphere and Upper Mantle: the Mediterranean Region, *J. Geophys. Res.*, *99*, 12,091-12,108, 1994.

3.1 Introduction

As demonstrated by De Jonge and Wortel [1990] and Richards and Engebretson [1990,1992] it is possible to predict the thermal structure of the mantle by making use of existing tectonic (in geological literature often called paleogeographic) reconstructions. In this study we will describe and apply a modelling procedure with which we calculate the temperature distribution. From this we derive a synthetic P-wave velocity model using estimates of the temperature dependence of the seismic velocity. Thus, the procedure enables us to compare the kinematic implications of geological and geophysical field observations with results obtained by seismic imaging of the lithosphere and mantle. In this way we provide a connection between the present deep (seismic) structure and shallow (tectonic) evolution of a region. We will show an application

of this modelling approach for different tectonic reconstructions of the evolution of the Alpine-Mediterranean area. We choose to study this particular region for the following two reasons.

- The geological evolution of the Mediterranean region has been studied extensively, resulting in several detailed reconstructions of the tectonic history. Recent studies describing the evolution of this area are for example those by Dercourt et al. [1986], Gealey [1988], and Dewey et al. [1989]. These authors agree in general on the sequence of geological events that has led to the present structure of the Mediterranean region. Their conclusions, however, show differences in the relative magnitude and timing of the motion and internal deformation of plates and plate fragments. Since the reconstructions, based on a very wide range of observations, provide internally consistent (Alvarez [1991]), yet often differing evolutionary scenarios, it appears that the present geological data set lacks the resolving power to determine one unique scenario. Some old, no longer active, convergent margins are in fact almost impossible to reconstruct by usual geological methods because there is no information on the original size of oceanic basins that have long since disappeared. With our modelling we add an extra constraint on the reconstructions by providing a means to test them against the independently determined seismic velocity structure.
- For this region, we have an estimate of the present P-velocity structure from delay-time tomography [Spakman, 1988; Spakman et al., 1993; Blanco and Spakman, 1993]. These tomographic results describe the three-dimensional structure of the lithosphere and mantle from the surface down to a depth of 1400 km. The detailed tomographic models for the Mediterranean mantle structure constitute the independent reference against which we test our model results.

In this study we use our modelling approach as a tool for the verification of geodynamical hypotheses that describe the tectonic evolution of a region. We predict the impact of the evolution on the seismic structure and test the predictions qualitatively against tomographic results. This implies that we take

the image of the mantle presented by delay time tomography as a reasonable approximation of the actual structure. An alternative viewpoint is that one considers this method as an analysis of the causes of the complicated velocity structure of the upper mantle as shown in tomographic results.

Note that a positive correlation between tomographic results and our forward modelling supports both the processes we interpret from the tectonic reconstruction and the reliability of the modelling approach. Forward models with a good correlation between predicted and tomographically determined structures yield an important implicit result in the form of a detailed thermal evolution, which is simultaneously consistent with observations of surface geology and with tomographic results. We can use this to predict other thermally determined quantities which can be tested against data sets, independent of both the seismological information and the tectonic assumptions. Two quantities that we will discuss are the total basin subsidence and the observed heat-flow density.

3.2 Forward Modelling Procedure

The modelling procedure consists of a sequence of steps from a tectonic reconstruction via a kinematic model of material flow, and calculation of temperatures to geophysical quantities. At each of these stages errors may occur. When comparing the modelling results with observations it is therefore useful to discern the following three categories of errors:

1 *Incorrect tectonic reconstruction.* With this type of error the modelling procedure itself may be correct, but the tectonic evolution considered is not. An example of this type of error is the modelling of a non-existent subduction zone. If we only had to deal with these errors this would be ideal, because these errors enable the verification of different tectonic hypotheses.

2 *Incorrect modelling approach.* In this category we group errors and unjustified simplifications of the modelling procedure. In our models this type of error may occur when compositional differences at deep levels in the mantle do have an important effect on P-wave velocity or when the temperature P-wave velocity relation is very different from values estimated from laboratory data.

3 *Incorrect comparison data.* This comprises the errors in the reported geophysical quantities against which we test our, possibly correct, forward model.

All three types of errors can potentially produce a complete misfit between model results and reference. However, work by Spakman et al. [1991, 1993] shows that type 3 errors for the delay-time tomography are often not that severe: in well sampled parts of the studied region the tomographic results are accurately resolved. Still, in poorly sampled parts the imaging errors in the tomographic results can be so large that we will only concentrate on comparing them with our forward models in a qualitative sense (geometry, sign, and order

of magnitude). Evidently, the modelling approach is limited by the scale and the resolution of the tectonic reconstructions. This means we will only model features down to typical sizes of tens of kilometres where we consider them important for the structure of the lithosphere and mantle.

Two fundamental assumptions about the nature of mantle processes and the cause of the seismic velocity structure are made in our modelling approach. We will explain these assumptions explicitly because the validity of the method as presented depends strongly on them.

In the first place, we assume that surface-tectonic processes cannot be considered separately from processes in the underlying mantle. The tectonic processes that occur near the surface are an expression of a dynamic lithosphere-mantle system. Horizontal motions are necessarily accompanied by vertical material flow, if only on the grounds of conservation of mass. Given the existence of a vertical - not entirely adiabatic - temperature gradient, it follows that the mantle will show thermal perturbations which are directly linked to processes observed at the surface. In the model the principal processes we consider are convergence (which we associate with subduction) and extension, possibly resulting in ocean floor spreading (which we associate with upwelling of mantle material).

Secondly, we assume that the presently observed three-dimensional structure of seismic velocities in and below the lithosphere can be determined from the distribution of temperatures. We will not use the possible compositional differences or anisotropy to calculate the seismic velocity structure. Since this assumption does not hold for crustal depths, we cannot model the seismic velocities at these shallow levels.

With these two assumptions, our premise is that tectonic evolution is reflected in the form of seismic velocity anomalies. In the following sections we will describe the subsequent stages of the modelling approach that lead from a tectonic reconstruction to the accompanying synthetic three-dimensional velocity model.

Stage 1: constructing a displacement field from a tectonic reconstruction

The modelling begins with the transformation of information in a tectonic reconstruction into a kinematic description of lithosphere and mantle processes. This conversion consists of the determination of the evolution of relative convergence velocities across plate boundaries [De Jonge and Wortel, 1990] and of in-plate displacements that describe the lithospheric extension processes. We assess the velocities on the surface of the Earth by tracking the position of reference points, on both upper and lower plate in a subduction process, and by calculating their relative motion for every interval given in the reconstruction. The time span of the kinematic description must comprise the processes that determine the mantle structure. As an example of the relative convergence information Figure 1 shows three stages of the development computed for the migrating plate contact near Italy.

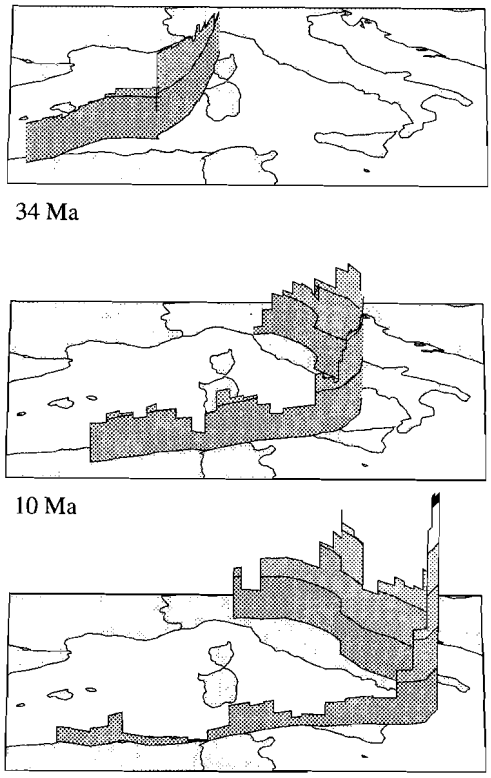

Figure 1. Evolutionary stages of the relative rate of convergence, perpendicular to the trench, according to the Dewey et al. reconstruction of the Tyrrhenian Sea. Height of the vertical bars denotes the velocity (shading at 1 cm/yr intervals), and horizontal position corresponds to that of the plate contact at the pertaining time.

Convergent plate boundaries. In the case of a convergent margin the vertical flow affecting the mantle is derived by assuming a subduction process that accommodates the convergence across the plate boundary during its evolution. Subduction is modeled in two dimensions for small segments of the plate contact (in a cross-section perpendicular to the margin in question) as a translation of lithospheric material along a predefined path into the mantle. This method is similar to that described by for example Minear and Toksöz [1970], Toksöz et al. [1971], Sleep [1973], Andrews and Sleep [1974], Toksöz and Hsui [1978], Hsui and Toksöz [1979], and Hsui et al. [1983]. Our modelling of subduction zones is a modification of these methods that allows for temporal variations in convergence rate. The reason for this modification lies in the fact that the relative velocities may vary from 0 to 7 cm yr^{-1} for a single plate

boundary during the evolution of the Mediterranean. To illustrate the effect of this, we show in Figure 2 the difference between three subduction zones that have the same cumulative relative convergence of 750 km. In this figure the top panels give the velocity development. There is only a small difference between figures 2a and 2b, while the time-averaged case of figure 2c clearly differs from the previous two; at depths of 200 to 400 km temperatures inside the subducted slab are 300 to 400 °C higher in the latter. From these cases we conclude that the convergence velocity changes we find in a tectonic reconstruction will have an effect on the final thermal structure. We can therefore not ignore them in our modelling.

The path followed by material descending into the mantle is controlled by the angle of dip of subduction. We have no direct information on this angle for the past evolution of the region. For parts of the Tyrrhenian and Hellenic subduction zones we can estimate the present dip angle from the outline of Wadati-Benioff zones (hypocentres from ISC catalogue). Usually, however, even the present dip angle of old subduction zones is not constrained by seismic observations because of the lack of seismicity. Furthermore, the complexity of the subduction zones in the studied region precludes a prediction of the exact geometry of the subducted slab (in less irregular settings such predictions may be more feasible: see Creager and Boyd [1991] for the Aleutian region as an example). Instead, we have tried to assess a realistic average value for the duration of the evolution of a subduction zone based on convergence velocity, average age, and composition of the subducted lithosphere. We take an angle ranging from 80° for old oceanic lithosphere and slow convergence down to 30 for very young oceanic or continental lithosphere. For a discussion of this lithospheric age dependence of slab dip we refer to Wortel and Vlaar [1978, 1988].

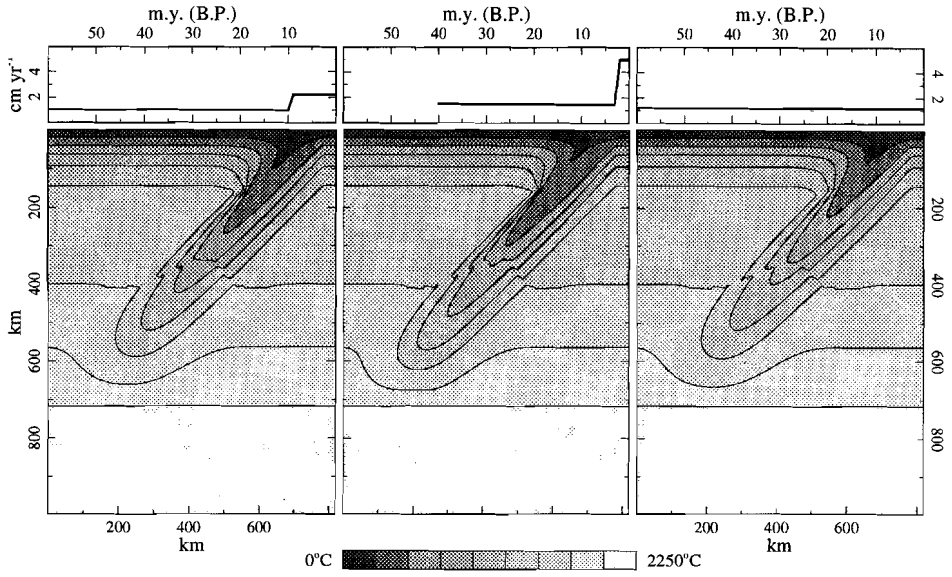

Figure 2. The effect of convergence velocity development (top panels) on thermal structure (bottom panels). Total convergence for all three cases is 750 km. a) High convergence velocity during the last 10 m.y. b) High convergence velocity during the last 3 m.y. c) Constant rate throughout. The first two cases (Figures 2a and 2b) represent a typical example of the difference between the DRC-I and DRW models discussed in the following section. Figure 2c would result from modelling only the total relative displacement for the duration of the evolution

Intra-plate extension. In intra-plate extension processes the vertical component of motion is derived by modelling extension as a time dependent pure shear deformation. This is an adaptation of the stretching model proposed by McKenzie [1978]. We extend the lithosphere to the amount required by surface motion in the reconstruction and we allow asthenospheric material to flow in from below to maintain a mass balance. For extension modelling the difference between a time-dependent velocity evolution and an averaged velocity becomes very important because quantities like surface heat flow density are strongly controlled by the most recent phases of the development.

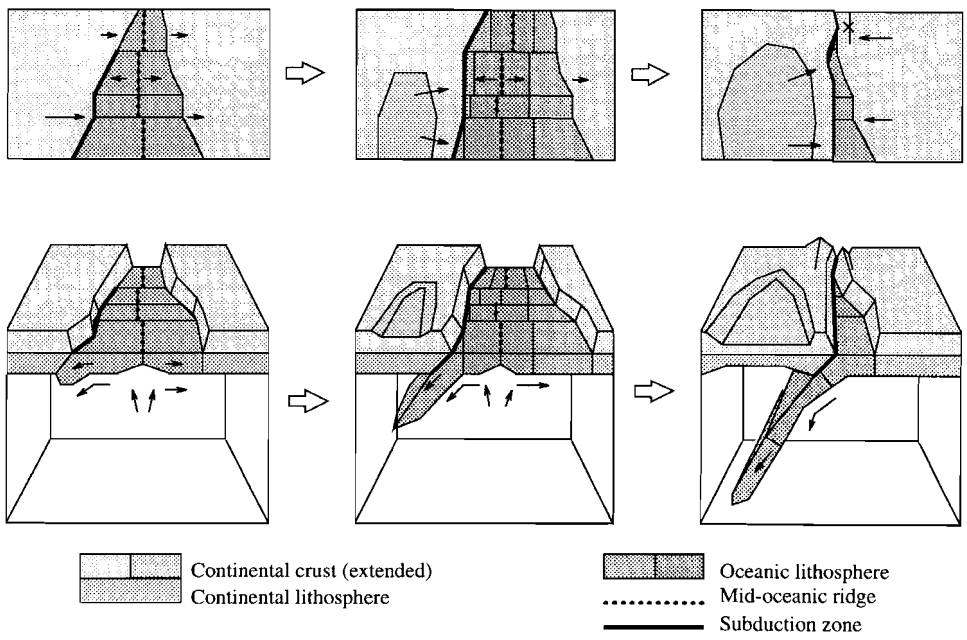

Figure 3. Schematic representation of the parameters and processes derived from the tectonic reconstructions. Plate kinematics in map view, with development from left to right, in the top panels. modelled corresponding mantle and lithosphere processes in the bottom panels.

Figure 3 summarizes the general concepts that we use to translate the tectonic reconstructions into the vertical velocity information required for further calculation. In this figure the top panels show simplified maps at three stages in the evolution, while the bottom panels show the corresponding mantle processes. The features in this figure that determine the thermal structure are (more or less in decreasing order of importance for the thermal model):

- position of subduction zones as a function of time,
- rate and direction of relative motion as a function of time,
- time of formation of lithosphere at mid-oceanic ridges,
- composition and initial thickness of continental lithosphere,
- timing and magnitude of extension processes.

We expect that the processes mentioned above will be able to produce most of the thermal structure of the lower lithosphere and upper mantle.

Stage 2: thermal model

We treat the determination of the development of the thermal structure of the mantle as an initial value convection-diffusion problem. The convective processes are given by the explicit flow field of the kinematic model described

above. The initial structure is also based on the tectonic reconstruction in the following manner:

Initially oceanic regions. When at the start of the modeled period oceanic lithosphere is present, the thermal structure is approximated by a cooling half-space with physical parameters for olivine. The time of formation of this lithosphere (derived from the tested reconstruction) controls the thermal age of this half-space. The possible contribution of a sedimentary cover is ignored in the determination of this initial structure.

Initially continental regions. In continental regions we approximate the initial structure by a standardized steady-state continental model. This structure consists of a crustal part, with a top layer of granitic and a bottom layer of dioritic composition and heat production, overlying a mantle part with a peridotite-eclogite composition [Rybach, 1987]. The thickness of the continental crust, before stretching or thrusting events have altered it, is estimated with data for unperturbed adjacent crustal thicknesses [Meissner, 1978] and from information in the tectonic reconstruction.

Initial mantle structure. For the material parameters in the deeper mantle part of the model we use an average olivine composition (94% Forsterite, eg. Schatz and Simmons [1972]). The thermal gradient is an adiabat for this composition. This gradient is only added after calculations with the 'potential temperature' [McKenzie, 1969; 1970]. In this way we can simply account for the adiabatic temperature rise with depth in both the subducted lithosphere and the surrounding mantle. The mantle geotherm also includes the contribution of the olivine phase transition near 400 km. This phase transition is approximated by an instantaneous fixed temperature rise of 150°C (between values reported by Bina and Wood [1987] and Turcotte and Schubert [1986]) if the material crosses the temperature dependent critical depth.

Thermal development of initial structures. We use the kinematics derived from the reconstruction to model material flow by (discrete) translation of the initial structure in small time steps (0.1 to 0.5 Myr) for the entire period of the tectonic evolution.

The thermal structure is derived for every time step by calculating the thermal diffusion. This is done by numerically solving the equation:

$$\frac{dT(\bar{x},t)}{dt} = \frac{1}{\rho C_p}\nabla\cdot\left(k(\bar{x},t)\nabla T(\bar{x},t)\right) + \frac{A}{C_p}$$

$$\approx \frac{k}{\rho C_p}\nabla^2 T(\bar{x},t) + \frac{A}{C_p} \qquad (k \text{ constant})$$

where: k= thermal conductivity, ρ= density, C_p= specific heat, and A= radiogenic heat production (which is used only in the crustal levels of continental lithosphere).

This differential equation is solved using an Alternating Direction Implicit (A.D.I.) finite difference method [Douglas, 1955, 1957; Peaceman and Rachford, 1955; Fairweather and Mitchell, 1967; Mitchell, 1969; Ames, 1977]. For the

boundary conditions used (an adiabatic temperature gradient through the bottom of the model, no heat flow through the sides, and a fixed temperature at the top) it is as accurate as for example a standard two-dimensional Crank-Nicholson operator.

Time-dependent three-dimensional temperature structure. The two-dimensional results (vertical sections spaced at 20-50 km intervals) are combined into a three-dimensional model after the thermal diffusion is evaluated. This approach has the disadvantage that possible heat loss out of the plane of the vertical sections is ignored. We expect that especially high-curvature structural features may be more accurately represented if the possibility of net lateral heat flow into, or out of a cross section is incorporated. Future developments will include the full three-dimensional modelling for those geometries.

Stage 3: from model temperature to geophysically observable quantities

The final stage of the thermal evolution - the present synthetic temperature structure of the mantle and lower lithosphere - can be compared with observations, although not directly; first we need to convert this model result to geophysically verifiable quantities. In this study we will address three possible conversions which are discussed below.

Seismic velocity perturbations. To convert the thermal structure to P-velocity perturbations we estimate a depth dependent temperature derivative of V_p. For this we use the elastic parameters of olivine in the following fashion. For the p-wave velocity we take:

$$V_P = \sqrt{\frac{K+\frac{4}{3}\mu}{\rho}} \quad \text{This yields for } \partial V_p/\partial T$$

$$\frac{\partial V_p}{\partial T} = \frac{1}{2V_p\rho}\left[\frac{\partial K}{\partial T}+\frac{4}{3}\frac{\partial \mu}{\partial T}+\alpha\left(K+\frac{4}{3}\mu\right)\right. \qquad 1)$$

where ρ= density, T=temperature, V_P= P-wave velocity, K=bulk modulus, and μ=shear modulus. The expansion coefficient α is given by:

$$\alpha = -\frac{1}{\rho}\frac{\partial \rho}{\partial T}.$$

We evaluate Equation 1 for several (extrapolated or measured) values of the elastic parameters at different temperatures and pressures. Assuming that Equation 1 holds at mantle conditions in the range that we are studying (the non-linearity of this equation near the solidus warrants caution in this respect) we arrive at a range of possible values shown in Figure 4. The calculations of the synthetic V_p structure are based on the average values denoted by the thick line. Seismic velocity anomalies (ΔV_p, not the actual velocity V_p) can now be calculated for every cell in the modeled volume using:

$$\Delta V_p = \frac{\partial V_p}{\partial T}_z [T - \bar{T}(z)] \qquad \textbf{2)}$$

In this expression $\bar{T}$ denotes the average (an estimate for the unperturbed) temperature at depth z. Note that both Equation 1 and 2 are only approximate, as $\partial V_p/\partial T$ is considered as a function of smoothly varying elastic parameters with depth, whereas in fact it is highly non-linear and depends on temperature and pressure. In a more sophisticated model one could consider including a more accurate description, but this is at present hardly warranted in view of the up to 100% differences between the available extrapolated laboratory data.

An important effect that follows from our depth-dependent $\partial V_p/\partial T$ is the decrease with depth observed in the temperature sensitivity of the mantle velocity structure. The right panel of Figure 4 illustrates this effect: the relative velocity anomaly as a result of a 100 °C low-temperature anomaly is shown for different depths. One can observe that the velocity perturbation resulting from a fixed thermal anomaly is four times smaller at the base of the model than at the top. This effect is also important for seismological observations: it implies that the velocity variations in the mantle will decrease with depth, even when subducted material would not heat up by thermal diffusion during its descent.

Thermal subsidence and heat flow density. We derive from the thermal model two other parameters: the thermal subsidence and the basement heat flow. We calculate the subsidence by requiring a constant pressure at a given 'compensation' depth as a result of the temperature and composition dependent density of a vertical column. In this model we take the compensation depth at 200 km from the (initial) top of the model. The total subsidence is obtained by incrementing the (water loaded) isostatic subsidence at every time-step. This synthetic cumulative subsidence can be compared with back-stripped stratigraphic data.

We calculate the basement heat flow density from the temperature gradient across the top layer (in the final stage of the thermal model) and the thermal conductivity of the crust at a given point. This quantity is strongly controlled by relatively shallow processes occurring during the extension of lithosphere. In both heat flow and subsidence calculations the contributions of a possible sedimentary cover or erosion have been ignored.

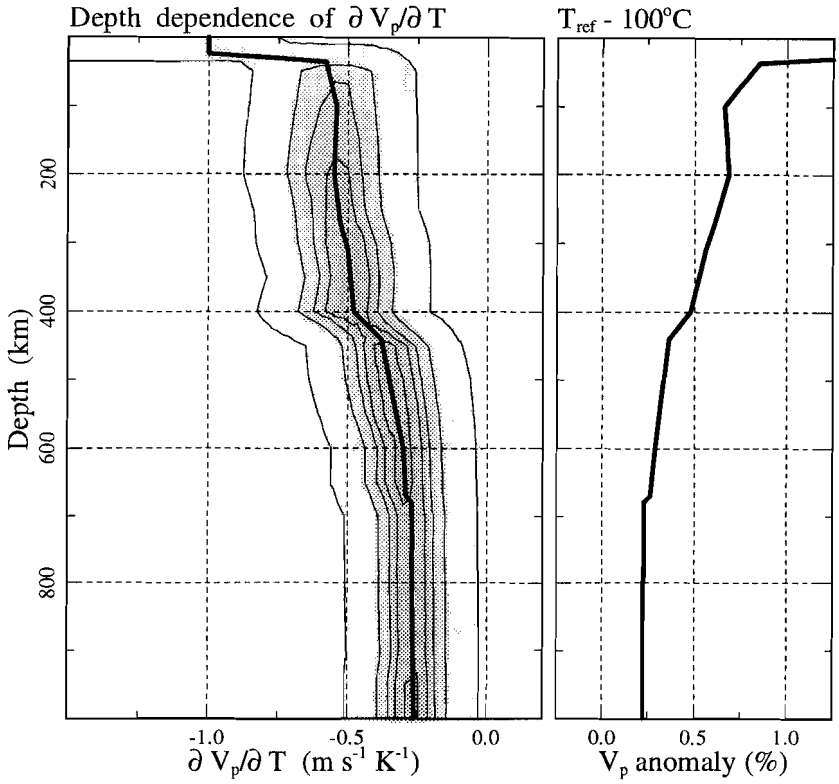

Figure 4. The left panel shows depth dependence of P velocity sensitivity to temperature: the grey area denotes the range, and the thick line the values used. Results obtained by a Monte Carlo evaluation of (extrapolated laboratory) results from Graham and Barsch [1969], Mizutani et al. [1970], Chung [1971], Anderson et al. [1972], Wang and Simmons [1972], Suzuki [1975], Sumino et al. [1977, 1983], Dziewonski and Anderson [1981], Suzuki et al. [1981, 1983], Turcotte and Schubert [1982], Sawamoto et al. [1984], Weidner et al. [1984], Bina and Wood [1987], Isaak et al. [1989], and Gwanmesia et al. [1990]. The right panel shows how the velocity anomaly that would result from a 100°C lower temperature decreases with depth (in percent of the ambient P velocity).

3.3 Application to the Evolution of the Mediterranean Region

We have selected two tectonic scenarios to which we apply our modelling approach: the reconstruction by Dercourt et al. [1986] and that of Dewey et al. [1989]. These tectonic reconstructions are not always uniquely interpretable; for the Dercourt et al. [1986] work we have made some supplementary assumptions, leading to two alternative models. As a result we predict three

possible mantle models based on two tectonic reconstructions.

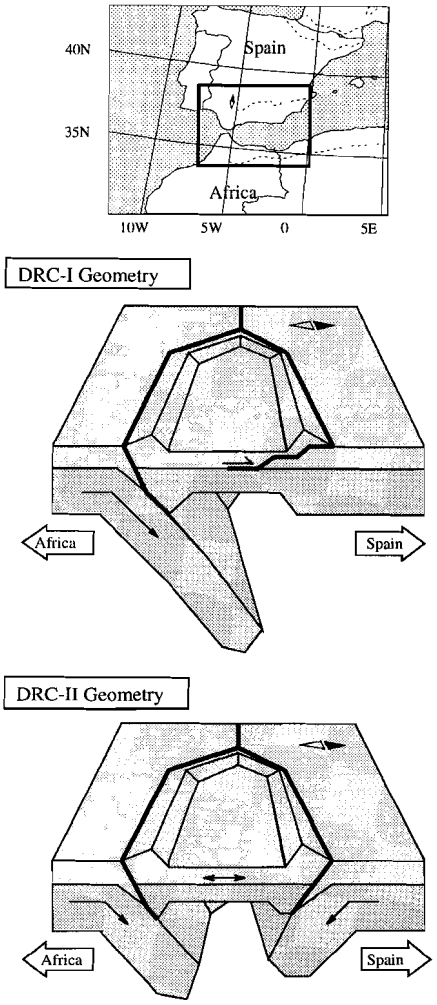

Figure 5. Possible interpretations of the geometry of the plate contact for the Alboran region. (see location map). Top panel, DRC-I model with a single subduction zone; bottom panel, DRC-II model with two oppositely dipping slabs.

The first two synthetic models, 'DRC-I' and 'DRC-II', are both based on the work by Dercourt et al. [1986]. In this reconstruction the evolution of the Tethys area is described in the form of a sequence of generalized tectonic maps which span a period of 150 Myr. We use the displacement during the last 110 Myr in this reconstruction with a modification for the Hellenic arc region (see Figure 7 for geographic names). In the Dercourt et al. [1986] work subduction at the Hellenic trench system begins in the Tortonian, preceded by a thrusting phase in which the precise nature of the plate contact is unspecified. In the modelling, however, we assume that this pre-Tortonian thrusting phase is also an expression of a subduction process. Note that this interpretation is not explicitly given in the tectonic reconstruction, but is based on geometrical arguments. It appears that there is not enough space available to allow for the pre-Tortonian Africa-Europe convergence of hundreds of kilometres without some subduction. The Dinaride-Hellenide thrust belt is, in our opinion, the most likely place for this subduction to occur. Conclusions from more recent work by Mercier et al. [1989] corroborate this modification.

Because of other uncertainties in our interpretation of the Dercourt et al. [1986] reconstruction, we will consider for the Alboran region two possible large scale plate configurations with the same surface expression. The model DRC-I is calculated assuming that the convergence at the plate boundary between Spain and Africa is accommodated at a single subduction zone with a large strike-slip component in the relative motion. With this interpretation the Betic Cordillera is formed

by shallow (on the model scale) processes not significantly influencing the deeper lithosphere and mantle. This configuration is similar to the one suggested by Biju-Duval et al. [1977].

An alternative for the evolution of the Alboran is evaluated in the DRC-II model in which we calculate the effect of two oppositely dipping slabs in the region. This is a direct translation of the tectonic evolution that is presented by Dercourt et al. [1986]. In figure 5 the geometrical difference between the two models is depicted.

The third model 'DRW' is based on the reconstruction presented by Dewey et al. [1989]. Whereas this reconstruction covers a smaller part of the Mediterranean (from Spain to Italy) and a shorter period (38 My), it shows more detail in both space and time. For the DRW model we did not need to make extra suppositions about the inter- and intra- plate kinematics implicit in the tectonic reconstruction. The volume of the model that is not covered by the tectonic reconstruction (Figure 6) is supplemented by results from the DRC-I model to facilitate comparison with the other images.

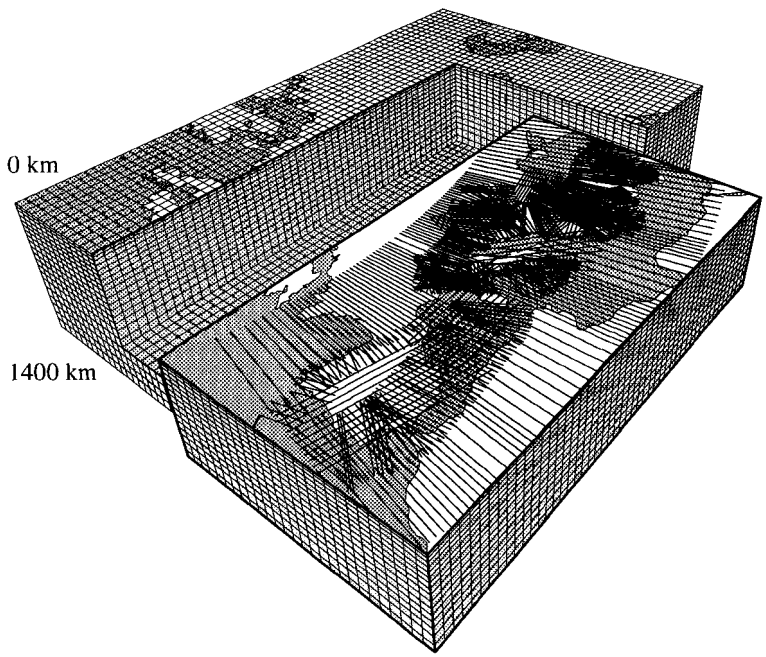

Figure 6. Cell model used for tomography (whole volume), lines on top of model are the traces of the two-dimensional sections evaluated for the DRC-I model (block inset). The data unique for the DRW model have almost the same distribution but are confined to the Thyrrenian Sea region. Cell size of the tomographic results is 0.8°x0.8° horizontally (approximately 90x90km) and 33 to 100 km vertically. Along-section resolution of the forward models is better than 10x7.5 km.

Synthetic mantle models

To compare our predicted mantle structure to that obtained with tomography we project the synthetic structure on the cell model that is used for the tomographic results of Spakman et al. [1993] (cells of figure 6). The grid has horizontal cell sizes of 0.8° and vertical sizes ranging from 33 km in the top layer to 100 km at the bottom. The reduction of detail of the synthetic models to that of the tomographic results means we lose some information present in our predicted velocity structure. However, it is this projected synthetic structure we expect to find in an ideal tomographic experiment when we correctly predict the mantle structure.

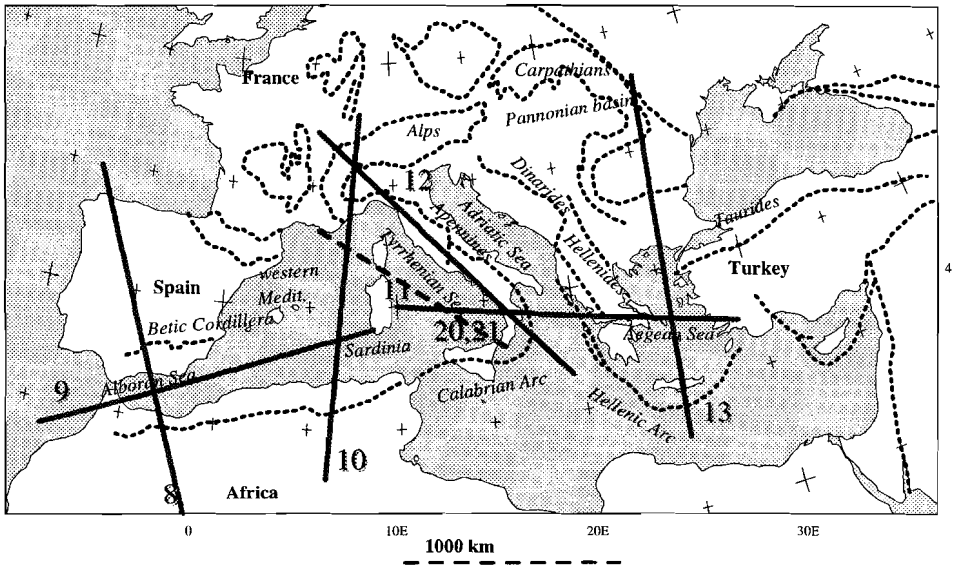

Figure 7. Location map of the study area. Main structural features are shown with dotted lines. Numbers and thick lines indicate the vertical cross sections through the models shown in Figures 8 to 13. The thick dashed line indicates the line of section for Figures 20 and 21.

Comparing the Dercourt et al. [1986] models: DRC-I and DRC-II. The effect of the geometrical difference between the DRC-I and DRC-II models is best investigated in vertical cross sections through the 3-D structure (for the location of these cross sections, see Figure 7). Figures 8 and 9 (page 74) show the synthetic structures across and along the main trend of the plate contact in the Alboran region. For later comparison the bottom panels of these figures show the image of the mantle obtained by seismic tomography. The dots in the figures denote earthquake hypocentres taken from the ISC-catalogue.

In Figures 8 and 9 the thermal calculations result in a only relatively small geometrical difference between the single slab DRC-I and the double slab DRC-II models. The reason is that the convergence on the northern subduction zone (of the Betic Cordillera) in the DRC-II model is so small and it has occurred so long ago (Oligocene) that a slab signature at the cell model resolution has merged with the surrounding structure. The synthetic structure of the mantle is dominated by the compositional difference between the continental and oceanic lithosphere and a diffuse remnant of the subduction of the African margin. More rapid convergence on the African side in the DRC-I model does result in a deeper reaching and more pronounced anomaly. The apparent decoupling of the subducted lithosphere from the surface on this margin is a result of modelling crustal material (with a high radiogenic heat production) in the topmost part of the subduction zone.

In the subsequent cross-sections we will show the effects of more recent phases of the development and of more pronounced kinematic differences by comparing the DRC-I results to results based on the DRW kinematic model.

A different evolution: The Dewey et al. [1989] based model DRW. For the western and central part of the Mediterranean the DRW model provides an alternative prediction of mantle structure. Figure 10 (page 76) shows a section located east of that of Figure 8, running from Algeria to the Alps. In this section, the extent of the high velocity region that results from subduction of the African plate is larger for the DRC-I model than for the DRW model. This results from the different evolution of Africa-Europe convergence in the underlying reconstructions: in the DRW model more of the motion is concentrated in the Apennine belt, while for DRC-I more convergence occurs at the African-Tyrrhenian margin. The high seismic velocities in left-hand side of the upper two sections of Figure 11 are an oblique section through the predicted Tyrrhenian slab. This high velocity region extends from the Calabrian arc down to a depth of 700 km. There is not a large difference between the DRC-I and DRW models as both reconstructions give approximately the same kinematics for the outward migration of the Calabrian arc. It is important to recall that the structure in the DRW model is determined from the evolution of the Mediterranean during only the last 38 My. The strong resemblance of DRC-I and DRW in this region therefore implies that here mantle structure is controlled by the later stages of the evolution. In this figure the high velocity structure on the right is an oblique section through the Hellenic slab (based on the DRC-I model in both synthetic images)

Figure 12 shows a section along the strike of the Apennines. For this section the predictions of the DRW model and those of the DRC-I model are clearly different. In the former a contiguous deep high velocity anomaly is modeled along the entire length of the Apennines, whereas the latter exhibits a distinctive vertical break between the high velocity structure below Calabria and the Northern Apennines. The cause of this difference is the same difference in convergence velocity as mentioned for Figure 10.

Finally, Figure 13 shows a cross-section of the Hellenic trench system; this part of the model is controlled entirely by the Dercourt et al. [1986] reconstruction supplemented with our assumption on pre-Tortonian subduction, as the evolution of the Hellenide margin is not included in the Dewey et al. [1989] work.

(continued on page 80)

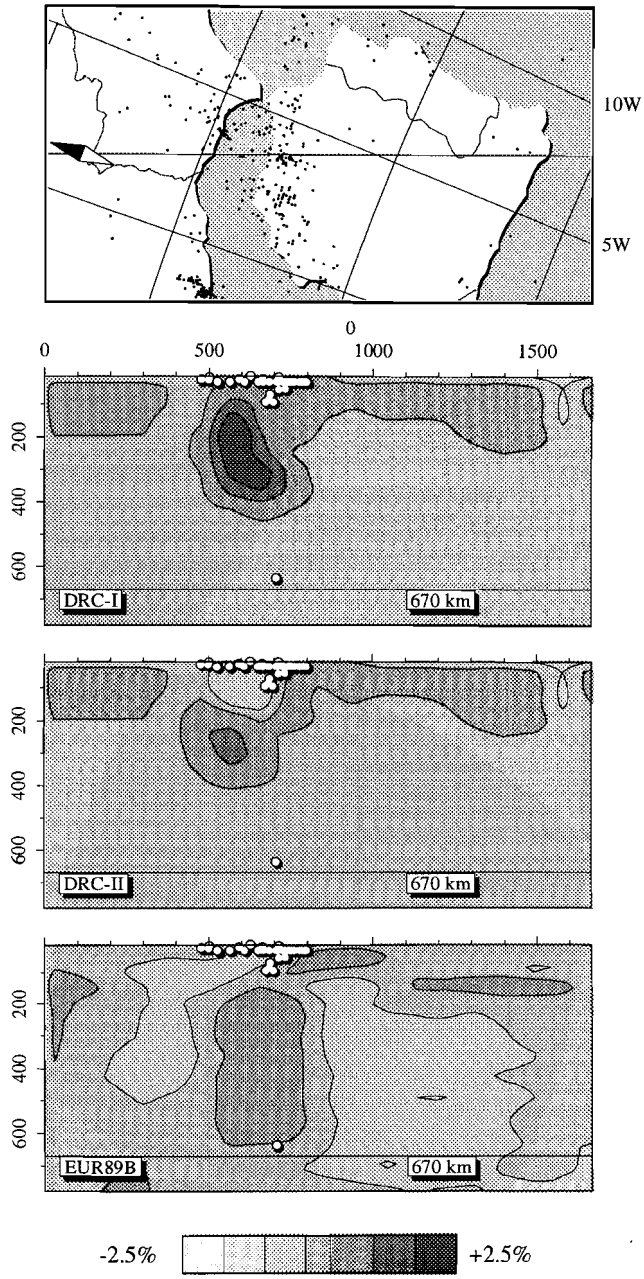

Figure 8. Vertical cross section perpendicular to the main trend of convergence in the Alboran region, through the synthetic (DRC-I and DRC-II) models and the seismic velocity structure imaged with tomography (EUR89B). Section location is shown in Figure 7. Circles denote recent seismicity, as given in the ISC catalogue.

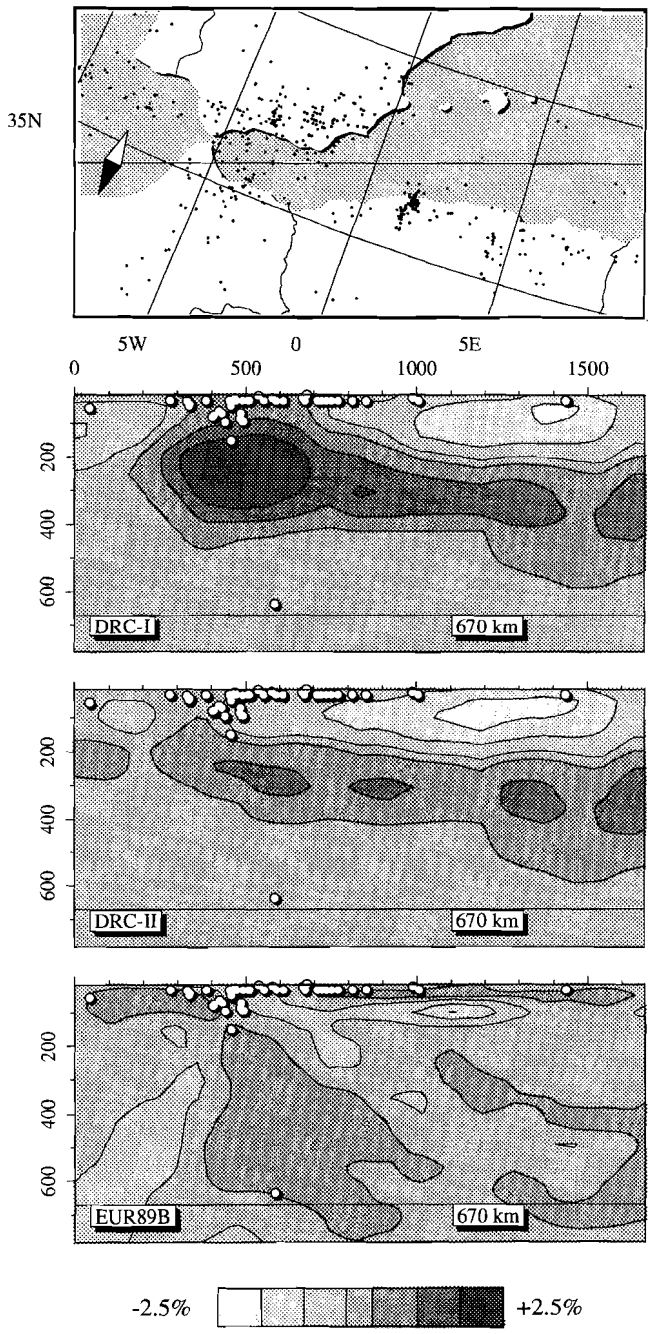

Figure 9. Vertical cross section parallel to the main trend of convergence in the Alboran region and perpendicular to Figure 8. Section location is shown in Figure 7.

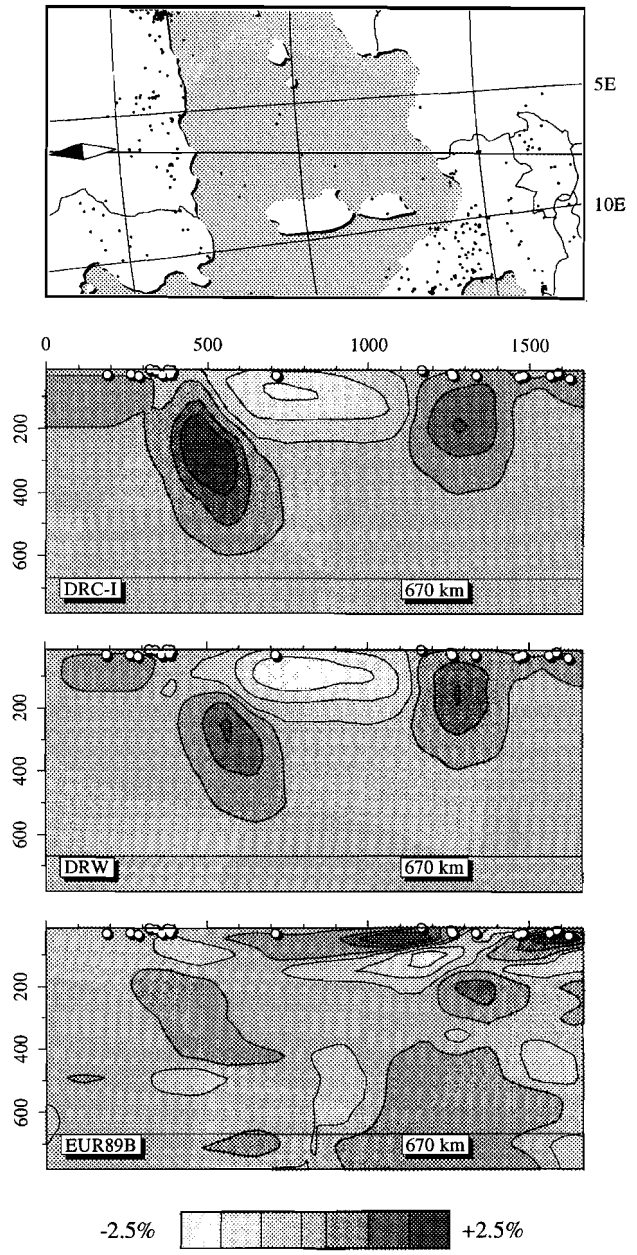

Figure 10. Vertical section crossing the Mediterranean from Algeria to Switzerland. The top panel is the synthetic model DRC-I, based on the *Dercourt et al.* [1986] reconstruction. The middle panel shows the DRW model, derived from the *Dewey et al.* [1989] work. The bottom panel shows the tomographic image. Section location is shown in Figure 7.

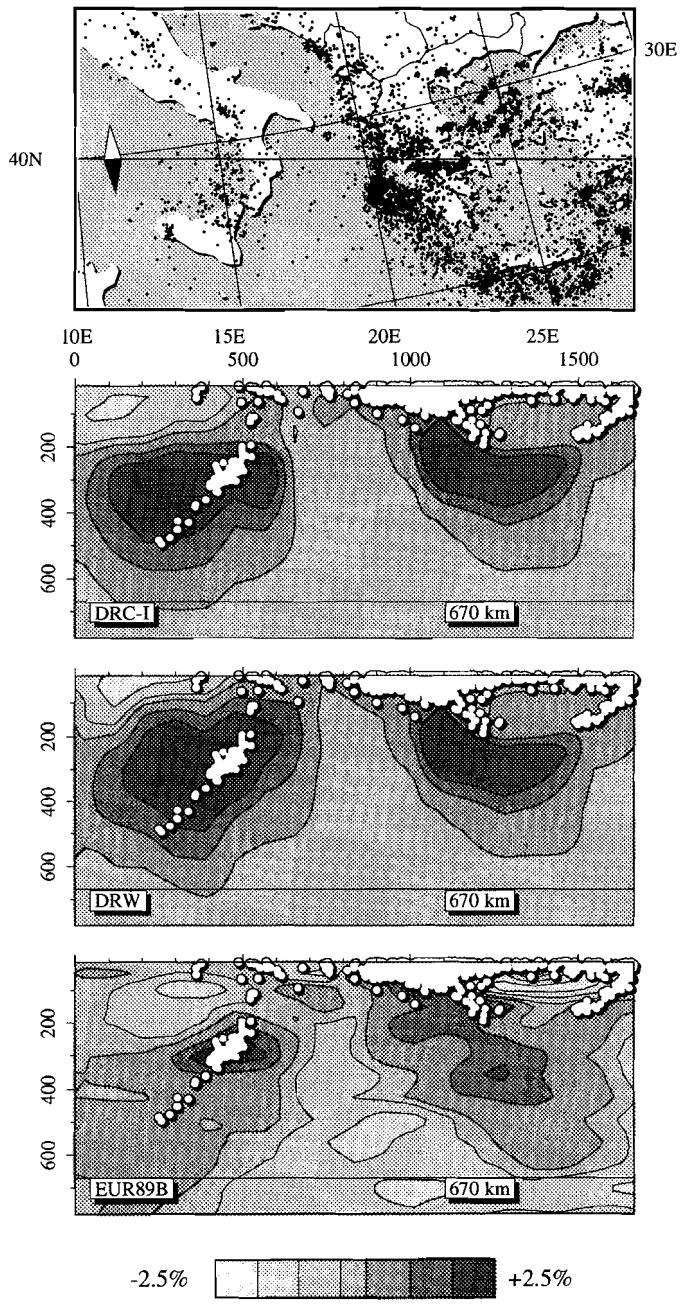

Figure 11 Vertical sections crossing both the Tyrrhenian (left) and Hellenic (right) subduction zones. The same models as in Figure 10 are shown. Section location is shown in Figure 7.

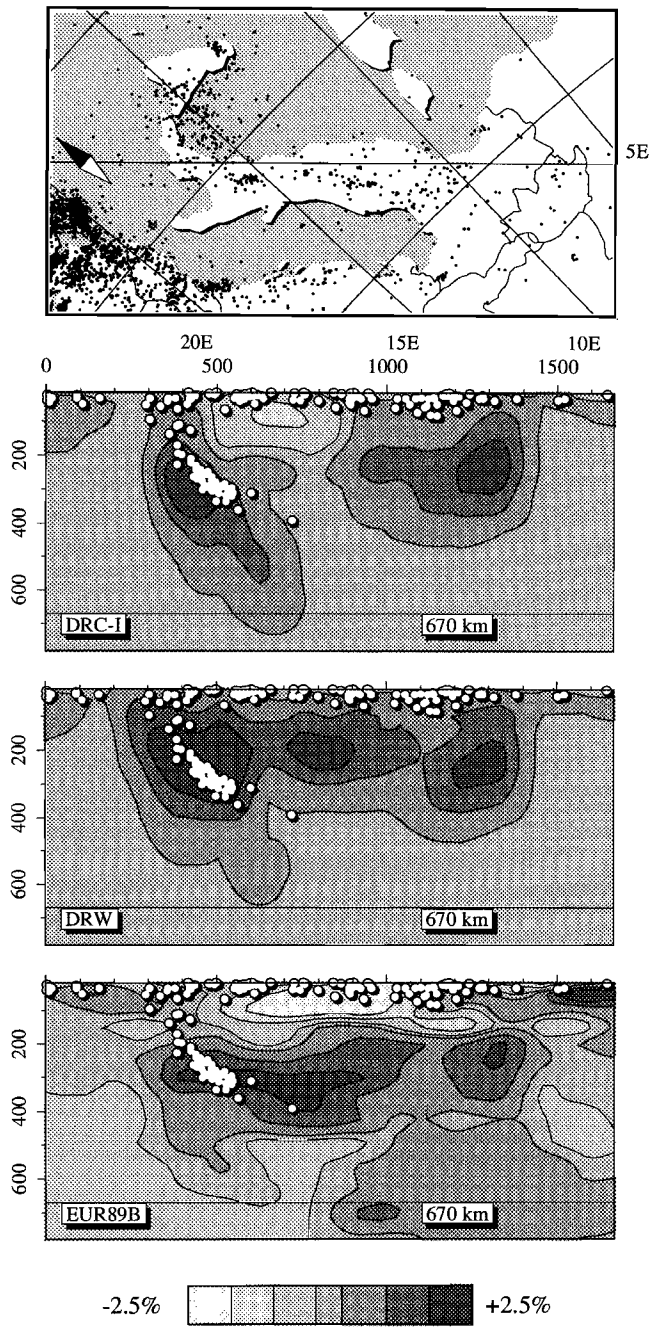

Figure 12. Section along the strike of the Apennine plate boundary. Section location is shown in Figure 7.

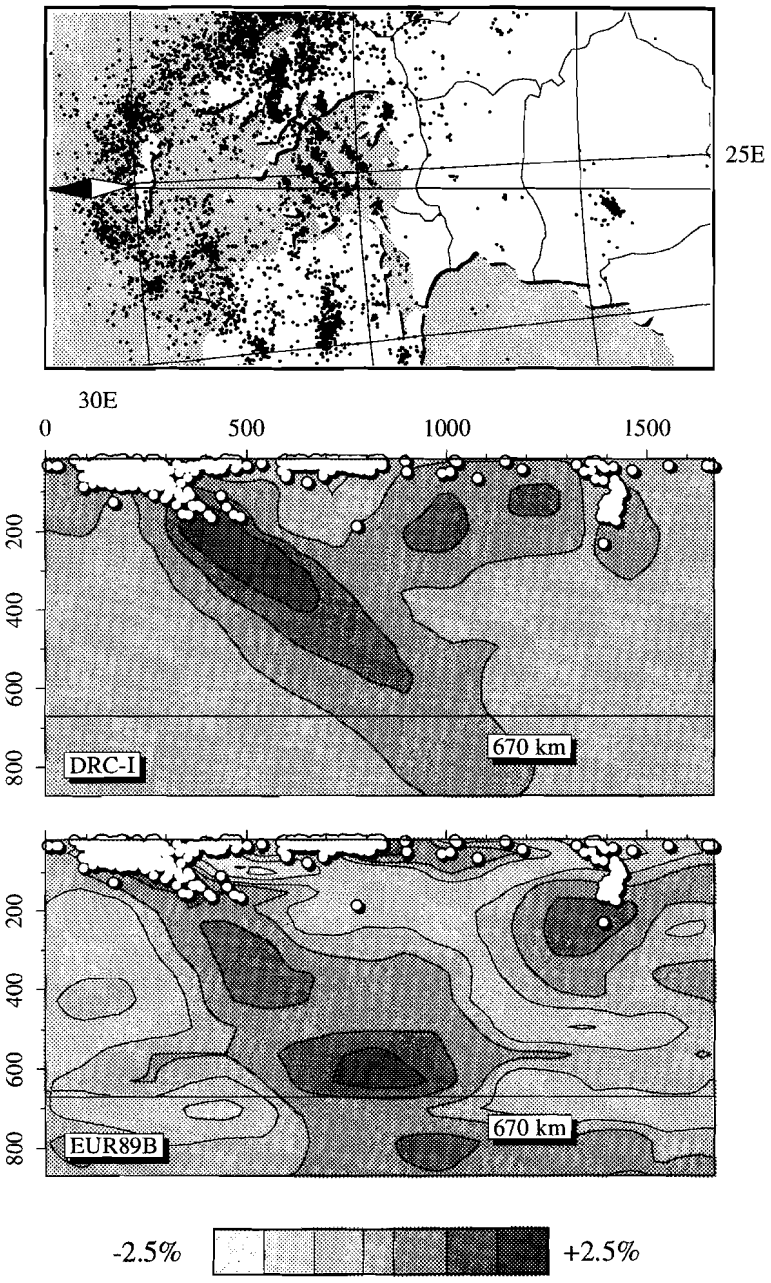

Figure 13. Section across the Hellenic trench; because data are only available in the reconstruction given by *Dercourt et al.* [1986] the DRW model is identical. Section location is shown in Figure 7

3.4 Comparing the synthetic velocity structure and tomographic results

In this section we will address the differences between the synthetic velocity structures and the tomographic results. At present, we will restrict ourselves to a qualitative comparison of the larger scale features observed in the synthetic models and the tomographic results. The reason for doing this is the fact that the tomographic analysis has its own type of errors, which may result in underestimating the amplitude of mantle anomalies actually present and in imaging artifacts related to lack of spatial resolution. A more quantitative analysis that also comprises the tomographic imaging problems is in preparation[†].

Vertical Sections.

The modelling results for the mantle in the Alboran region (Figure 8) exhibit a structure that is distinctly different from that imaged with tomography. For this particular region Blanco and Spakman [1993] have demonstrated that a subducted slab with spatial dimensions comparable to that shown in the bottom panel of Figure 8 can explain the tomographic results. They also demonstrated that a subducted slab with high velocities up to the surface could be resolved. Therefore, we are inclined to conclude that the modelling approach contains some error for this region. Whether this error resides in the kinematics (type 1) or in the model calculations (type 2) is uncertain. At present, the inability to reliably determine what type of error we make for this region means we cannot decide between the two possible geometries of the DRC-I and DRC-II (figure 4) interpretation.

The tomographic image below the African margin of the Western Mediterranean (Figure 9, right hand side and Figure 10) is considered poorly resolved in the tomographic results (type 3 error), so a comparison cannot be made directly. The sections more to the east generally show a better fit between tomographic and synthetic results. The patterns of the high velocity regions associated with the Tyrrhenian and Hellenic subduction zones shown in Figure 11 and 13, and the high velocity structure below the Apennines and Alps in Figure 12 agree spatially to within a few cells with the tomographic results. The amplitudes of velocity heterogeneity in the predicted structure are generally larger. In Figure 12 the better correlation of the DRW model with tomographic results for the deeper subducted lithosphere leads us to conclude that the large-scale plate motions may be better represented in the Dewey et al. (1989) reconstruction.

Horizontal sections.

In the following figures we will show horizontal slices through the models. We primarily address the comparison with tomographic results where the spatial resolution (as discussed by Spakman et al. [1993]) is sufficiently high.

[†](Chapter 4)

The top panels depict the velocity anomaly based on the DRW model. The rectangle denotes the area covered by the Dewey et al. [1989] tectonic scenario. The middle panel shows the velocity anomalies based on the Dercourt et al. [1986] reconstruction (DRC-I hypothesis: a single slab in the Alboran). In the bottom panel we show the tomographic results (EUR89B) for the same depth.

95 km. Figure 14 shows the velocity structure at a depth of 95 km. One important difference between the DRC-I and the DRW model, is absence of a clear subduction at this level below the Apennines in DRC-I (despite its presence in the kinematic scenario). The reason for this is the lower time resolution provided in the DRC-I model (only two stages at 10 and 0 Ma). As a result, the (modeled) heat flow from the adjacent extensional area of the Tyrrhenian Sea (low velocity structure off the west coast of Italy) overprints the signature of subduction more strongly than it does in the DRW model (in which much of the extension is concentrated in the last 4 Million years). Neither of our synthetic models produces the marked velocity minimum (suggesting anomalously high temperatures) under the Apennines that is observed with P-wave travel times and also in S-wave studies [Panza et al., 1980; Panza, 1984; Snieder, 1988; Zielhuis, 1992].

The correlation between synthetic structure and tomographic results in other regions is better: the Hellenic-Dinaric system and the 'root' of the Alps are recognizable as high velocity structures in all panels. Low seismic velocities resulting from extension in the western Mediterranean and in the Aegean Sea are also present in both synthetic models. Although it must be remarked that the magnitude of the velocity perturbation for the latter region is less pronounced than in the tomographic results. This discrepancy is again most likely a result of the implicit averaging that takes place in the DRC-I model: the formation of the Aegean Sea occurred in the last few million years, but the tectonic reconstruction describes only two stages of this development (at 10 Ma and present).

195 km. Figure 15 shows a section at a depth of 195 km. A striking change with respect to the previous level is seen in all panels. The circum-adriatic high velocity belt and also the near parallel high velocity zones in Turkey, which were in the previous figure only present in the synthetic sections, now show up in the tomographic results. Along the North African margin the tomographic results exhibit a number of small positive velocity anomalies, which may well belong to a more continuous high velocity zone like the one computed for the predicted structure. The poorer resolving power of the seismological data for this part of the Mediterranean may prevent a more accurate imaging of the velocity structure.

Deeper structure. The improved correlation that we inferred for Figure 15 is also found in Figures 16, 17 and 18 (at depths of 245, 360 and 425 km respectively). We observe in our synthetic models a distinct signature of the tectonic evolution of the region. Specifically the effects of young (Calabrian and Hellenic) and old (Alpine, Carpathian, and Tauride) subduction processes can be recognized. The shape of the circum-Adriatic cold (high velocity) regions

correlates very well with the tomographic results on the scale of a few cells of the tomographic image. An important feature to note both in the synthetic and tomographic results is the southward shift of the locus of maximum high velocity anomalies: the older subduction zones of the Alpine belt in the north have a less pronounced signature than the younger subduction zones of the Calabrian and Hellenic arcs.

In Figures 18 and 19 a correlation between the predicted structure and the tomographic results still exists, but the predicted high-velocity anomaly below the Alboran and Italy is more pronounced in the tomographic results than it is in our modelling. The absence of high velocity material at larger depth below the Alps in the synthetic models (Figure 19) may indicate that we have not modeled all the convergence that has occurred, this would imply that in this region the period (approximately 100 m.y.) we have considered in our kinematic model is still not long enough. This does not explain the absence of high velocity material below the Carpathians, where relatively recent subduction has taken place. We conclude that in this region, we may make a type 1 or type 2 error.

(continued on page 89).

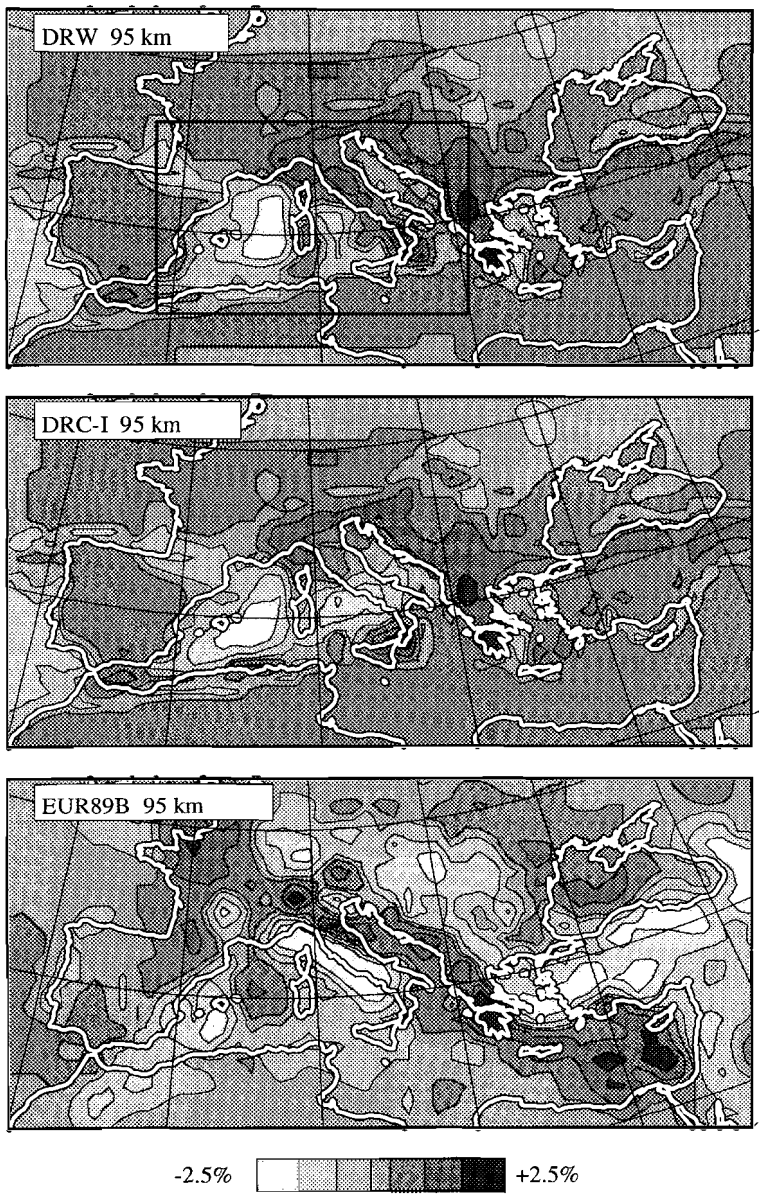

Figure 14. Regional P-wave velocity structure of the Mediterranean at a depth of 95 km. The top panel shows the synthetic structure based on the *Dewey et al.* [1989] reconstruction (inside the rectangle), the middle panel is based on the *Dercourt et al.* [1986] reconstruction, and the bottom panel is the tomographic model EUR89B. The shading denotes the relative deviation from the radial earth reference velocity, based on work by *Dziewonsky and Anderson* [1981] for the synthetic structure.

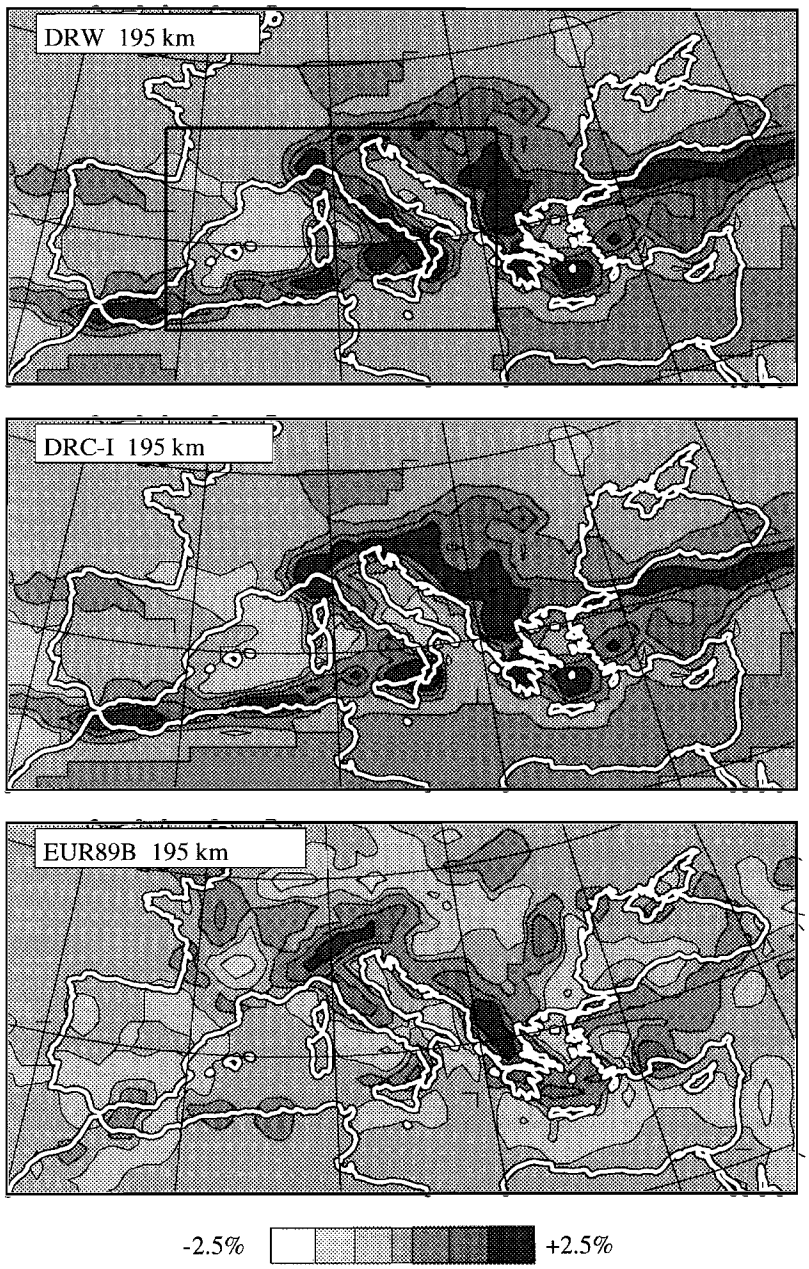

Figure 15. Regional P-wave velocity structure at a depth of 195 km. Panel ordering and legend the same as in Figure 14.

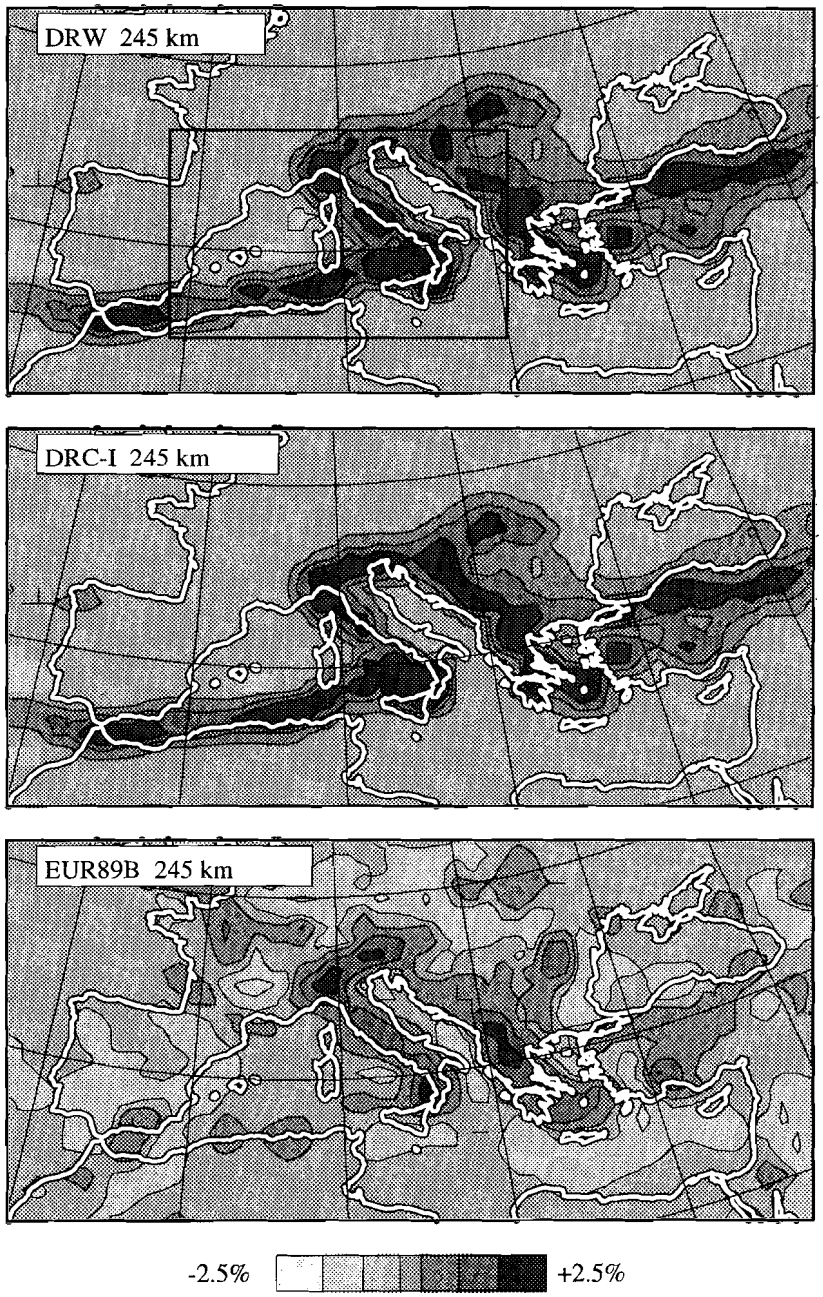

Figure 16. Regional P-wave velocity structure at a depth of 245 km. Panel ordering and legend the same as in Figure 14.

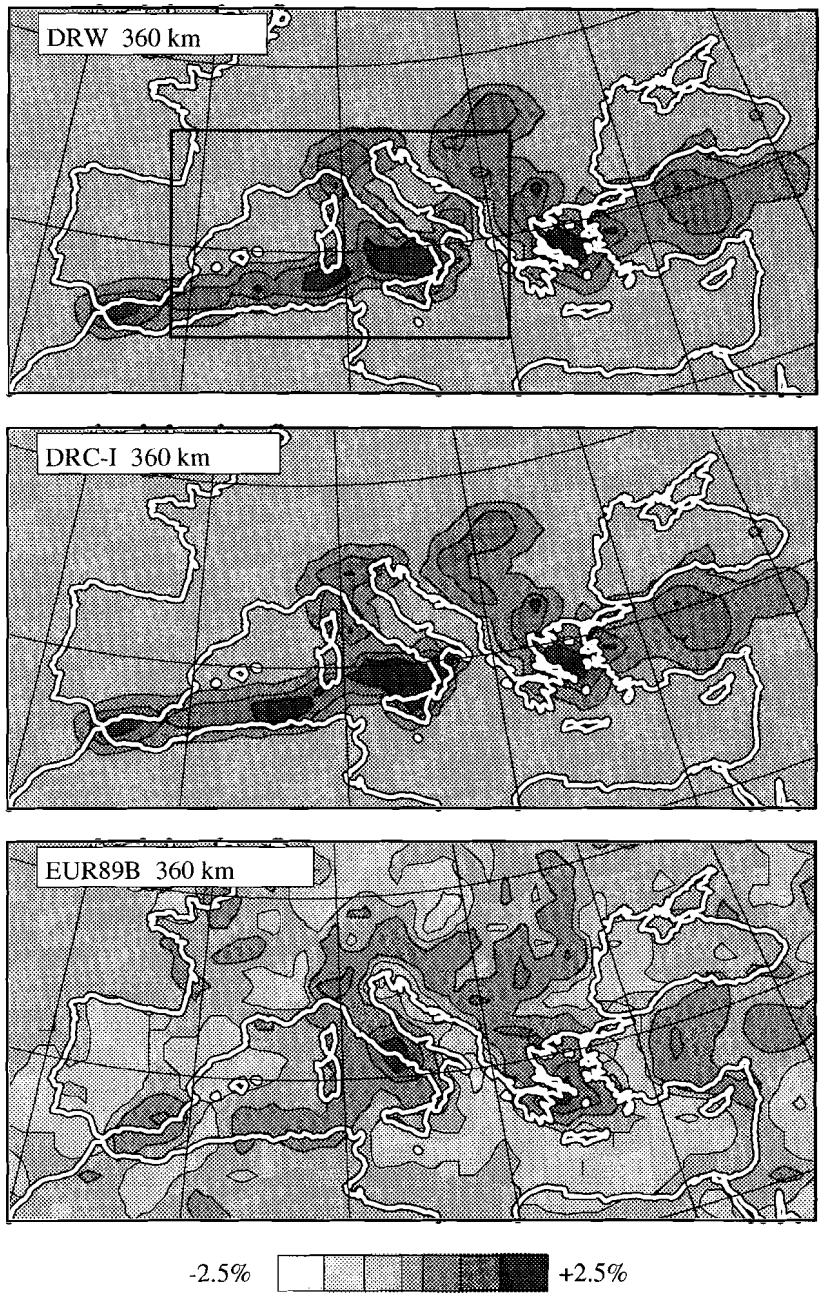

Figure 17. Regional P-wave velocity structure at a depth of 360 km. Panel ordering and legend the same as in Figure 14.

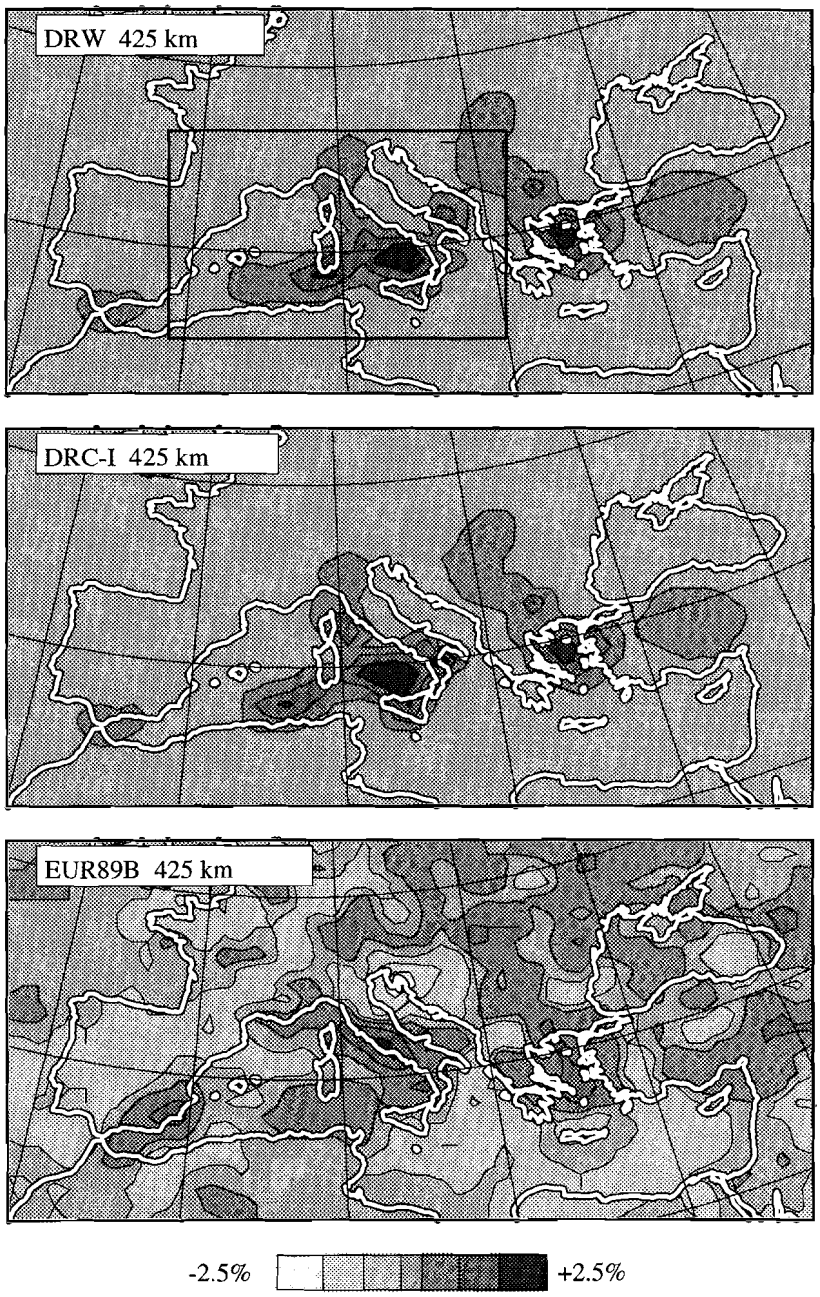

Figure 18. Regional P-wave velocity structure at a depth of 425 km. Panel ordering and legend the same as in Figure 14.

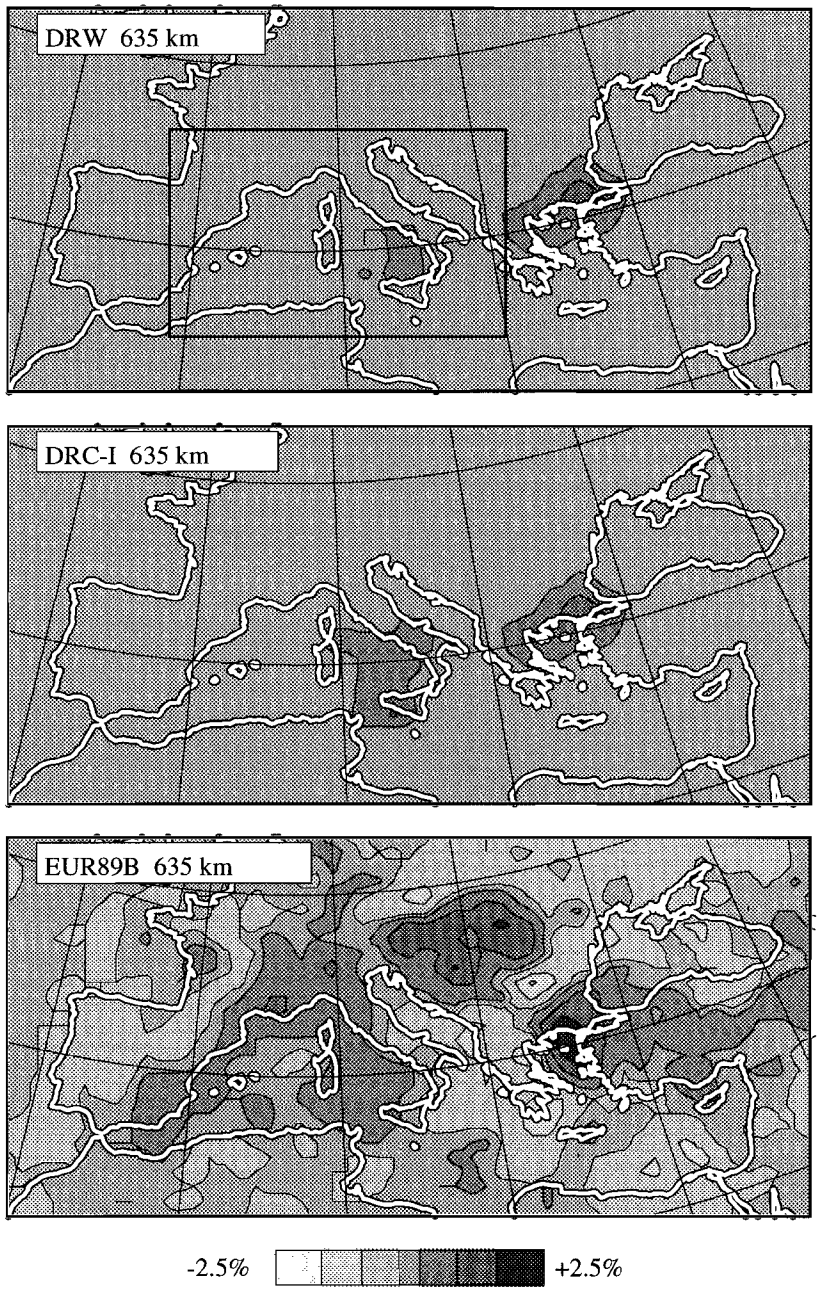

Figure 19. Regional P-wave velocity structure at a depth of 635 km. Panel ordering and legend the same as in Figure 14.

3.5 Reliability and limitations of the modelling approach

The synthetic models of the Mediterranean mantle can in some parts of the region predict the tomographic images of seismic velocity structure, but there are also notable discrepancies between the two results. We find the best correlation with our synthetic models in those regions which are covered reliably by the tomographic results (e.g., Figures 11 and 13). A close comparison of the predicted and the tomographically imaged mantle structure is hampered by the fact that the spatial resolution of the tomographic results varies considerably with position in the mantle [Spakman et al. 1993]. A significant and characteristic difference between the synthetic models and the tomographic images, however, is seen in Figure 12. In this along-strike section of the Apennine margins we predict a continuous high velocity slab in the synthetic models. The tomographic results on the other hand shows marked low velocities in the structure around depths of 100-200 km. In the horizontal section at 95 km (Figure 14) this discrepancy is present as the anti-correlation of anomaly patterns below the Apennines. The kinematic description of surface displacement can still be essentially correct (no type 1 error), but our modelling results for the current subduction zones as continuous slabs may not be justified everywhere in the Mediterranean. We may be simplifying the complex late stages of the subduction process too much (an error of type 2). Spakman et al. [1988], Spakman [1990], and Wortel and Spakman [1990,1992] discuss a possible explanation for the discontinuous slab images: they propose the subducted lithosphere may have become detached from the surface during some late stage of the evolution. This process may also play a role in the Alboran region [Blanco and Spakman, 1993] and the Carpathian region [Wortel and Spakman, 1993]; it would explain how our synthetic models predict the right amount of subducted lithosphere at the wrong depth in the mantle. We deliberately do not include these detachment processes in the calculations, since we want to restrict the modelling assumptions to those properties that can be derived from the tectonic reconstructions used. In this way the differences between model results and the tomographic image can give us further insight in the processes occurring at depth in the mantle.

As a result of this complication, both the DRC-I and DRW synthetic structures exhibit only a partial agreement with the tomographic images for the lower lithosphere and uppermost mantle. At deeper levels our models show a better fit with the tomography; the geometry and magnitude of the expected cold regions below the Mediterranean and the high velocity structures found with tomography are similar in the regions imaged well by tomography. Overall we conclude that the reconstructions by Dercourt et al. [1986] and Dewey et al. [1989] both represent good reconstructions for the meso-scale evolution of the Mediterranean region. For a more quantitative explanation of the (mis)match of our predicted models and the tomographic results, it is necessary to determine how well the synthetic mantle models can be imaged with tomography (De Jonge, Spakman and Wortel, in prep.)

3.6 Shallow detail

The comparison of the P-velocities determined by forward modelling of the kinematics and those found by seismic tomography is a good test for discriminating between the larger scale convergence-dominated processes in the region, but for the detailed analysis of extensional processes the resolution provided by tomography can be too coarse. Since extension processes are an important part of the evolution of the young back-arc basins of the Mediterranean, we want to compare our thermal results to bathymetry and heat flow, data sets primarily sensitive to the thermal structure of the lithosphere. For the top layer of the model we calculate the heat-flow and subsidence that accompany the extension predicted by the tectonic reconstructions. These parameters are also important if the thermal models of the lithosphere and upper mantle are used to constrain the internal thermal evolution of sedimentary basins. The following results are based on the same kinematic and compositional parameters as the regional models, however, they are presented at the higher resolution of the thermal calculations (i.e., without projection on the tomographic grid of figure 6).

Basin subsidence.

Figure 20 is a section through the Tyrrhenian Sea and the Gulf of Lion (along the dashed line in Figure 7). In the three panels we show the measured depth and predicted 'isostatic' depth of these basins. We derive the subsidence from pure shear thinning of a continental crust with constant initial thickness (30 km). The timing and stretching factors were chosen to comply with the horizontal surface motion of the reconstruction. Stretching is then followed by thermal subsidence using a simple isostatic control. The present bathymetry (which of course includes sediments) and the modeled (with only water loading) show a reasonable correspondence. With effects of sedimentary cover and erosion, the fit between model and observation will even improve because erosion reduces the height of the uplifted blocks, while a low density sedimentary infill (especially in the older basin between Sardinia and France) would give a smaller depth of this basin. We have not modeled these refinements because the difference between results from the DRC-I and DRW models is small for the time integrated changes in bathymetry. This means that subsidence of basins is not a very strict criterion for comparing different reconstructions.

Heat flow density.

Figure 21 shows the present, interpolated, heat flow based on observations by Hutchinson et al. [1985], compared with predicted basement heat flow density from modeled lithospheric structure after stretching. The line of this section is the same as that of figure 20. Here, the grey area denotes the range of uncertainty of the actual heat flow measurements. Thick lines in the lower

two panels show the heat flow calculated from the intra-plate deformation implicit in the tectonic reconstruction. Note that the main difference between the kinematics underlying the DRC-I and DRW models is not the total amount of extension, but rather the relative timing and position of the extensional phases. Differences between the lower two curves are mainly a result of the larger detail in time that is given in the Dewey et al. [1989] reconstruction (eight stages between 38 and 0 Ma against only four for the Dercourt et al. [1986] work). The strong dependence of heat flow density on the most recent extensional history means we can verify especially the modelling of the later stages of internal lithospheric deformation with observations of this quantity.

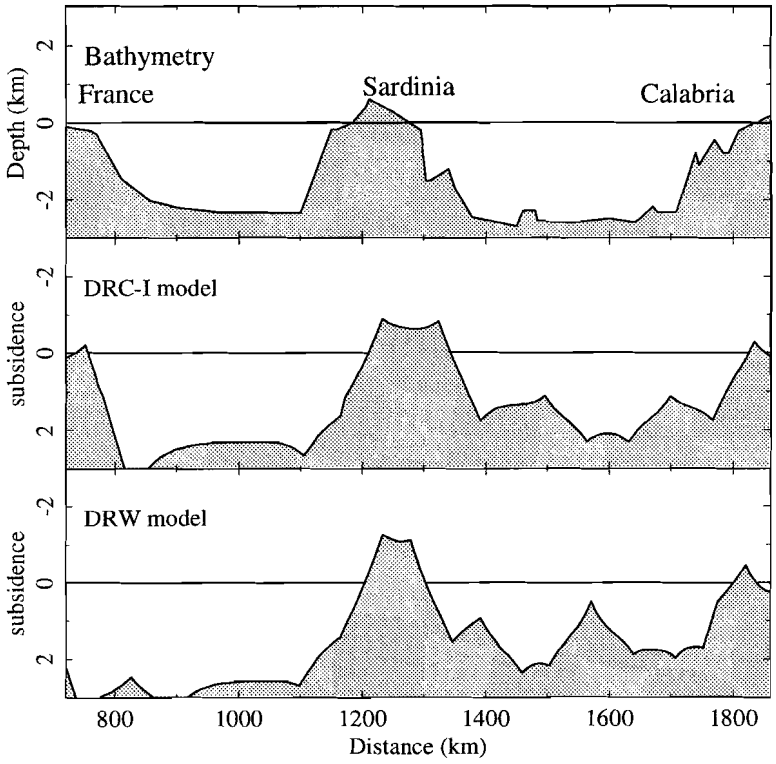

Figure 20. Bathymetry based on forward modelling (bottom two panels) compared with the actual depth of the Tyrrhenian sea (top panel). The section crosses from the south coast of France over Sardinia to Calabria. Section location shown in Figure 7.

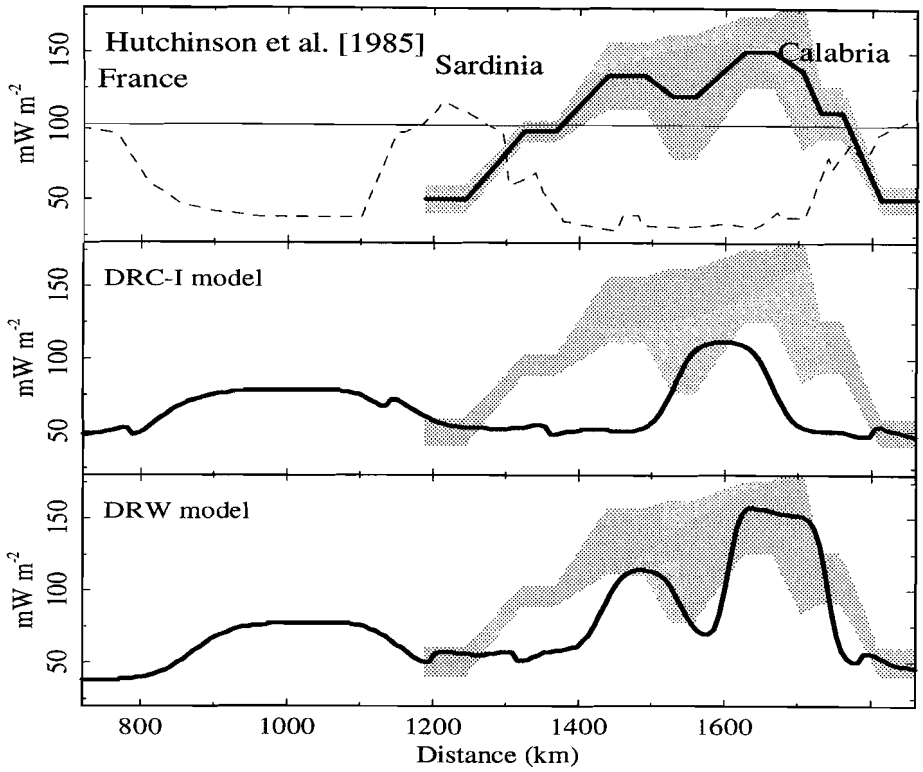

Figure 21. Heat flow density, as predicted from forward modelling (drawn line in bottom two panels) compared with heat flow measurements (top panel, grey areas denote the observational error range) by *Hutchinson et al.* [1985]. Section location the same as in the previous figure, the dashed line in the top panel shows the seafloor topography for reference.

3.7 Discussion and Conclusions

Our forward modelling of the thermal and seismic-velocity structure of lithosphere and upper mantle provides a link between tectonic reconstructions and models of the seismic velocity structure of the lithosphere and mantle. For the Mediterranean, the mantle structure predicted from regional extension and subduction with complex geometry and timing can be compared to available tomographic results. The most important mismatch between predicted models and the tomographic model is found in regions where the late stage development of subduction may have led to detachment of the subducted slab.

In general, however, the tectonic reconstructions proposed by Dercourt et al. [1986] and Dewey et al. [1989] both produce a good agreement between mantle predictions and tomographic results at scales of 100 to 200 km and larger. The

predicted models are furthermore consistent with basin bathymetry and basement heat flow observations.

We therefore conclude that the imaged seismological structure of the Mediterranean can be largely explained by our modelling results for subduction and extension using the kinematic boundary conditions provided by tectonic reconstructions. The correlation between forward models and tomographic results also implies that much of the P-wave velocity structure imaged by tomography results from thermal anomalies associated with conductive heat transfer between the mantle and (subducted) lithosphere.

The higher resolution in space and time given in the Dewey et al. [1989] reconstruction yields a better prediction of heat flow and of seismic velocities for the Tyrrhenian region. Furthermore, we conclude that the period that needs to be considered for the evolution of the Mediterranean is at least 40 m.y. for the rapidly converging plate boundaries of the Calabrian and Hellenic arcs and possibly two to three times that for the slower moving boundaries, since even effects of subduction processes that occurred 100 million years ago can be recognized in both the predicted mantle structure and in the tomographic results.

Acknowledgements:
M. R. de Jonge is funded by NWO/AWON (Netherlands Organisation for Scientific Research, Earth Sciences branch), project 751-354-019.
This study is carried out in the frame-work of Pionier Project PGS 76-144 'Detailed Structure and Dynamics of the Upper Mantle', which is funded by NWO.
We thank the reviewers H. M. Benz, T. Hearn, and D. Moser for their thoughtful comments.

References:

Alvarez, W., Tectonic evolution of the Corsica-Apennines-Alps region studied by the method of successive approximations, *Tectonics, 10*, 936-947, 1991.

Ames, W. F., *Numerical Methods for Partial Differential Equations*. 365 pp., Academic Press, New York, 1977.

Anderson, D. L., C. Sammis, and T. Jordan, Composition of the mantle and core, in *The Nature of the Solid Earth*, edited by E. C. Robertson, J. F. Hays, and L. Knopoff, pp. 41-66, McGraw-Hill, New York, 1972.

Andrews, D. J., and N. H. Sleep, Numerical modelling of tectonic flow behind island arcs, *Geophys. J. R. Astr. Soc., 38*, 237-251, 1974.

Biju-Duval, B., J. Dercourt, and X. Le Pichon, From the Tethys ocean to the Mediterranean seas: A plate tectonic model of the evolution of the western alpine system, in *Structural History of the Mediterranean Basins*, edited by B. Biju-Duval and L. Montadert, pp. 143-164, Technip, Paris, 1977.

Bina, C. R., and B. J. Wood, Olivine-spinel transitions: Experimental and thermodynamic constraints and implications for the nature of the 400-km seismic discontinuity, *J. Geophys. Res., 92*, 4853-4866, 1987.

Blanco, M. J., and W. Spakman, The P-wave velocity structure of the mantle below the Iberian peninsula: Evidence for subducted lithosphere below southern Spain, *Tectonophysics, 221*, 13-34, 1993.

Chung, D. H., Elasticity and equations of state of olivines in the Mg_2SiO_4-Fe_2SiO_4 system, *Geophys. J. R. Astr. Soc., 25*, 511-538, 1971.

Creager, K. C., and T. M. Boyd, Kinematic flow model of the Aleutian slab, *J. Geophys. Res., 96*, 2293-2307, 1991.

De Jonge, M. R., and M. J. R. Wortel, The thermal structure of the Mediterranean upper mantle: A forward modelling approach, *Terra Nova, 2*, 609-616, 1990.

Dercourt, J., L. P. Zonenshain, L.-E. Ricou, V. G. Kazmin, X. Le Pichon, A. L. Knipper, C. Grandjacquet, I. M. Sbortshikov, J. Geyssant, C. Lepvrier, D. H. Perchersky, J. Boulin, J.-C. Sibuet, L. A. Savostin, O. Sorokhtin, M. Westphal, M. L. Bazhenov, J. P. Lauer, and B. Biju-Duval, Geological evolution of the Tethys from the Atlantic to the Pamirs since the Lias, in *Evolution of the Tethys*, edited by J. Auboin, X. Le Pichon, and A. S. Monin, *Tectonophysics, 123*, 241-315, 1986.

Dewey, J. F., M. L. Helman, E. Turco, D. H. W. Hutton, and S. D. Knott, Kinematics of the western Mediterranean, in *Alpine Tectonics*, edited by M. P. Coward, D. Dietrich, and R. G. Park, *Geol. Soc. Lond. Spec. Publ., 45*, 265-283, 1989.

Douglas, J., On the numerical integration of $\frac{\partial^2 U}{\partial x^2}+\frac{\partial^2 U}{\partial y^2} = \frac{\partial U}{\partial t}$ by implicit methods, *J. Soc. Ind. Appl. Math., 3*, 1955.

Douglas, J., A note on the alternating direction implicit method for the numerical solution of heat flow problems, *Proc. Am. Math. Soc., 8*, 409-412, 1957.

Dziewonsky, A. M., and D. L. Anderson, Preliminary reference Earth model, *Phys. Earth and Plan. Int., 25*, 297-356, 1981.

Fairweather, G., and A. R. Mitchell, A new computational procedure for a.d.i. methods, *Soc. Ind. Appl. Math. J. on Num. Anal., 4*, 163-170, 1967.

Gealey, W. K., Plate tectonic evolution of the Mediterranean-Middle East region, *Tectonophysics, 155*, 285-306, 1988.

Graham, E. K., and G. R. Barsch, Elastic constants of single-crystal forsterite as a function of temperature and pressure, *J. Geophys. Res., 74*, 5949-5972, 1969.

Gwanmesia, G. D., S. Rigden, I. Jackson, and R. C. Liebermann, Pressure dependence of elastic wave velocity for β-Mg_2SiO_4 and the composition of the earth's mantle, *Science, 250*, 794-797, 1990.

Hsui, A. T., B. D. Marsh, and M. N. Toksöz, On melting of the subducted oceanic crust: Effects of induced mantle flow, *Tectonophysics, 99*, 207-220, 1983.

Hsui, A. T., and M. N. Toksöz, The evolution of thermal structures beneath a subduction zone, *Tectonophysics, 60*, 43-60, 1979.

Hutchinson, I. , R. P. von Herzen, K. E. Louden, J. G. Sclater, and J. Jemsek, Heat flow in the Balearic and Tyrrhenian Basins, western Mediterranean, *J. Geoph. Res., 90*, 685-701, 1985.

Isaak, D. G., O. L. Anderson, T. Goto and, I. Suzuki, Elasticity of single-crystal forsterite measured to 1700K, *J. Geophys. Res., 94*, 5895-5906, 1989.

McKenzie, D. P., Speculations on the consequences and causes of plate motions, *Geophys. J. R. Astr. Soc., 18*, 1-32, 1969.

McKenzie, D. P., Temperature and potential temperature beneath island arcs, *Tectonophysics, 10*, 357-366, 1970.

McKenzie, D. P., Some remarks on the development of sedimentary basins, *Earth and Plan. Sci. Lett., 40*, 25-32, 1978.

Meissner, R., Th. Wever, and E. R. Flüh, The moho in Europe - implications for crustal development, *Ann. Geophys., 5B*, 357-364, 1987.

Mercier, J. L., D. Sorel, P. Vergely and K. Simeakis, Extensional tectonic regimes in the Aegean during the Cenozoic, *Basin Research, 2*, 49-71, 1989.

Minear, J. W., and M. N. Toksöz, Thermal regime of a downgoing slab and new global tectonics, *J. Geophys. Res., 75*, 1397-1419, 1970.

Mitchell, A. R., *Computational methods in partial differential equations*, 255 pp., Wiley, London, 1969.

Mizutani, H., Y. Hamano, Y. Ida, and S. Akimoto, Compressional wave velocities of fayalite, Fe_2SiO_4 spinel and coesite, *J. Geophys. Res., 75*, 2741-2747, 1970.

Panza, G. F., The deep structure of the Mediterranean-Alpine region and large shallow earthquakes, *Mem. Soc. Geol. It., 29*, 5-13, 1984.

Panza, G. F., St. Mueller, and G. Calcagnille, The gross features of the lithosphere-asthenosphere system in Europe from seismic surface waves and body waves, *PAGEOPH, 118*, 1209-1213, 1980.

Peaceman, D. W., and H. Rachford, The numerical solution of parabolic and elliptic differential equations, *J. Soc. Ind. Appl. Math., 3*, 28-41, 1955.

Platt, J. P., and R. L. M. Vissers, Extensional collapse of thickened continental lithosphere: a working hypothesis for the Alboran Sea and the Gibraltar arc, *Geology, 17*, 540-543, 1989.

Richards, M. A., and D. C. Engebretson, The history of subduction, the distribution of hotspots, seismic heterogeneity, and the large scale structure of mantle convection, *EOS trans. AGU, 71*, 1575, 1990.

Richards, M. A., and D. C. Engebretson, Large-scale mantle convection and the history of subduction, *Nature, 355*, 437-440, 1992.

Rybach, L., A petrological model of the lower continental crust, derived from seismic velocities and from radioactive heat production, *Ann. Geoph., 5B*, 403-408, 1987.

Sawamoto, H., D. J. Weidner, S. Sasaki, and M. Kumazawa, Single-crystal elastic properties of the modified spinel (beta) phase of magnesium orthosilicate, *Science, 224*, 749-751, 1984.

Schatz, J. F., and G. Simmons, Thermal conductivity of earth materials at high temperature, *J. Geophys. Res., 77*, 6966-6983, 1972.

Sleep, N. H., Teleseismic P-wave transmission through slabs, *Bull. Seismol. Soc. Am., 63*, 1349-1373, 1973.

Snieder, R., large scale waveform inversions of surface waves for lateral heterogeneity -II: Application to surface waves in Europe and the Mediterranean, *J. Geophys. Res., 93*, 12067-12080, 1988.

Spakman, W., Upper mantle delay-time tomography. With an application to the collision zone of the Eurasian, African and Arabian plates, Ph.D thesis, 200 pp., Utrecht University, Utrecht, 1988.

Spakman, W., M. J. R. Wortel, and N. J. Vlaar, The Hellenic subduction zone: A tomographic image and its geodynamic implications, *Geoph. Res. Lett., 15*, 60-63, 1988.

Spakman, W., S. van der Lee, R. D. van der Hilst, Structure of the European-Mediterranean upper mantle to a depth of 1400 km: Preliminary results from P delay-time tomography (abstract), *Terra Abstracts EUG, 3*, 173, 1991.

Spakman, W., S. van der Lee, R. D. van der Hilst, Travel-time tomography of the European-Mediterranean mantle down to 1400 km, *Phys. Earth Plan. Int., 79*, 3-74, 1993.

Sumino, Y., O. L. Anderson and I. Suzuki, Temperature coefficients of elastic constants of single crystal MgO between 80 and 1300 K, *Phys. Chem. Min., 9*, 38-47, 1983.

Sumino, Y., O. Nishizawa, T. Goto, I. Ohno and M. Ozima, Temperature variation of elastic constants of single-crystal forsterite between -190° and 400°C, *J. Phys. Earth, 25*, 377-392, 1977.

Suzuki, I., Thermal expansion of periclase and olivine and their anharmonic properties, *J. Phys. Earth, 23*, 145-159, 1975.

Suzuki, I., O. L. Anderson, and Y. Sumino, Elastic properties of single-crystal forsterite Mg_2SiO_4 up to 1200 K, *Phys. Chem. Min., 10*, 38-46, 1983.

Suzuki, I., K. Seya, H. Takei, and Y. Sumino, Thermal expansion of fayalite, Fe_2SiO_4, *Phys. Chem. Min., 7*, 60-63, 1981.

Toksöz, M. N., J. W. Minear, and B. R. Julian, Temperature field of a downgoing slab, *J. Geophys. Res., 76*, 1113-1139, 1971.

Toksöz, M. N., and A. T. Hsui, Numerical studies on back-arc convection and the formation of marginal basins, *Tectonophysics, 50*, 177-196, 1978.

Turcotte, D. L., and G. Schubert, *Geodynamics: Applications of Continuum Physics to Geological Problems*, 450 pp., Wiley, New York, 1982.

Wang, H., and G. Simmons, Elasticity of some mantle crystal structures 1. Pleonaste and hercynite spinel, *J. Geophys. Res., 77*, 4379-4392, 1972.

Weidner, D. J., H. Sawamoto, and S. Sasaki, single-crystal elastic properties of the spinel phase of Mg_2SiO_4, *J. Geophys. Res., 89*, 7852-7860, 1984.

Wortel, M. J. R., Seismicity and rheology of subducted slabs, *Nature, 296*, 553-556, 1982.

Wortel, M. J. R., and W. Spakman, Structure and dynamics of subducted lithosphere, arc migration, and the geodynamic evolution of the Mediterranean region, *EOS Trans. AGU, 71*, 1633, 1990.

Wortel, M. J. R., and W. Spakman, The dynamic evolution of the Apenninic-Calabrian, Hellenic, and Carpathian arcs: a unifying approach, *Terra Abstracts EUG, 5*, 97, 1993.

Wortel, M. J. R., and W. Spakman, Structure and dynamics of subducted lithosphere in the Mediterranean region, *Proc. Kon. Ned. Akad. v. Wetensch, 95*, 325-347, 1992.

Wortel, M. J. R., and N. J. Vlaar, Age-dependent subduction of oceanic lithosphere beneath western South America, *Phys. Earth Plan. Int., 17*, 201-208, 1978.

Wortel, M. J. R., and N. J. Vlaar, Subduction zone seismicity and the thermo-mechanical evolution of downgoing lithosphere, *PAGEOPH., 128*, 625-659, 1988.

Zielhuis, A., S-wave velocity below Europe from delay-time and waveform inversions, Ph.D thesis, 148 pp., Utrecht University, Utrecht, 1992.

Chapter 4

Testing forward models with tomographic inversion results; testing tomographic inversion results with forward models[†]

Appearances to us in four ways: for either things appear as they are;
or they are not, and do not even appear to be;
or they are, and do not appear to be;
or they are not, and yet appear to be.
Further, in all these cases to form a right judgement is the office of an educated man.
Epictetus, The Discourses, 101

Abstract. We compare model predictions of mantle structure based on different reconstructions of the tectonic evolution of the Alpine-Mediterranean region with independent models obtained by a tomographic inversion of delay times. The aim of this comparison is to decide which of the studied tectonic reconstructions best describes the actual development of the region. We first study the imaging properties of the tomographic inversion. For that purpose, we perform resolution experiments with different predicted synthetic models of mantle structure. The results of the experiments give insight into the magnitude and nature of imaging artefacts of the tomographic inversion and allow the identification of poorly and well resolved parts of the model. Specifically, we find that features of the mantle structure, like the extent of aseismic slabs and possible detachment of subducted lithosphere, can be resolved well. Using the obtained resolution estimates, we can decide where the forward models provide a good prediction of the actual mantle structure. We find that none of the tested tectonic reconstructions results in a completely accurate prediction of the seismic velocities obtained with tomography. For many subregions of the Alpine-Mediterranean area, however, we can identify the best parts of the tested reconstructions. Furthermore, we can draw conclusions on the nature of mantle processes from the misfit between tomographic results and forward models.

[†] This chapter has been submitted for publication without the footnotes as; M. R. de Jonge, W. Spakman, and M. J. R. Wortel, Geodynamic evolution of the Alpine-Mediterranean region: a tomographic analysis, *J. Geophys. Res.*, 1995.

4.1 Introduction

During the last decade detailed reconstructions of the geological evolution of parts of the Alpine-Mediterranean region have been proposed [Dercourt et al., 1986, Dewey et al., 1989, and Dercourt et al., 1990]. These reconstructions give a description of the evolution of orogenic belts, plate boundaries, extensional basins, and of the distribution of different types of crust. In creating a tectonic reconstruction, it is often necessary to supplement the geological data with assumptions on the tectonic processes, e.g. on the maximum size of destructed oceanic basins and the associated amount of convergence across plate boundaries. For this and other reasons, different studies have resulted in a number of reconstructions of the tectonic evolution of the Alpine-Mediterranean region.

We will study which of these reconstructions provides the best description of the actual evolution by exploiting information on the present lithosphere and mantle structure provided by tomographic investigations. In this study we use the link between tectonic reconstructions and seismic velocity structure as proposed by De Jonge and Wortel [1990] and De Jonge et al. [1993; 1994]. These authors have developed a forward modelling strategy to predict the seismic velocity structure of the mantle and lithosphere from tectonic processes. The forward modelling consists of three steps. Firstly, the surface kinematics taken from the reconstruction is translated into a three-dimensional material flow model of the lithosphere and mantle. Secondly, the temperature evolution of lithosphere and mantle is calculated with the prescribed kinematics and thermal diffusion. Finally, the three-dimensional temperature structure is converted to a predicted P-wave velocity structure. De Jonge et al. [1993, 1994] have applied this method to different reconstructions of the Alpine-Mediterranean region to produce a number of mantle predictions.

Detailed models of the structure of the Alpine-Mediterranean mantle are available from tomographic inversion of seismological data [Spakman, 1990, 1991; Spakman et al., 1988, 1993; and Remkes and Spakman, 1993]. Because the forward and inverse models are based on different methods and data they are completely independent.

The independence of the forward and inverse models implies we can test the results obtained by forward modelling with results of the tomographic inversion. The premise for the comparison of forward and inverse models is that the forward model derived from the best tectonic reconstruction yields the best prediction for the present-day lithosphere and mantle structure. However, due to various modelling errors neither the tomographic nor the forward models are perfect descriptions of the Earth's mantle structure. De Jonge et al. [1994] distinguished the following three causes for misfit between results of the two methods:

Type-1 error. The misfit between forward and inverse models is caused by adopting an incorrect tectonic scenario to determine the history of material

flow in the mantle. Too little plate-convergence given in a reconstruction, for instance, results in too short slabs predicted in the forward model.
Type-2 error. The misfit between forward and inverse models stems from incorrect approximations in the forward modelling method and is essentially independent of the tectonic reconstruction employed. Examples are oversimplification of subduction zone geometry and incorrect conversion of temperature to P-wave velocities.
Type-3 error. The misfit is caused by errors in the tomographic images of the structure due to poor seismic data quality and lack of spatial resolution. Lack of resolution in the down dip direction of a subducted slab can for instance lead to spurious mapping of the depth penetration of the slab.

Because of the complicated interaction of these three types of errors De Jonge et al. [1994] could only give a qualitative interpretation of the differences between the results of the forward and inverse modelling methods. We will attempt to identify and isolate the three types of errors in the present study to draw more quantitative conclusions.

In the first part of this paper we will briefly describe the forward models of De Jonge et al. [1993, 1994] and the inverse models of Spakman et al. [1993] and of Remkes and Spakman [1993]. In the second part we will describe a technique with which we analyse the influence of type-3 modelling errors. The technique is similar to that used by Spakman et al. [1989] for the investigation of the spatial resolution for imaging subduction in the North West Pacific. The third part of the paper deals with the detailed application in a large number of tomographic experiments with the aim of isolating type-3 errors. Finally, the fourth part deals with the comparison of various forward and tomographic models. In this last section we will assess the quality of the different tectonic reconstructions. After identification of the modelling errors, both the fit and the misfit between predicted and imaged mantle structure give valuable information on the geodynamic processes that shaped the Alpine-Mediterranean region from the Middle Mesozoic onwards.

The main theme of the present study is to make a detailed comparison of forward and inverse models with the aim to study the quality of different tectonic reconstructions by identifying type-1 misfit errors. A second objective is to study the link between surface tectonics and seismic velocity structure. On a global scale a similar approach has been followed for this purpose by Richards and Engebretson [1992]. As important spinoff results we will also obtain valuable information on the actual lithosphere and mantle structure by identifying type-3 errors (which takes us a step further in the interpretation of information contained in the tomographic images). Furthermore, by identifying type-2 misfit errors we obtain information on the nature of mantle processes.

4.2 Forward and inverse models of the Alpine-Mediterranean region

Forward models

Predictions of the Alpine-Mediterranean mantle structure have been obtained with a method developed by De Jonge and Wortel [1990], and De Jonge et al. [1993,1994]. The forward models were derived with the objective to test various tectonic reconstructions of the Cenozoic evolution. The tectonic reconstruction published by Dercourt et al. [1986] was used to compute the mantle prediction models called DRC-I and DRC-II. The model DRW is based on the reconstruction of the Western Mediterranean by Dewey et al. [1989] and extended with parts of DRC-I in other regions. All three models are described in de Jonge et al. [1994]. The model DRC-III [De Jonge et al., 1993] is based on the tectonic reconstruction of the Northern Tethys by Dercourt et al. [1990] and also extended with parts of DRC-I. Parameters controlling the forward models are changes in the shape or position of plates and plate-boundaries and the type of lithosphere involved in tectonic processes (thermal state and composition). Forward modelling comprises the translation of the temporal and spatial development of surface tectonics into a three-dimensional kinematic model of lithosphere and mantle flow. To construct the flow field assumptions on the nature of tectonic processes in the region need to be made. Relative convergence across plate boundaries is associated with subduction. Divergence and increase in surface area of plates are associated with upwelling of asthenosphere and intra-plate extension or oceanic spreading. The three-dimensional flow model controls the advective component of heat transport in numerical modelling of lithosphere and mantle temperatures. The final result of the thermal modelling procedure is a prediction of the present temperature field of the lithosphere and mantle.

The various predictions (DRC-I, DRC-II, DRC-III and DRW, see also table 2) are all characterised by a complex three-dimensional geometry of thermal anomalies related to subduction and extension processes. For comparison with tomographic models temperature anomalies are converted to P-wave velocity anomalies using a depth-dependent derivative of P-wave velocity to temperature ($\partial V_p/\partial T$) (see De Jonge et al. [1994]). Resulting velocity anomalies are subsequently projected on a cell-model with the same dimensions as used for tomographic inversion (Figure 1). Cell sizes are 0.8° by 0.8° laterally and cell thicknesses range from 33 km (in the lithosphere) to 100 km (at a depth of 1400 km).

More details on the forward modelling procedure can be found in De Jonge et al. [1994]. We remark that several type-2 errors may result, for example, by assuming subduction instead of lithospheric thickening, by using average material properties throughout the mantle, or from the inaccuracy of the depth-dependent value of $\partial V_p/\partial T$ determined from laboratory experiments.

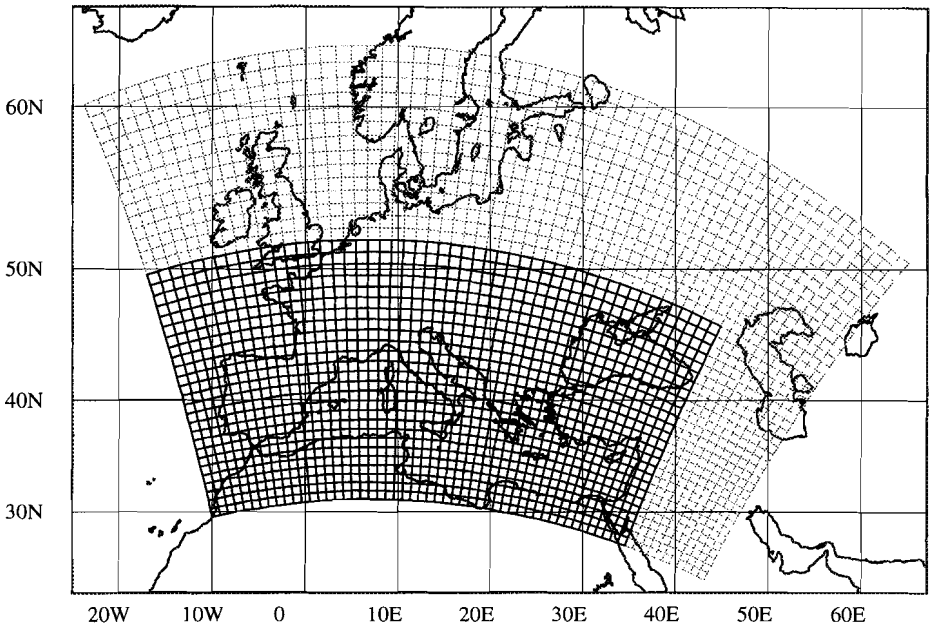

Figure 1. Cell grid used in the tomographic inversion. The resolution experiments discussed in this paper are limited to the part of the cell model that is predicted from the tectonic reconstructions used (denoted by the thicker grid lines), although the tomographic computations are performed for the whole grid. The model spans a depth range from the surface down to 1400 km

Inverse models

For the comparison with forward model results we employ the tomographic models EUR89B of Spakman et al. [1993] and EUR93 of Remkes and Spakman [1993]. The tomographic models are obtained from the inversion of P-wave delay-times and they are completely independent of the forward models. As tomographic inversion forms an important part of the present study we will give a brief and simplified description of the basic procedure.

Tomographic models are calculated from P-wave delay times as regularized least-squares solutions of the matrix equation **d=Am**, where **d** is the delay-time data vector, **m** is the model vector, and **A** is the coefficients matrix relating data to the model. With "regularized least squares" is implied that the system **d=Am** is solved under additional constraints on model smoothness and model amplitude. A detailed description of the method can be found in Spakman and Nolet [1988] and Spakman [1991]. It is important to note that the matrix system **d=Am** is a discrete and linearized approximation of the actual nonlinear tomographic problem. Linearization is performed with respect to a

one-dimensional reference model of the Earth's P-wave velocity structure. Spakman et al. [1993] and Remkes and Spakman [1993] used the method developed by Van der Hilst and Spakman [1989] to find regional reference models from the P-wave delay times reported by the International Seismological Centre (ISC). Two regional reference models are shown in Figure 2. The model PM2 is used to determine the tomographic model EUR89B [Spakman et al., 1993] and the model PM4 is used for EUR93 [Remkes and Spakman, 1993].

The model vector **m** consists of three parts: velocity anomalies in cells (Figure 1) by which the mantle structure is discretized, earthquake mislocation parameters, and station correction parameters. Consequently, the coefficients matrix **A** also consists of three parts: coefficients derived from the illumination of the mantle by seismic ray-paths connecting earthquakes and stations, coefficients describing earthquake mislocation, and coefficients for the determination of station corrections, respectively. Therefore, the tomographic method simultaneously fits velocity heterogeneity, earthquake mislocation vectors, and station corrections to the data. In Figure 3 the pertinent quantities are schematically illustrated for a single ray-path (i.e. one row of **d=Am**).

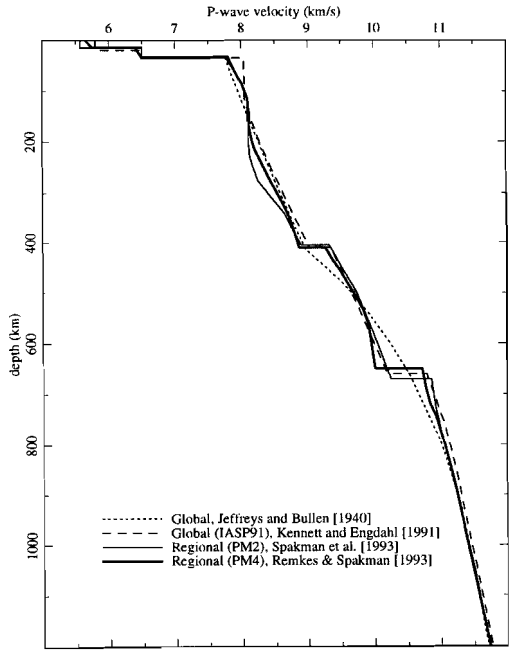

Figure 2. Radial P-wave velocity models, thick lines show the regional reference velocity PM4 (used for EUR93) and PM2 (used for EUR89B). For comparison also the global Jeffreys-Bullen [Jeffreys and Bullen, 1940] and IASP91 [Kennett and Engdahl, 1991] models are shown

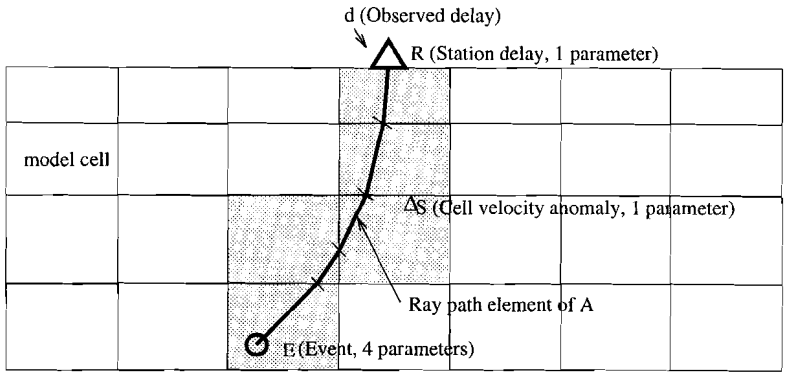

Figure 3. Schematic representation of a single event-station pair in the tomographic inversion, determining one equation of matrix A. The delay time is related to parameters describing the station R, the event E, and contributions from velocity anomalies ΔS along ray-path segments.

In this study we will employ the matrix **A** used by Remkes and Spakman [1993] for determining model EUR93. These authors use a different tomographic approach than Spakman et al. [1993] and a more detailed parameterization of the model. We will display results from both EUR89B and EUR93 in our analysis to illustrate the robustness of the tomographic solution with respect to changes in the reference model and model parameterization, and to provide a link with model EUR89B, which has been extensively described by Spakman et al. [1993].

4.3 Procedure for comparison of forward and inverse models

De Jonge et al. [1993, 1994] made a qualitative comparison of the tomographic model EUR89B with various forward models of mantle structure. They could, however, not distinguish effects of errors in the tectonic reconstruction (type-1) from effects of errors in the tomographic mapping (type-3) in their appraisal of the misfit between inverse and forward models. In the present study we will set up a more quantitative method of comparison that allows discrimination between mapping errors and other errors causing model misfit. Consequently, our analysis will (1) give a detailed assessment of the quality of tomographic mapping of the Alpine-Mediterranean mantle in addition to the resolution analysis presented by Spakman et al. [1993] and (2) allow the study of the quality of tectonic reconstructions of this region. We will identify type-3 errors with sensitivity analysis in which synthetic models of velocity heterogeneity are used [Spakman and Nolet, 1988 and Humphreys and Clayton, 1988].

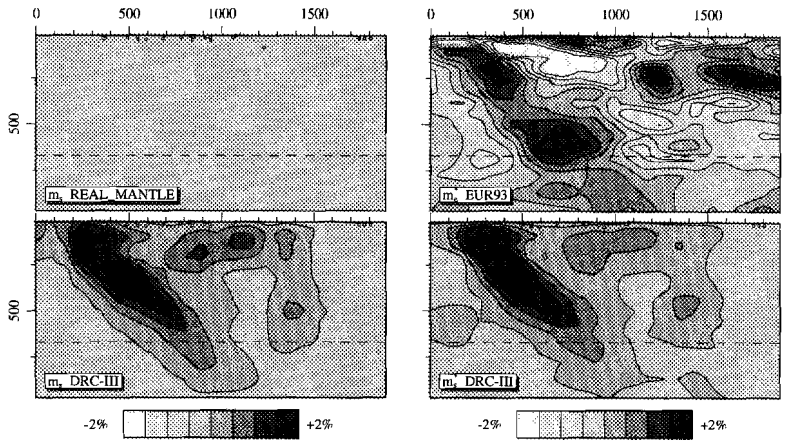

Figure 4. Four cross-sections through different representations of the mantle structure. Top left: real mantle (empty as it is unknown), top right: the tomographic inversion result EUR93 by Remkes and Spakman [1993], bottom left: a prediction of mantle structure (DRC-III by de Jonge et al. [1993]), and bottom right: the tomographic image of this predicted structure

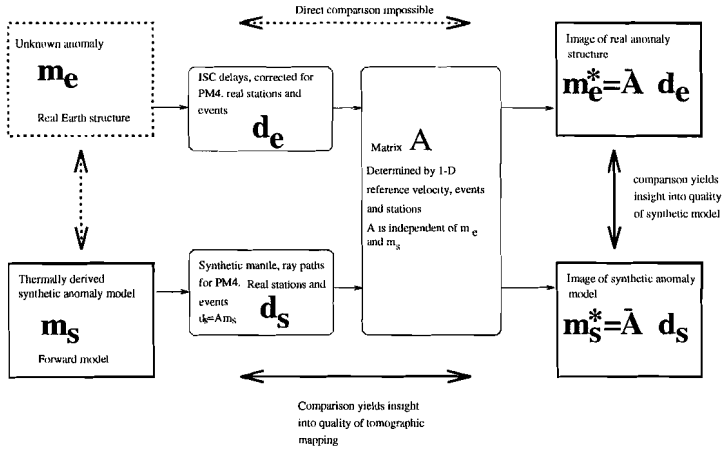

Figure 5. Schematic representation of the models shown in Figure 4 and their interrelation. The first part of this study will focus on the quality of mapping of the synthetic model $\mathbf{m_s}$ (bottom left) onto its tomographic image $\mathbf{m_s^*}$ (bottom right), to assess the quality of tomographic mapping in this region in general. The second part will focus on the comparison of the image of the synthetic model $\mathbf{m_s^*}$ (bottom right) and the image of the actual mantle structure $\mathbf{m_e^*}$ (top right) to study the quality of the synthetic models.

The procedure for comparing forward and inverse models is schematically depicted in Figures 4 and 5. In Figures 4 and 5 we denote mantle structure by the four corner panels: the real mantle $\mathbf{m}_e$, the mantle prediction $\mathbf{m}_s$ (a forward model), and their tomographic images $\mathbf{m}_e^*$ and $\mathbf{m}_s^*$, respectively. The tomographic image $\mathbf{m}_e^*$ is a mapping of the actual Earth structure: it is obtained as a regularized least-squares solution of $\mathbf{d}_e=\mathbf{Am}$, in which $\mathbf{d}_e$ is the data vector of delay times. The image $\mathbf{m}_s^*$ is obtained by first computing synthetic delay times $\mathbf{d}_s$ (by the forward computation $\mathbf{d}_s = \mathbf{Am}_s$), and next solving the system $\mathbf{d}_s=\mathbf{Am}$ for $\mathbf{m}_s^*$.

Ultimately we want to draw inferences on the quality of the synthetic model $\mathbf{m}_s$ relative to the actual mantle structure $\mathbf{m}_e$ (left-hand arrow in Figure 5). We need to make two comparisons to achieve this: firstly between $\mathbf{m}_s$ and its mapping $\mathbf{m}_s^*$ (bottom arrow in Figure 5), and secondly between $\mathbf{m}_s^*$ and $\mathbf{m}_e^*$ (right-hand arrow in Figure 5). The first comparison will demonstrate how well tomography (data, ray-paths, and inversion method) can image mantle structure. From this step we derive the importance of type-3 (tomographic imaging) errors. The second comparison gives insight into the differences between actual and predicted mantle structure and thereby into type-1 and type-2 errors (incorrect tectonic scenario and imperfect numerical modelling, respectively). These two steps are detailed below.

The first comparison comprises the studying of spatial resolution of velocity anomalies obtained in the tomographic mapping of $\mathbf{m}_s$ on $\mathbf{m}_s^*$. The typical scale of anomalies in $\mathbf{m}_s$ is of the order of a few hundred km and anomaly amplitudes are of the order of a few percent with respect to the ambient mantle (reference velocity). We investigate resolution in a series of experiments using different models $\mathbf{m}_s$. The effect of data errors is studied by adding synthetic noise to $\mathbf{d}_s$. Both random and systematic errors will be used. We will show that the spatial resolution for mapping typical structures (three-dimensional slab geometry) is indeed sufficiently high to proceed with the second comparison.

We can then carry out the comparison of $\mathbf{m}_e^*$ with various images $\mathbf{m}_s^*$, based on different tectonic reconstructions. In parts of the model where spatial resolution is high the comparison between $\mathbf{m}_e^*$ and $\mathbf{m}_s^*$ directly leads to inferences about the relation between $\mathbf{m}_e^*$ and $\mathbf{m}_s$ and between $\mathbf{m}_e$ and $\mathbf{m}_s$. We will show that in well resolved regions a number of important differences between $\mathbf{m}_e^*$ and $\mathbf{m}_s^*$ exist. These spatially resolved differences provide us with a means to assess type-1 and type-2 misfit errors between the prediction $\mathbf{m}_s$ and the actual mantle $\mathbf{m}_e$.

In parts of the model where the spatial resolution is not high, the identification of type-3 errors will still help to assess the quality of the tomographic image $\mathbf{m}_e^*$ and to separate type-3 from type-1 and type-2 errors in a qualitative sense. The identification of type-1 and type-2 errors enables us to draw conclusions on the quality of the tectonic reconstructions and on the nature of mantle processes in the evolution of the region, respectively.

Limitations of the method of resolution analysis

Before we conduct the resolution experiments, we need to address three potential drawbacks of sensitivity analysis with synthetic velocity models [Spakman, 1991; Van der Hilst et al., 1993].

(1) Sensitivity analysis can only give insight into the resolving power provided by the reference ray-paths employed. The ray-paths from which the matrix **A** is constructed are computed from a one-dimensional reference model. However, due to the lateral velocity heterogeneity reference ray-paths need not coincide with the actual ray-paths. We try to minimize ray-path effects by using regional reference models for the average mantle structure [Spakman et al., 1993; Remkes and Spakman, 1993].

(2) Real data and errors (reading-, mispick-, implicit modelling-, and mislocation errors) need not have the same statistics as synthetic data and synthetic noise. Furthermore, the synthetic data are perfectly consistent with reference ray-paths, since these data are computed by integration along the ray-paths. For the real data it is unknown how well these correlate with the reference ray-paths (and therefore with mantle structure). In our experiments synthetic data errors, added to $\mathbf{d}_s$, consist of two components: a normally distributed random error plus a systematic component related to 'distant' mantle heterogeneity (e.g. slabs in the mantle of the NW Pacific).

(3) Lévêque et al. [1993] have demonstrated that a good recovery of detail in sensitivity tests does not guarantee good recovery of larger structures. The latter problem can be avoided by using synthetic models with different characteristic scales of anomalies. The synthetic models used by Spakman et al. [1993] combined with synthetic models used in the present study fulfil this requirement. These models test the sensitivity of the inversion to resolve the structure on scales between 40 and 1000 km.

In view of the forementioned uncertainties, sensitivity analysis cannot provide formal proof for the *existence* of the mantle anomalies imaged. However, the use of a regional reference model, of different synthetic velocity anomaly models, and of both random and systematic errors in the synthetic data, substantially reduces the possibility of making incorrect inferences about the spatial resolution for actual mantle structure. With this in mind we perform the following experiments.

4.4 Assessing the quality of tomographic mapping

In this section we will study the potential type-3 errors of the tomographic imaging by means of a number of experiments. The experiments are performed with different synthetic structures $\mathbf{m}_s$, all based on the forward model DRC-III [de Jonge et al., 1993], and highlighting different aspects of the mantle structure. Also, different levels of noise are added to the delay-time data derived from the synthetic structure. An overview of the experiments is shown in Table 1.

General experiment description

In experiments TEST-1, TEST-2 and TEST-3 we investigate the spatial resolution and amplitude recovery for mapping the entire DRC-III model. Especially the effects of density of ray-paths, random noise, and systematic noise will be addressed. These tests do not give insight into possible ray-path smearing effects in the interior of slabs. We need to investigate, for example, whether slab images like the ones shown in the right-hand panels of Figure 4 can be a result of a much shallower penetrating slab that is artificially enlarged due to lack of resolution in the dip direction. The second group of experiments, TEST-4 through TEST-8, are designed to address these anomaly smearing effects and to study spatial resolution within slabs. These tests are also motivated by a number of discrepancies between forward and inverse models. With these experiments we will especially study the resolution for assessing the continuity of subducted slabs. For the experiments TEST-4 to TEST-8 we will use mantle models that are modified from DRC-III so that imaging errors can be easily recognized. The modified models should not be considered to describe the real mantle structure of the Alpine-Mediterranean region; they are only used for sensitivity analysis. An overview of the geographical names associated with the tectonic features we will discuss in the following sections is shown in Figure 6.

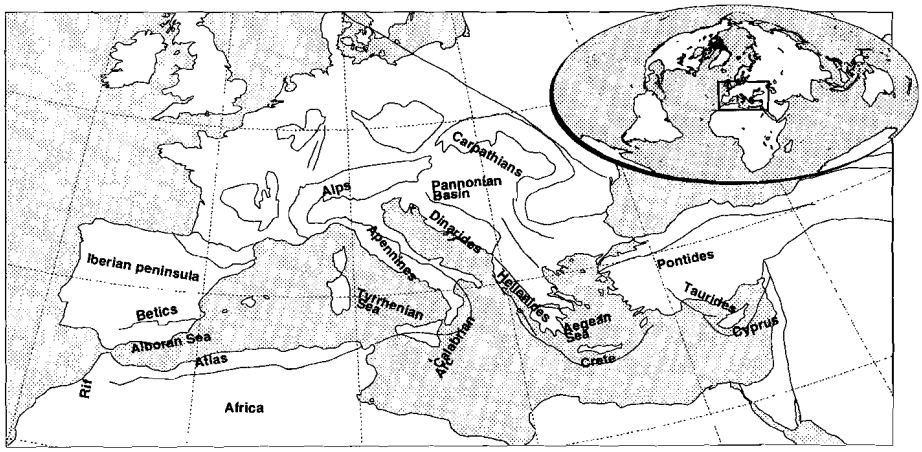

Figure 6. Location map of the study area.

Table 1. Overview of the mantle models $\mathbf{m}_s$ used for the resolution tests.

name	model/inversion feature	random noise	systematic noise
TEST-1	noise free, station and event locations fixed	-	-
TEST-2	moderate noise level, also inversion for station and event corrections	0.5s	-
TEST-3	high noise level, also inversion for station and event corrections	0.75s	-0.75s
TEST-4	no structure below 410km, high noise level	0.75s	-0.75s
TEST-4b	no structure below 410km, moderate noise level	0.5s	-
TEST-5	no structure below 145 km, high noise level	0.75s	-0.75s
TEST-5b	no structure below 145km, moderate noise level	0.5s	-
TEST-6	no structure between 120 and 410 km, high noise level	0.75s	-0.75s
TEST-6b	no structure between 120 and 410 km, moderate noise level	0.5s	-
TEST-7	no structure between 120 and 170 km, high noise level	0.75s	-0.75s
TEST-7b	no structure between 120 and 170 km, moderate noise level	0.5s	-
TEST-8	resolution for shallow low velocity layer, moderate noise level	0.5s	-

All experiments are performed with the matrix **A** from Remkes and Spakman [1993]. We have used the same regularization parameters and number of iterations (30) for the LSQR algorithm [Paige and Saunders, 1982] to calculate the least-squares solution. The 1.7 million ray-paths that determine the matrix are calculated with the PM4 reference velocity structure and with actual seismic events and stations. Because of the distribution of stations and events, the ray-paths sample the model volume unevenly (Figure 7). The best sampling is obtained in the central part of the model, while poorly sampled areas are most notable along the North African margin (especially near the Iberian peninsula and Tunisia, at the southern edge of the model). The variation in ray density affects the amplitude recovery when only a limited number of LSQR iterations are carried out. In general low ray density correlates with an underestimation of anomaly amplitudes, while high density correlates with good amplitude recovery. It is therefore important to take the ray density into consideration when interpreting tomographic results.

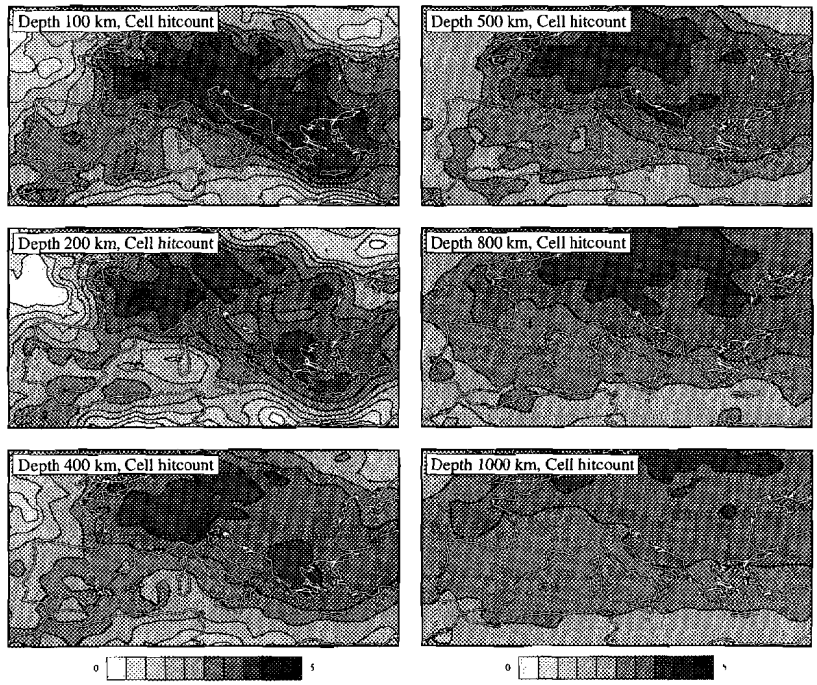

Figure 7. ^{10}log of the number of rays intersecting a cell of the model volume ('hitcount'), shown at different depths. Ray geometry is computed from the reference model PM4 (Figure 2).

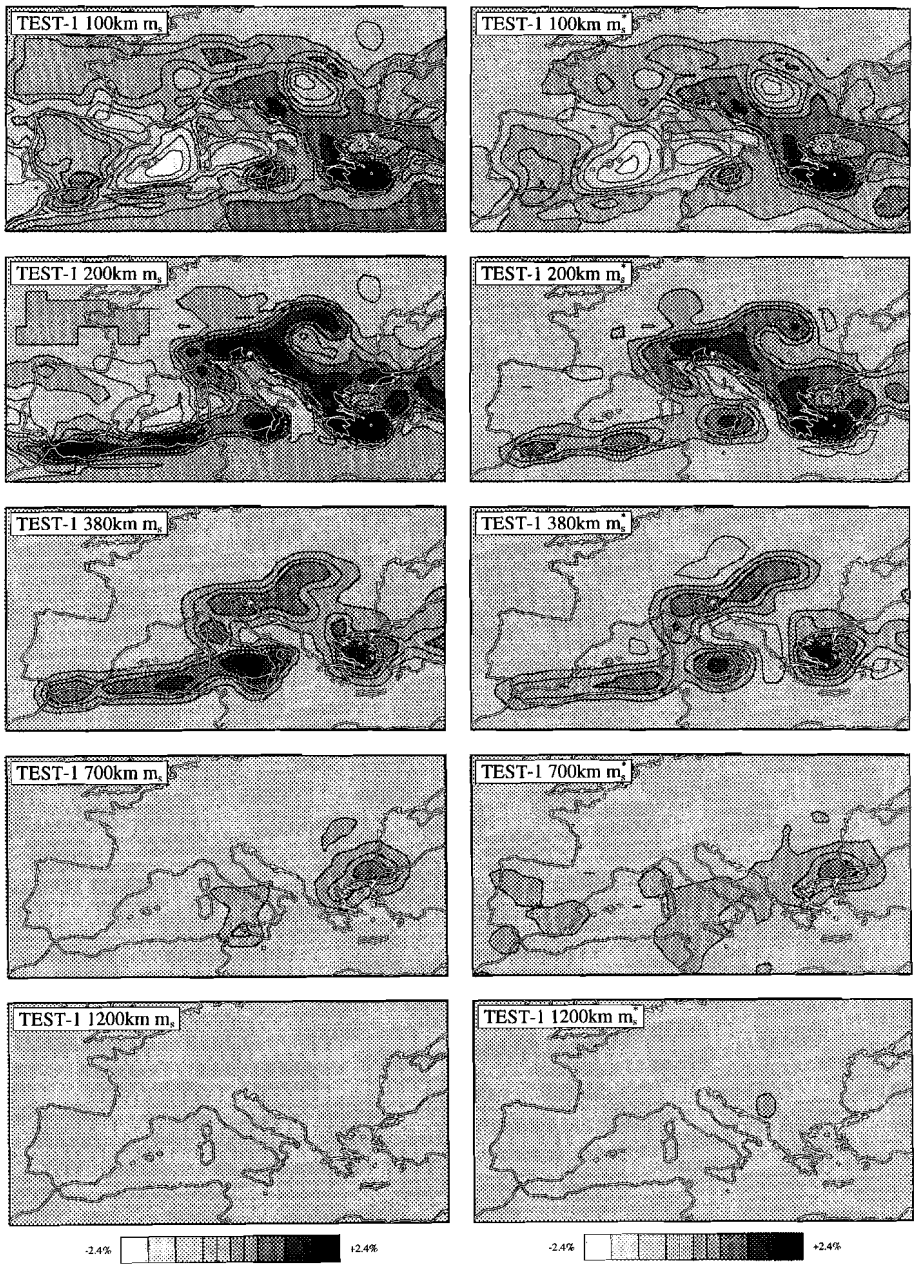

Figure 8. TEST-1, forward model $\mathbf{m_s}$ (left) and its tomographic image $\mathbf{m_s}^*$ (right), displayed are some selected slices. Velocity anomalies are plotted as percentages of the ambient mantle velocity (PM2 for EUR89B and PM4 for the others). The left column also shows the forward model for Figures 9 and 10.

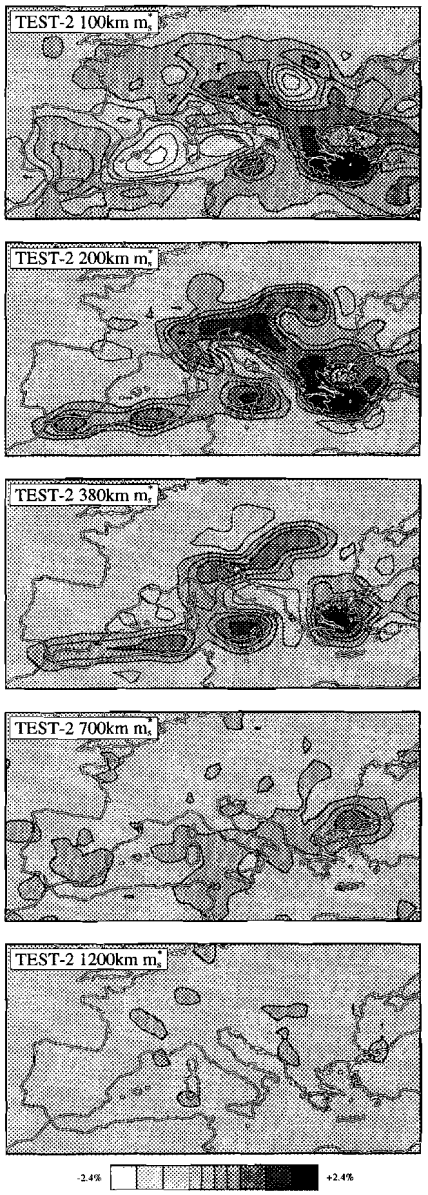

Figure 9. TEST-2, tomographic image of the forward model of TEST-1 (shown in the left column of Figure 8), in the presence of normally distributed synthetic random noise with μ=0 s and σ= 0.5 s in the delay-time data vector.

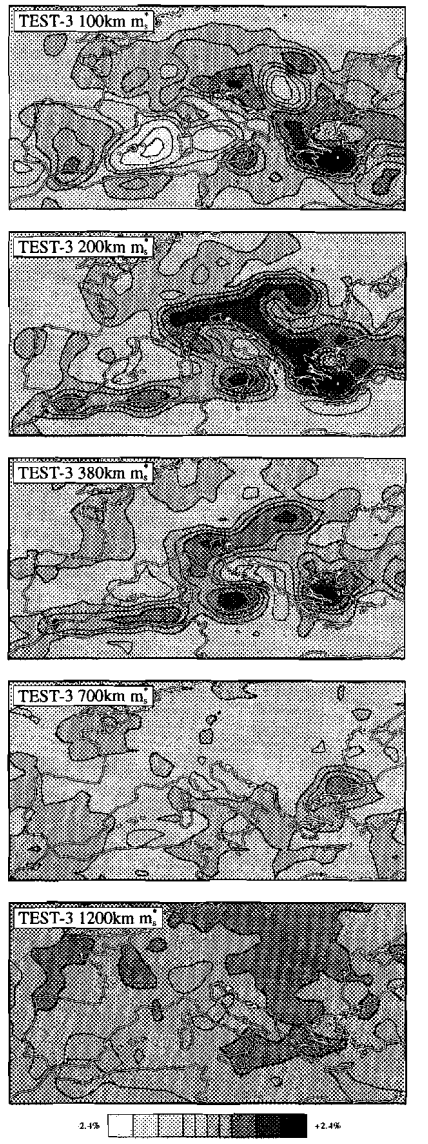

Figure 10. TEST-3, tomographic image of the forward model of TEST-1 (left column of Figure 8) with an additional high-velocity layer at 1200km depth, in the presence of synthetic normally distributed random noise (μ=0 s, σ=0.75 s for events inside the cell model and μ=-0.75 s, σ=0.75 s for teleseismic events).

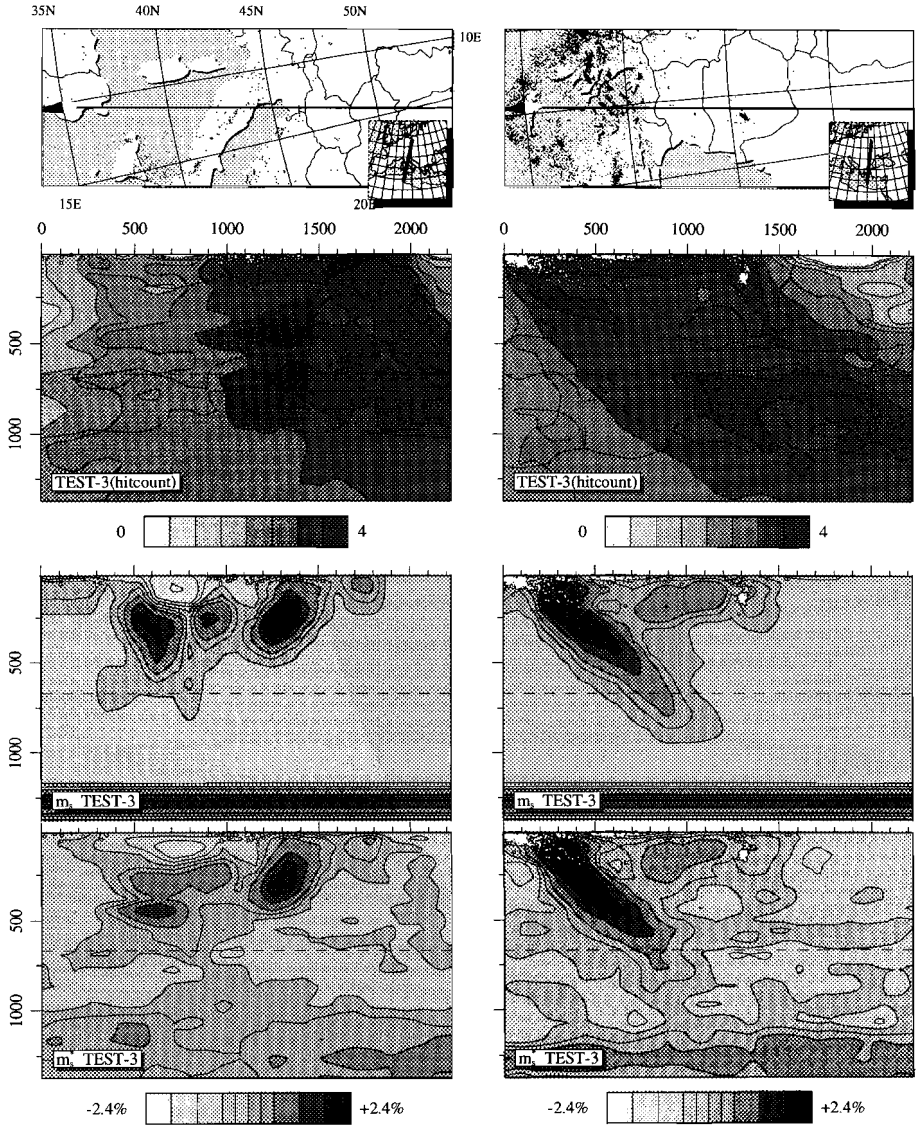

Figure 11. Vertical cross-sections through the results of TEST-3. Sections displaying the ^{10}log of the hitcount (top), the forward model (middle) and its tomographic image (bottom) are shown.

Experiments

TEST-1. The best resolved image is based on noise-free synthetic delay times (the equation $\mathbf{d}_s=\mathbf{A}\mathbf{m}_s$ is then consistent). This test allows us to separate effects of varying ray density from effects of noise on the tomographic image. Also, the result of this inversion serves as a reference for comparison with subsequent results. Imaging artefacts are primarily related to lack of resolution as 'anomaly smearing' along dominant ray directions and insufficient convergence due to the limited number of LSQR iterations. Figure 8 shows the results of this experiment. In regions that are well sampled by ray-paths, we find only small differences between $\mathbf{m}_s$ and $\mathbf{m}_s^*$. Both the amplitude and the spatial distribution of the anomalies in $\mathbf{m}_s$ are quite accurately imaged in $\mathbf{m}_s^*$. Notable differences in amplitude recovery are caused by an imperfect sampling of the cells by rays (largest differences occur in the least sampled cells, see Figure 7) combined with incomplete convergence to the least-squares solution of the LSQR algorithm. This test shows that the seismic rays derived from the stations and events, are sufficient to resolve mantle structure in the Mediterranean region as described by the DRC-III model. Amplitude recovery is near 90% in the best sampled areas (e.g. the Alps and the Aegean area). Amplitude recovery in the poorly sampled areas is much less (e.g. below the North African margin, the Iberian peninsula, and Turkey), but a good correlation between anomaly patterns in $\mathbf{m}_s$ and $\mathbf{m}_s^*$ remains. Low-amplitude resolution artefacts, which are visible in the slices at 700 km and 1000 km, result from a lack of depth resolution.

TEST-2. With this experiment we assess the sensitivity of the inversion to moderate, random, data errors. For this purpose we add normally distributed random noise to $\mathbf{d}_s$ with an average value $\mu=0$ s and standard deviation $\sigma=0.5$ s. The result is shown in Figure 9. As in TEST-1 the correspondence between input structure ($\mathbf{m}_s$) and tomographic image ($\mathbf{m}_s^*$) is quite good. The effects of noise on the image are reflected by the more irregular shapes of the artefacts that were already present in results of TEST-1. Amplitude recovery of the anomalies ranges from 80% in the well-sampled areas to 20% in some poorly sampled regions, e.g. below the African margin. The spatial variation of the anomaly patterns is imaged well throughout the model volume.

TEST-3. The cell model we use for the inversion covers only a small part of the Earth's mantle (Figure 1). However, in our inversion we also use data from events and stations at teleseismic distances (e.g. the North Western Pacific). It is important to find out to what extent delay-time signal acquired outside the cell model may be mapped into spurious heterogeneity inside the model. In the model parameterization, station parameters and event mislocation parameters are also (besides their literal purpose) included with the aim to absorb delay-time signal acquired outside the cell model. For TEST-3 we add noise to the synthetic delay times with a systematic component of $\mu=-0.75$s, $\sigma=0.75$s for all rays originating outside the model volume, and random noise with $\mu=0$s, $\sigma=0.75$s for all other rays. The systematic noise component mimics strong, on average positive, velocity anomalies outside the model volume (the

signal to noise ratio in this experiment is approximately 1). We furthermore modify the mantle model $\mathbf{m}_s$ by adding a high-velocity layer (of +2% anomaly value) at a depth between 1200 and 1300 km inside the model volume. Rays coming in from distances larger than 60° sample this high-velocity layer. Figures 10 and 11 show the result of the inversion in horizontal and vertical sections through the model. The recovery of anomaly amplitudes of $\mathbf{m}_s$ is typically 70% for the well -sampled areas. In both the well and the poorly recovered regions the anomaly patterns are mapped well. The artificial high velocity layer at 1200 km depth shows up in the inversion results and it does not leak significantly into spurious slab structure inside the model volume. Furthermore, amplitudes of imaging artefacts are still small compared to the structure present in the input model.

Comparison of calculated station delays and event location corrections for this inversion and those of TEST-1 and TEST-2 shows that the systematic errors introduced in TEST-3 are largely accommodated by these parameters. This test leads us to conclude that the tomographic method (ray-paths, model parameterization and inversion) can image mantle structure $\mathbf{m}_s$ well, even in the presence of high noise levels and of an on average faster mantle outside the model.

As already mentioned, TEST-1 to TEST-3 give no clear indication on the possibility of internal smearing within the modelled slabs. The next tests deal with this potential problem.

(continued on page 117)

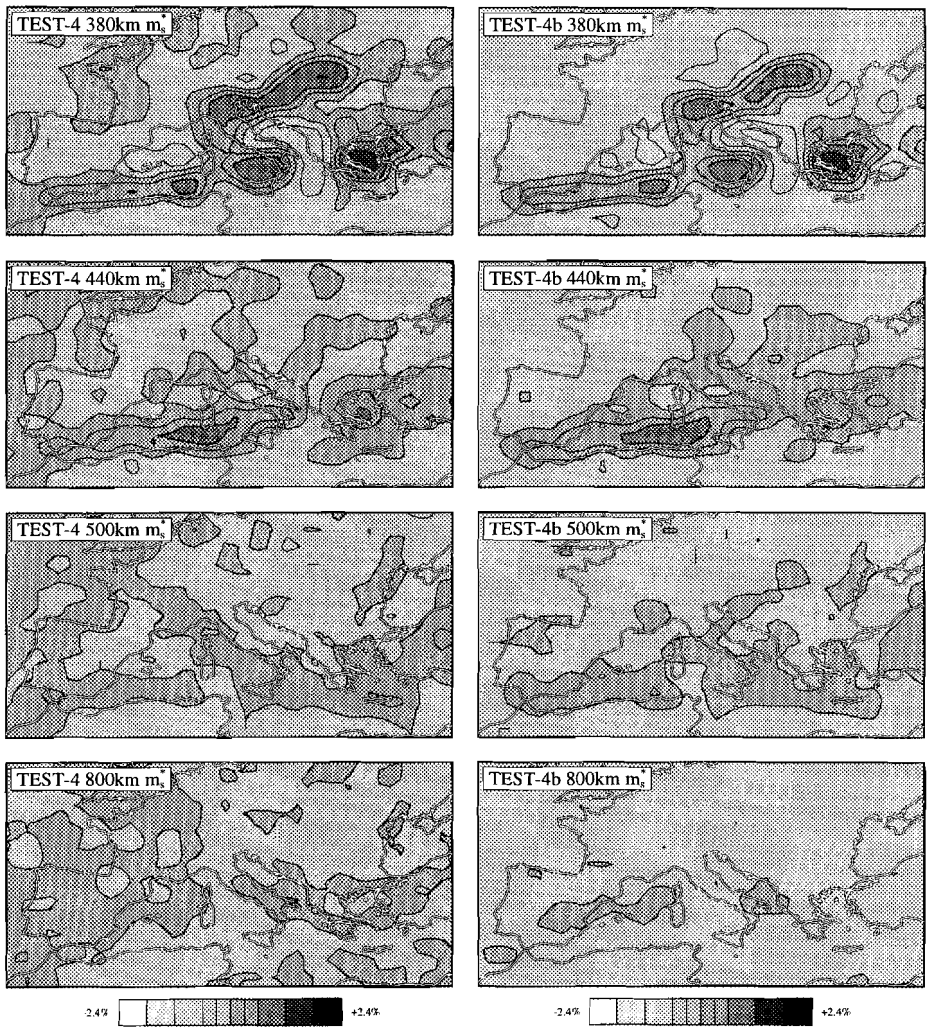

Figure 12. TEST-4. The forward model was truncated at 410km depth. Shown are tomographic results with synthetic noise levels μ=0/-0.75 s and σ= 0.75 s in TEST-4 and μ=0 s and σ= 0.5 s in TEST-4b. All imaged structure below the top panels consists of down-dip 'smearing' of the velocity structure.

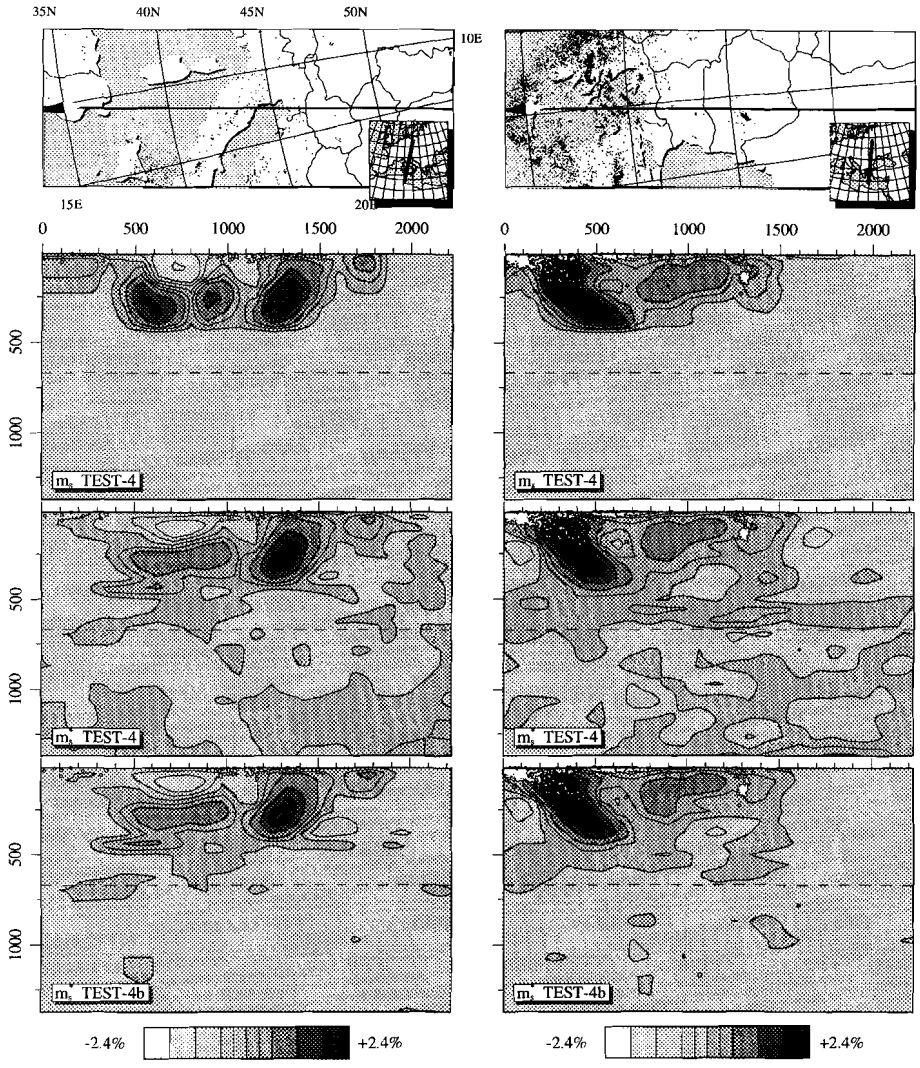

Figure 13. TEST-4. Vertical sections through the same models as shown in Figure 12. The top panel shows the truncated input model.

TEST-4 and TEST-4b. For TEST-4 and TEST-4b we modify $\mathbf{m}_s$ by setting all amplitudes of anomalies to 0% below 410 km depth before calculating $\mathbf{d}_s$. The inversion is subsequently carried out with two different noise levels. In TEST-4 we add the same high random and systematic errors that we used for TEST-3. For comparison, TEST-4b is performed with the same mantle model $\mathbf{m}_s$, but using only normally distributed noise of μ=0 s, σ=0.5 s (the same as in TEST-2). The purpose is to investigate the possibility that slab-like images below 410 km are generated by a combination of structure above 410 km and anomalous high-velocity structures outside the model volume. The results of the two experiments are illustrated with Figure 12.

The top row of panels in this figure show the imaged structure in the cell layer immediately above 410 km, where structure is still present in the input model $\mathbf{m}_s$. At this depth the results should be well comparable to TEST-3 and TEST-2, except where lack of depth resolution is significant. In the second row of Figure 12 we observe that 40 km below the cutoff level the velocity anomalies correlate with those in the overlying level, which indicates that signal from the overlying level leaks downwards. This effect is strongest for the North African margin (which is poorly sampled by ray-paths) and it also exists to a smaller extent below the Aegean. For the Alpine (ss) and Dinaride chains vertical leakage is much less. Amplitudes of the artefacts associated with this smearing are generally less than 0.6%. In the Aegean region, at a depth of 500 km (90 km below the cutoff level), the amplitude of artefacts has decreased to less than 0.3% in the vicinity of the 3% anomalies. Below 600 km random imaging errors predominate. Figure 13 illustrates the results in two cross-sections. The left-hand side of the left panels shows the poorly sampled North African margin, while the right-hand side shows the well-sampled Alpine belt. The right panels give a cross-section through the (also well-sampled) Aegean region. Smearing of anomalies in the depth direction is restricted to the first 50 to 100 km below 410 km for the well-sampled regions. Below the North African margin a similar pattern is found, with somewhat stronger and deeper reaching artefacts due to poorer sampling. Results of TEST-4 exhibit more imaging artefacts than those of TEST-4b because of the higher systematic and random noise levels imposed on the synthetic delay-time data. We conclude from these tests that slab images deeper than 410 km are neither generated by structure above this level nor by an anomalous high-velocity mantle outside the model volume.

(continued on page 122)

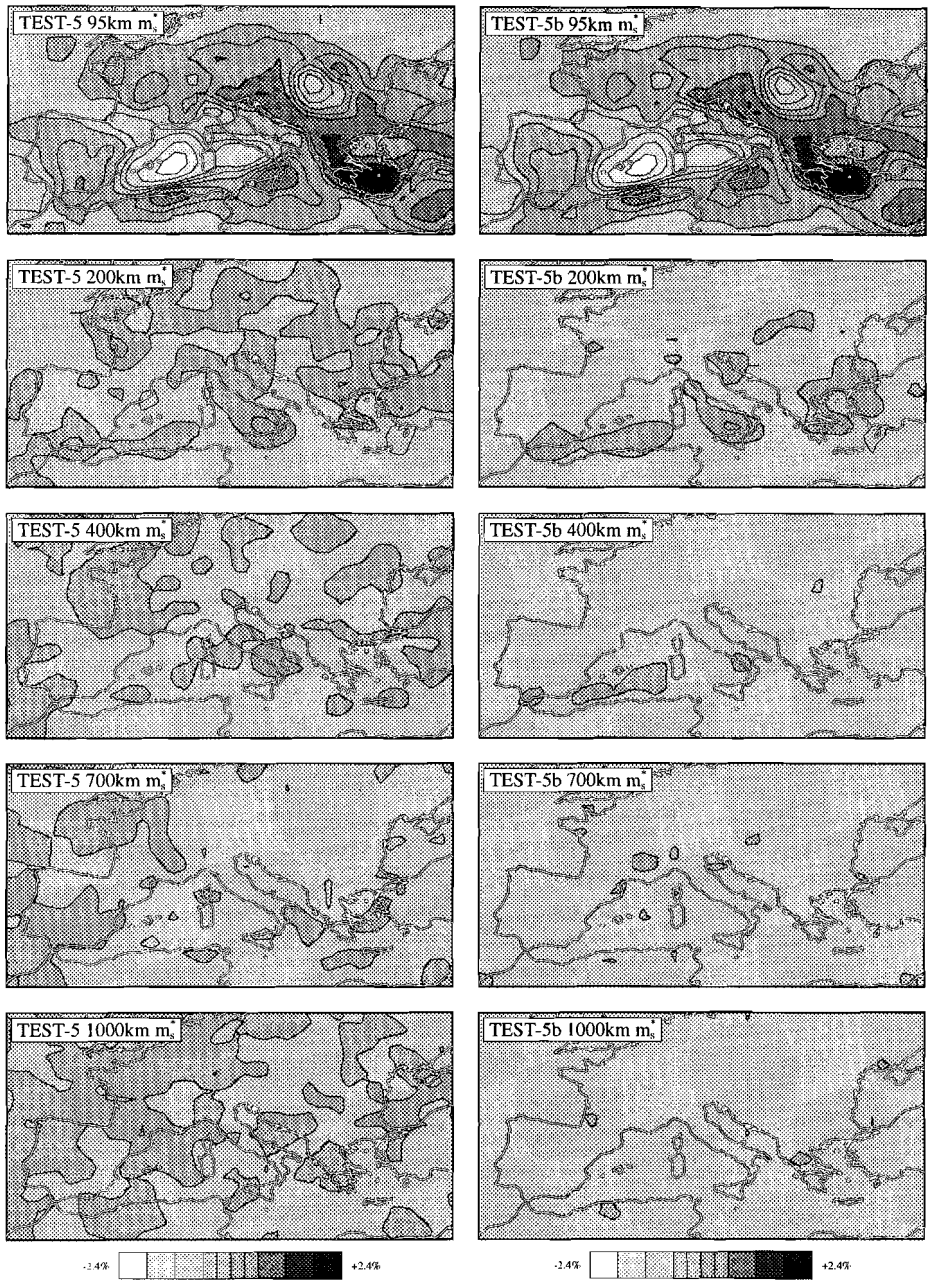

Figure 14. TEST-5. All velocity structure in the synthetic model was moved vertically to the depth level above 145 km. Shown are tomographic results with synthetic noise levels μ=0/-0.75 s and σ= 0.75 s in TEST-5 and μ=0 s and σ= 0.5 s in TEST-5b.

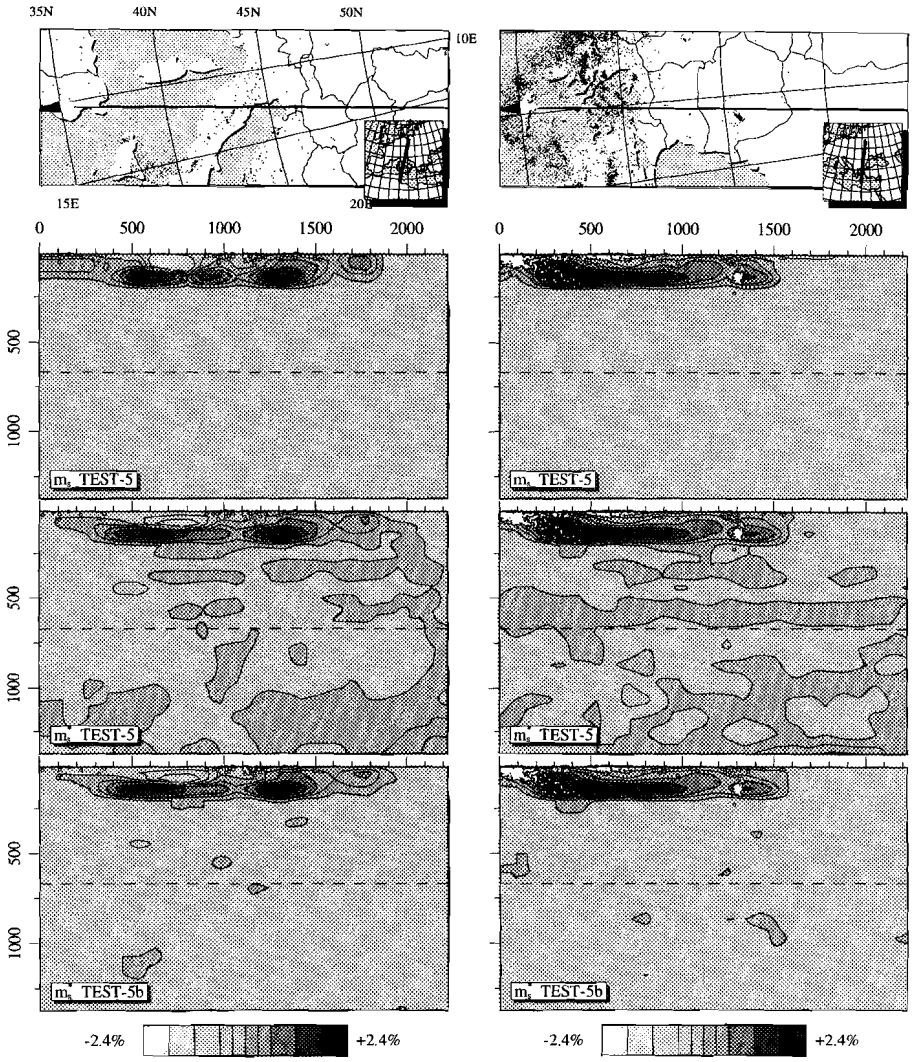

Figure 15. TEST-5. Vertical section through the models shown in Figure 14.

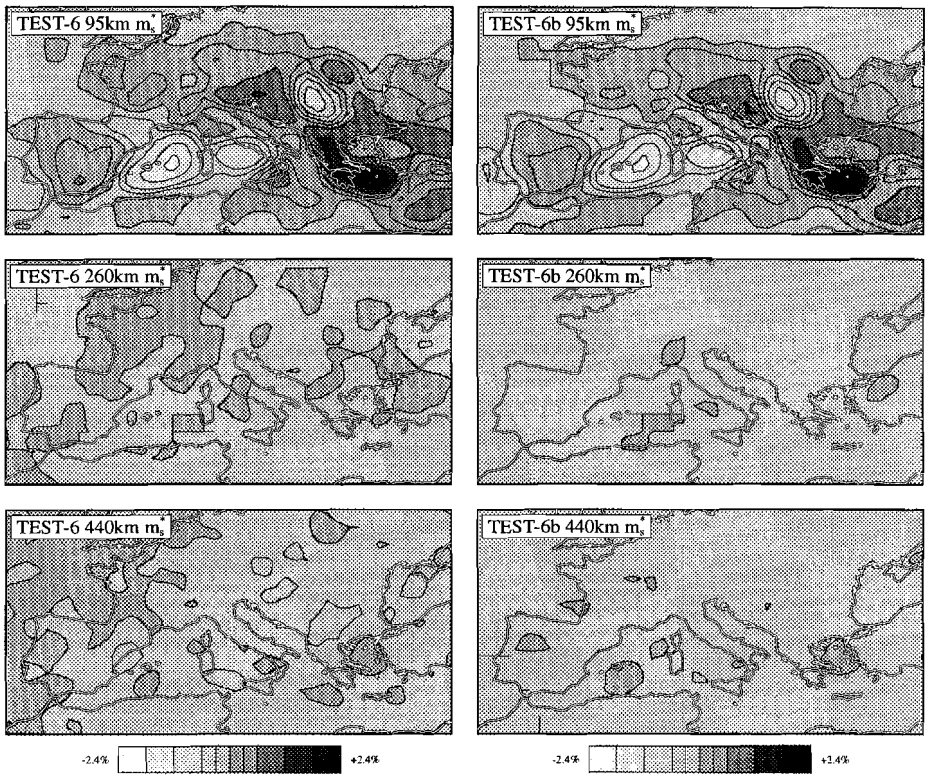

Figure 16. TEST-6. Resolution test for discontinuous slabs. Input models are set to 0% between 170 and 410 km. Shown are tomographic results with synthetic noise levels μ=0/-0.75 s and σ= 0.75 s in TEST-6 and μ=0 s and σ= 0.5 s in TEST-6b.

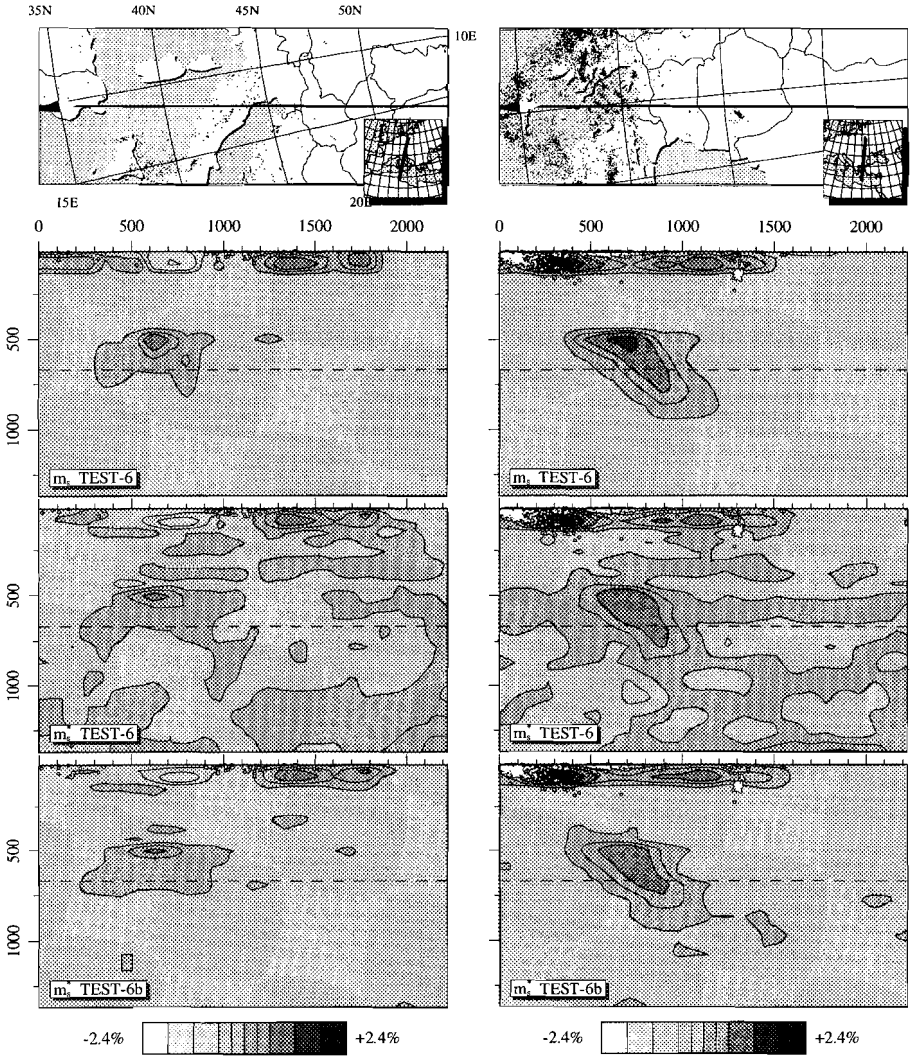

Figure 17. TEST-6. Vertical sections through the models shown in Figure 16

TEST-5 and TEST-5b. The problem we address in TEST-5 and TEST-5b is similar to that of TEST-4 and TEST-4b. Here we use a mantle model that only contains structure in the upper 145 km, to study an unperturbed mantle combined with a very heterogeneous lower lithosphere. We create the synthetic lithosphere anomalies for this model by vertical summation of the DRC-III structure to produce a model $\mathbf{m}_s$ that correlates laterally, but not in depth, with DRC-III. The P-velocity anomalies are scaled to reach a maximum of 6% to maintain a realistic upper limit on the amplitude of the velocity structure. Synthetic noise levels are the same as those used in TEST-4 and TEST-4b (Table 1). Figure 14 shows results of TEST-5 and TEST-5b in horizontal cross-sections and Figure 15 in vertical cross-sections. The inversion does not result in severe leakage of the high-amplitude velocity anomalies from the lithosphere into the underlying mantle: amplitudes of artefacts are well below 0.3%. We conclude from TEST-5 that vertical smearing of lithosphere structure (above 145 km) does not generate slab images in the upper mantle (between 145 km and 410 km), not even in the presence of high noise levels.

TEST-6 and TEST-6b. The experiments TEST-6 and TEST-6b are performed with a mantle model designed to further study the resolution at upper mantle depths. The input structure $\mathbf{m}_s$ contains no anomalies between depths of 120 and 410 km. Normally distributed, random and systematic noise components are added as in TEST-4 and TEST-4b, respectively. In Figure 16 the top and bottom panel rows show the structure just above and below the void depth interval, all structure visible in the middle row therefore consists of imaging artefacts. Figure 17 again gives two cross-sections computed from TEST-6. We observe that wide gaps in a synthetic subduction zone are well imaged in the inversion results. Structure in the overlying and underlying layers does not leak significantly into the depth range between 120 and 410 km and structure below 410 km is still imaged reliably.

(continued on page 125)

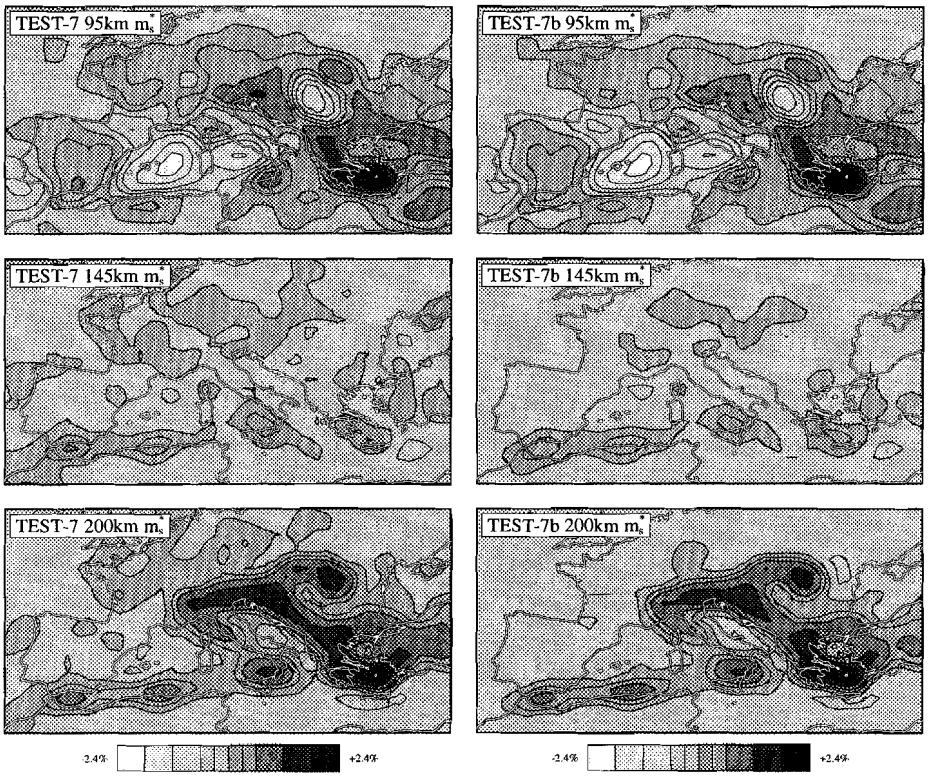

Figure 18. TEST-7. Resolution test for discontinuous slabs. Input models are set to 0% between 120 and 170 km (middle row is empty). Shown are tomographic results with synthetic noise levels μ=0/-0.75 s and σ= 0.75 s in TEST-7 and μ=0 s and σ= 0.5 s in TEST-7b.

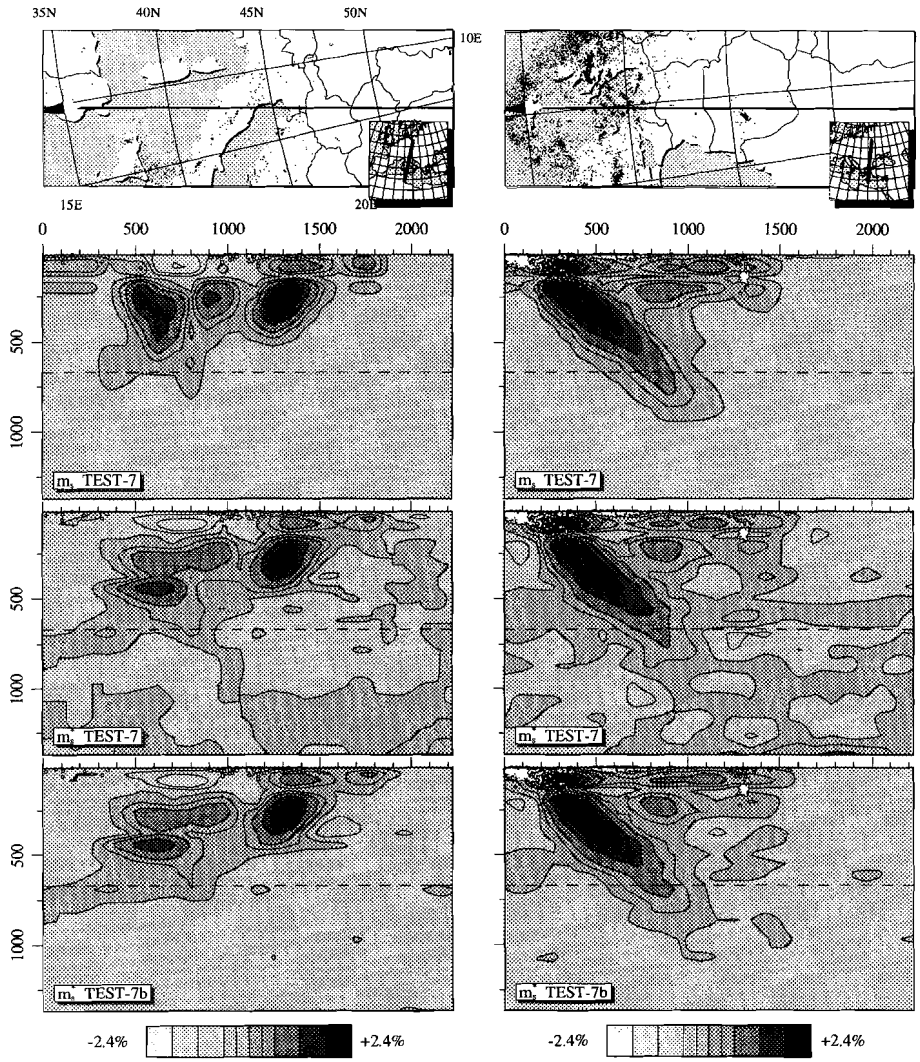

Figure 19. TEST-7. Vertical sections through the models shown in Figure 18.

TEST-7 and TEST-7b. This experiment is aimed at studying the depth resolution for small scale structure near a depth of 150 km (especially inside the subducted slab). We create the mantle structure for experiments TEST-7 and TEST-7b by replacing the anomaly amplitudes between 120 and 170 km from the velocity structure of DRC-III by 0% values. This depth range is interesting because here gaps are observed in slab images of the models EUR89B and EUR93 (real data inversions). These gaps have been interpreted as indications for slab detachment ('break-off') [Spakman et al., 1988; Wortel and Spakman, 1992,1993]. In TEST-7 and TEST-7b the synthetic noise is again the same as that of TEST-4 and TEST-4b, respectively. Figure 18 illustrates the results for three layers (above, inside, and below the gap) and Figure 19 for vertical cross-sections. For the less sampled areas (e.g. the African margin), we observe that a narrow gap in the high-velocity structure will *not* be imaged at this depth level, but it is well resolved in well sampled areas (Alps and Aegean). Therefore, at depths around 150 km vertical ray-path smearing may obscure the finer detail of the mantle structure in poorly sampled regions, but not in well sampled parts of the model.

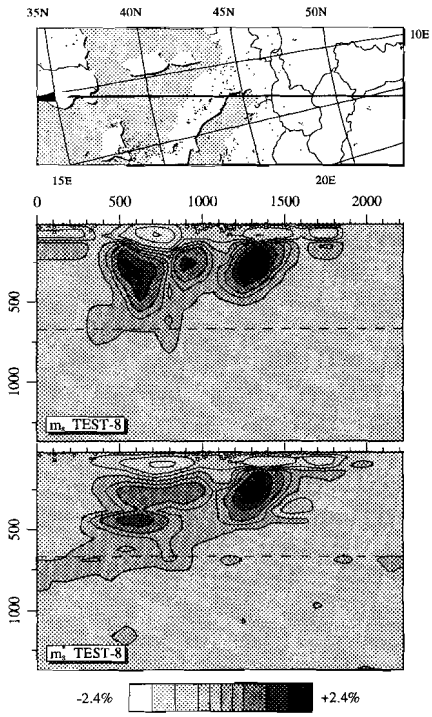

Figure 20. TEST-8. Resolution test for a low-velocity layer. Input models created by inverting the sign of anomalies above 170 km. Shown are tomographic results with synthetic noise levels μ=0 s and σ= 0.5 s.

TEST-8. Because the features predicted from forward modelling consist mainly of high velocity material, TEST-8 is added specifically to investigate the effect of low-velocity heterogeneity. In this test the mantle structure $\mathbf{m}_s$ contains an artificial low velocity layer between 18 and 170 km (produced by inverting the sign of the structure of DRC-III in this depth range). Most ray-paths sample this layer. The results of this experiment are shown in Figure 20. We find that the low-velocity layer is accurately imaged in both well and poorly sampled areas.

Conclusions on the imaging quality of the tomographic mapping

The previous experiments were dedicated to the problem of how well the complex three-dimensional slab structure of the Alpine-Mediterranean region can be imaged by seismic travel-time tomography. We conclude from our experiments that the tomographic method (rays, reference models, and inversion method) employed by Spakman et al. [1993] and Remkes and Spakman [1993] can well image the predicted mantle structure of the Alpine-Mediterranean region. The tomographic image $\mathbf{m}_s^*$ shows a good correlation with its input structure $\mathbf{m}_s$, both in spatial distribution and in amplitude of the anomalies in regions with high ray-path sampling (TEST-2, TEST-3). When the sampling of rays is less dense, the recovered image exhibits an underestimate of the velocity structure, but the correlation of spatial extent and sign of the anomalies remains good. From the experiments we also infer that the effects of anomaly smearing in the interior of slabs are only minor (TEST-4, TEST-5, TEST-6). Furthermore the resolution for small scale features (with both positive and negative velocity anomalies) is good in regions where the ray sampling is moderate to high (TEST-7, TEST-8).

In poorly sampled parts of the model volume the exact position of the leading edge of a subduction zone is imaged with an uncertainty of approximately 100 km (TEST-2, TEST-3). This means that in those regions the type-3 misfit errors make comparison of the depth extent of predicted subducted slabs and tomographic images less feasible. We observe that, for the poorly sampled parts of the mantle, the imaged amplitude of the anomalies and the resolution of finer detail is significantly less than that for the well-sampled regions.

We conclude that high-velocity material outside the studied volume does not lead to significant type-3 errors in the form of slab-shaped anomalies, neither in the moderate nor in the high noise level tests (TEST-4b to -7b and TEST-4 to -7, respectively). The station corrections and event origin time errors for which is inverted absorb most of the delay-time signal acquired along ray segments outside the model volume. Overall, we find that the results corroborate the inferences of Spakman et al. [1993]. These authors, however, based their conclusions on synthetic models that do not correlate in any sense with the actual mantle structure in the region.

4.5 Assessing the quality of the tectonic reconstructions

The imaging quality found for mapping $\mathbf{m}_s$ on $\mathbf{m}_s^*$ (the bottom path of Figure 5) gives similar confidence that the solution of $\mathbf{Am}=\mathbf{d}_e$ will also yield a reliable image $\mathbf{m}_e^*$ of the real mantle structure $\mathbf{m}_e$ (the top path of Figure 5). Since we can now separate the type-3 misfit from other sources of discrepancy we can use the image $\mathbf{m}_e^*$ to test the quality the forward models. We will first study

the overall correlation of anomalies in a typical $\mathbf{m}_s^*$ and $\mathbf{m}_e^*$, and subsequently we will address the differences between models based various tectonic reconstructions.

Overall fit of forward and inverse results

With the forward modelling approach of de Jonge et al. [1993, 1994], the structure of the mantle is predicted under the assumption that subduction zones consist of large plate-like bodies extending down from the surface into the mantle. These authors noted from a direct comparison of $\mathbf{m}_s$ and $\mathbf{m}_e^*$ that, although at deeper levels of the mantle the general correlation between the two models was good, there are many differences visible between forward models and tomographic images of the Alpine-Mediterranean mantle. In this section we will compare the image $\mathbf{m}_s^*$ of one of their models (DRC-III by de Jonge et al. [1993]) with EUR93 of Remkes and Spakman [1993].

In Figure 21 we show horizontal cross-sections through the forward model ($\mathbf{m}_s$), its image ($\mathbf{m}_s^*$), and the inverse model ($\mathbf{m}_s^*$). From inspection of Figure 21 we conclude that $\mathbf{m}_e^*$ and $\mathbf{m}_s^*$ exhibit anomaly patterns with very similar spatial scale and spatial variation.

All predicted models and their images have higher anomaly amplitudes than the tomographic results above 450 km and lower amplitudes below this depth. This suggests that the depth-dependent $\partial V_p/\partial T$ of de Jonge et al. [1993,1994] introduces a minor type-2 misfit. The uncertainty range these authors give for this parameter is approximately 30%, so a scaling error of 1% anomaly value in the largest predicted velocity anomalies is within the expected accuracy of the forward modelling. It is in fact possible to vary the value $\partial V_p/\partial T$ within this error margin so that the anomaly amplitudes in synthetic models show a much closer correspondence to the tomographic results. If such variations can be shown to have physical meaning, they contain important information on the in-situ temperature dependence of elastic and anelastic properties of mantle material.

Differences between DRC-III and EUR93 may result from the fact that in DRC-III no processes are modelled that produce low-velocity structures at large depth. Therefore, these low-velocity regions in EUR93 cannot be present in DRC-III. Another difference results from the fact that the high velocity region below the Ukrainian shield observed in the top rows of EUR93 was not part of the DRC-III model. Furthermore, the models resulting from the inversion of real delay times show more detail than the predicted models.

Closer inspection of Figure 21[†] shows in the shallowest level (100km) a good correlation between $\mathbf{m}_s$ and $\mathbf{m}_s^*$, which means type-3 errors are limited.

[†] Next page: Figure 21. Horizontal cross sections through a typical synthetic model (DRC-III by de Jonge et al. 1993], its tomographic image and a model based on tomographic inversion of real delay-times (EUR93 by Remkes and Spakman [1993]).

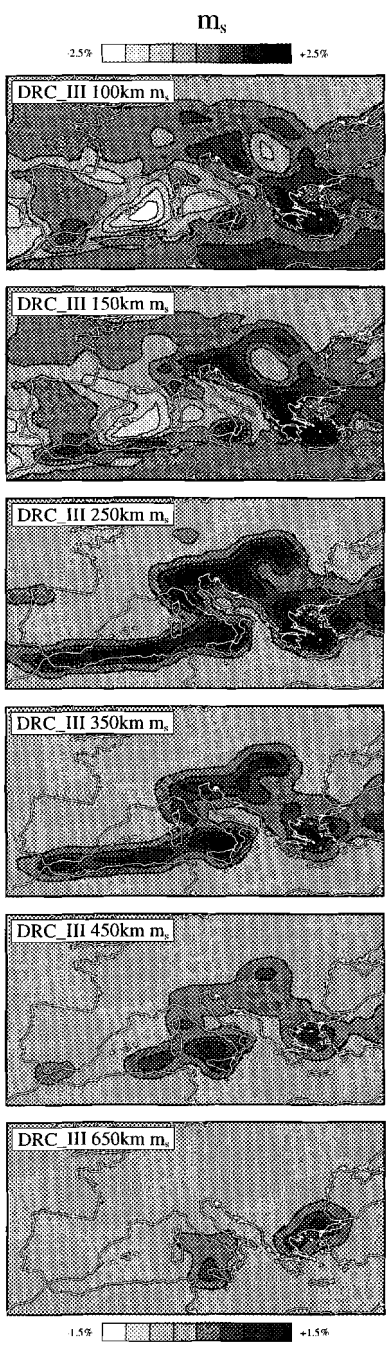

Figure 21.

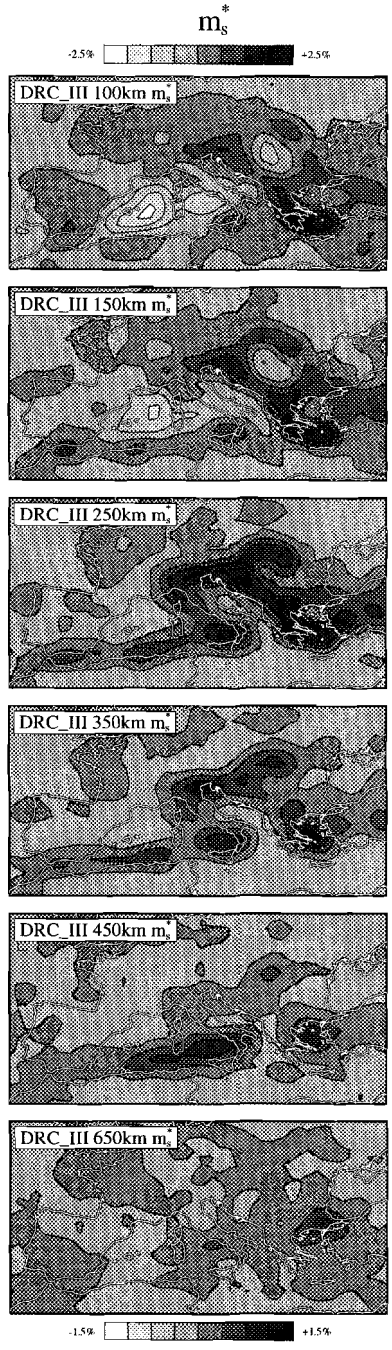

Figure 21. continued.

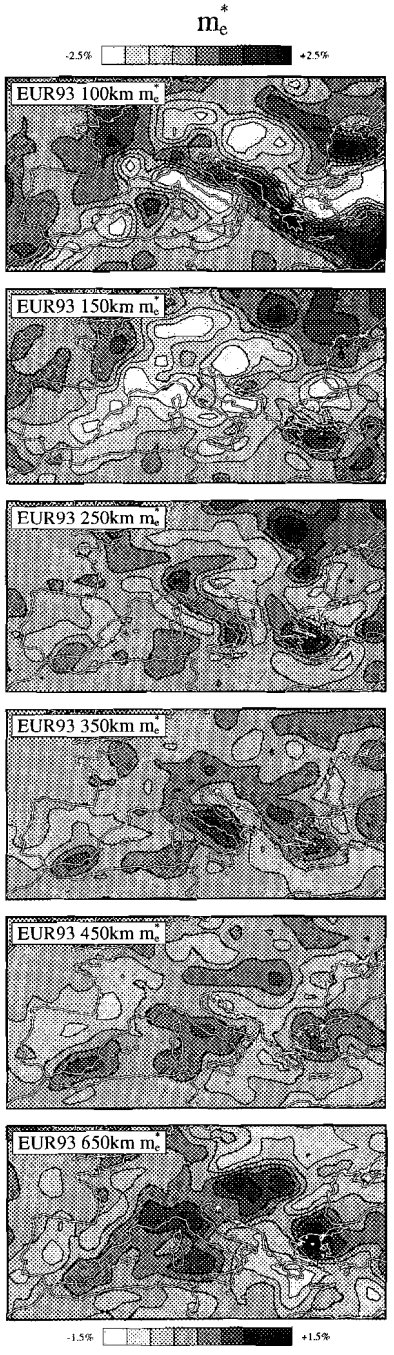

Figure 21. continued.

We find on the other hand a poor correlation between $\mathbf{m}_s^*$ and $\mathbf{m}_e^*$. A cause of this discrepancy may be a type-2 error: in the forward models the effect of variation of lithosphere composition on the velocity anomalies is ignored.

The second row of Figure 21 shows sections through the models at 150 km. At this depth level all synthetic models tested show the same pattern of discrepancies between forward and inverse models: the pronounced low-velocity structure below the Apennines and the Calabrian Arc that is imaged in EUR93 is absent in DRC-III. In vertical sections through EUR93 and EUR89B, this low-velocity region appears to cut across high velocity features. This observation led Spakman et al. [1988] and Wortel and Spakman [1992] to propose the hypothesis that subducted slabs may have become detached from the surface in these regions. If this process causes the structure, the forward models again exhibit a type-2 error because detachment of lithosphere is not modelled.

The third row of Figure 21 shows a depth level (250km) where the correspondence between DRC-III and EUR93 models is better. The general structure of high-velocity anomalies associated with the Alps, the Apennines, the Hellenides, and the Alboran region is present in all slices. Below the African margin, the marked drop in magnitude in the mapping of $\mathbf{m}_s$ on $\mathbf{m}_s^*$ (type-3 misfit) explains why the tomographic image shows only a minor effect of this subduction. This effect is also visible when comparing the lower left corners of the panels:

the large anomaly below southern Spain, predicted from the tectonic reconstruction, is imaged as a rather small anomaly both in the inversion of the predicted model delay times and in the inversion of real delay times. A similar observation can be made for the eastern side of the Mediterranean region. Especially below the Tauride and Pontide chains in Turkey the predicted structure is imaged with reduced amplitude, which also explains the lower amplitudes found in the tomographic model EUR93. The reduced recovery of signal in regions with low ray-path coverage is a typical example of a type-3 error. Note also that the predicted high-velocity structure below the Carpathians and Dinarides is not found in EUR93 at this depth.

The fourth row of Figure 21 shows that the correlation between DRC-III and EUR93 has improved at 350 km depth; the only significant discrepancy at this depth is the absence in EUR93 of the high-velocity material predicted below the Carpathians. In the fifth row (at 450 km) the Carpathian anomaly has all but disappeared in DRC-III, whereas it now begins to show up in EUR93.

In the sixth row (at 650 km) the structure associated with subduction in the southern part of the model (Alboran, Apennines, and Hellenic arc) is still predicted fairly accurately. However, high-velocity anomalies that are not predicted with the forward modelling are still present in EUR93. These high velocity regions are associated with subduction below the Alps, Carpathians and Dinarides. We hypothesize that for the Carpathians this material represents the high velocity material predicted for the shallower sections, because the volume of lithosphere subducted appears to be correctly predicted (between 0 and 450 km depth for DRC-III, between 450 and 650 km depth for EUR93). This would constitute a type-2 misfit error associated with slab-detachment. A similar type-2 error may be present for the Dinarides, where high-velocity anomalies are found in EUR93 at large depth and in DRC-III at lesser depth. Below the Alps, however, the total amount of subducted material in DRC-III is substantially less than the structure of EUR93 would imply. In this case the tectonic reconstruction has given too little plate-convergence in this region (type-1 error).

The type-2 misfit errors introduced by ignoring the detachment does not preclude assessment of type-1 errors because the bulk amount of subducted lithosphere can still be accurately predicted; it is only its location in the mantle that causes the misfit between predicted and tomographic models. When we compare the results of different tectonic reconstructions in the next section, we can take this into account by focusing on the volume of the anomalies and not on their exact position.

We can furthermore corroborate the conclusion of De Jonge et al. [1993, 1994] that the tectonic reconstructions and the forward modelling method provide a useful tool to predict the structure of the lithosphere and mantle, and that conversely the tomographic images obtained from the inversion of seismic delay times can serve as a test for different tectonic hypotheses.

Table 2. Different forward models of the mantle structure ($\mathbf{m}_s$) tested in this section.

Model	Description
DRC-I	Based on Dercourt et al. [1986] reconstruction
DRC-II	DRC-I, alternative development of the Alboran region
DRC-III	DRC-I + Alpine tectonics from Dercourt et al. [1990]
DRW	DRC-I + Tyrrhenian tectonics from Dewey et al. [1989]

Comparison of different forward models

We will now investigate forward models for the Alpine-Mediterranean region controlled by different tectonic reconstructions (DRC-I, DRC-II, DRC-III and DRW, see also Table 2). Recall that the models follow from translating surface kinematics directly into the corresponding mantle flow, and have not been further constrained with a posteriori knowledge of the actual tomographic inversion results. This point needs to be stressed because it would be equally possible to construct forward models that are also controlled by explicit assumptions on slab-detachment. Such forward models can produce a better fit with tomographic results because they would possess the gaps in subduction zones as described for the panels at 150km of Figure 21, but their use as an independent test for the validity of tectonic reconstructions would be impeded.

Bearing this in mind, we will study the differences between some indicative parts of various forward models. These differences illustrate the type-1 errors and they thereby give an indication of the relative merits of the forward models.

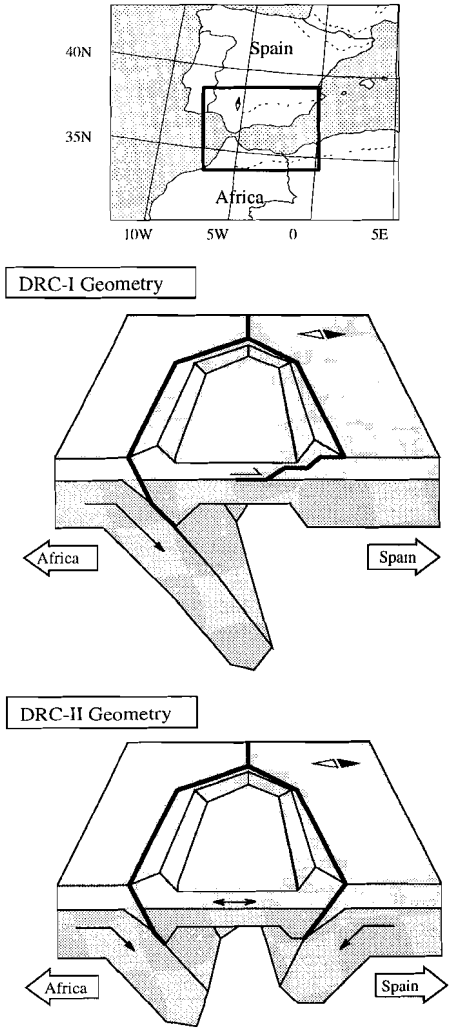

Figure 22. Schematic view of the tectonic setting and location of two possible reconstructions of the Alboran region, resulting in the DRC-I and DRC-II models of Figure 23.

Comparison of DRC-I and DRC-II. The models DRC-I and DRC-II are both essentially based on the tectonic reconstruction by Dercourt et al. [1986]. The difference between the two forward models exists in modelling either a single or a double subduction zone in the Alboran region (between Spain and Africa). Figure 22 shows a sketch of the two possible subduction geometries. De Jonge et al. [1994] have found that neither of these models produces a mantle prediction ($\mathbf{m}_s$) that compares well to tomographic results ($\mathbf{m}_e^*$, EUR89B of Spakman et al. [1993]). Their preliminary conclusion was that the tectonic reconstruction for this region was not very reliable (a type-1 error). However, when we compare the DRC-I and DRC-II $\mathbf{m}_s$ models shown in Figure 23 with their respective tomographic images $\mathbf{m}_s^*$ we see that in this region the tomographically recovered synthetic structures differ strongly from the original models (a type-3 error). Therefore, the tectonic reconstruction underlying these models may be better than a direct comparison of $\mathbf{m}_s$ and $\mathbf{m}_e^*$ suggests. The interpretation of a type-1 error by De Jonge et al. [1994] should be reconsidered in view of this type-3 error. From comparing the imaged synthetic structures $\mathbf{m}_s^*$ with EUR93 $_e^*(\mathbf{m})$ we conclude that the tomographic mapping of the actual mantle structure (bottom two panels of Figure 23) shows a closer resemblance to the image of DRC-I (left column of Figure 23). The correspondence with the (double slab) DRC-II model shown in the right column of Figure 23 is much less. Specifically, the (imaged) vertical extent of the subducted slab and the recovered amplitude of the velocity anomaly correspond better for DRC-I.

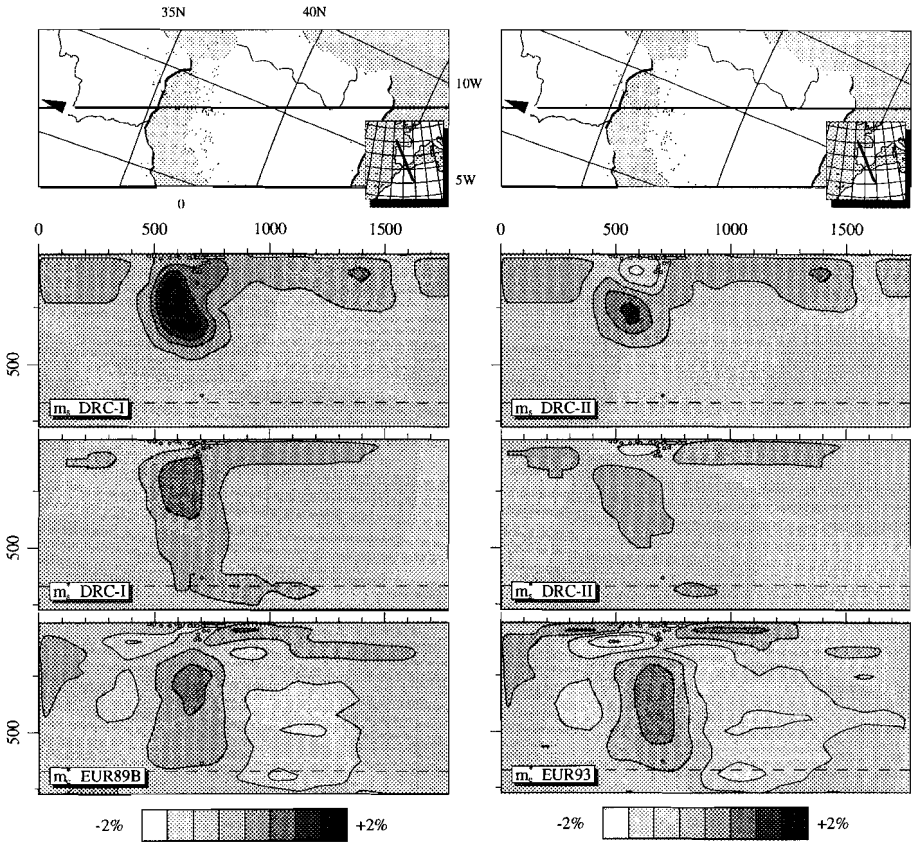

Figure 23. Two possible forward models of the Alboran region and inversion results (DRC-I and DRC-II). Bottom panels show the inversion results EUR93 by Remkes and Spakman [1994] and EUR89B by Spakman et al. [1993].

Our interpretation for plate-tectonic processes is therefore that the plate contact between Africa and Spain is better described in a setting dominated by a single subduction zone.

The low velocity layer overlying the African side of the top of the Alboran slab (as visible in $\mathbf{m}_e^*$) is not clearly found in either DRC-I or DRC-II. The resolution tests performed in the previous sections and those carried out by Blanco and Spakman [1993] suggest that this feature is not an artefact of the tomographic imaging. We therefore conclude that in this region an anomalously low velocity may be actually present above the subducted slab, which is in

accordance with the detachment interpretation given by Blanco and Spakman [1993] and Platt and Vissers [1989].

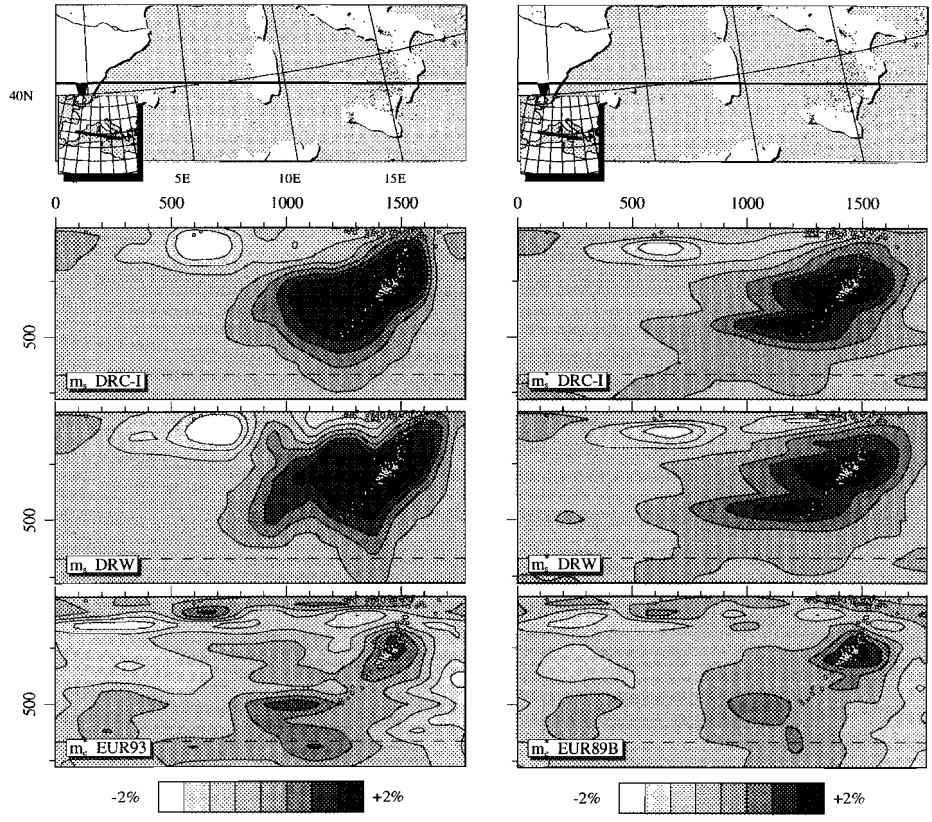

Figure 24. Comparison of two forward models of the Calabrian arc (DRC-I and DRW) and the inversion results of real seismic data (EUR89B and EUR93).

Comparison of DRC-I and DRW. The mantle models DRC-I and DRW are based on two different tectonic reconstructions of the development of the Tyrrhenian region. The model DRC-I is described in the previous section; the kinematics of the Tyrrhenian region for DRW are derived from the tectonic reconstruction by Dewey et al. [1989]. Figures 24 and 25 show two cross-sections through the model volumes. In Figure 24 we see that the predicted

mantle structure below the Calabrian arc does not differ strongly for the two reconstructions. This is not surprising because the underlying kinematic scenarios (for the Oligocene to Present) according to Dercourt et al. [1986] and to Dewey et al. [1989] are almost identical for this part of the arc. Both tectonic scenarios explain a subducted slab in the region that looks like the one found in the inversion of delay-time data (bottom panel).

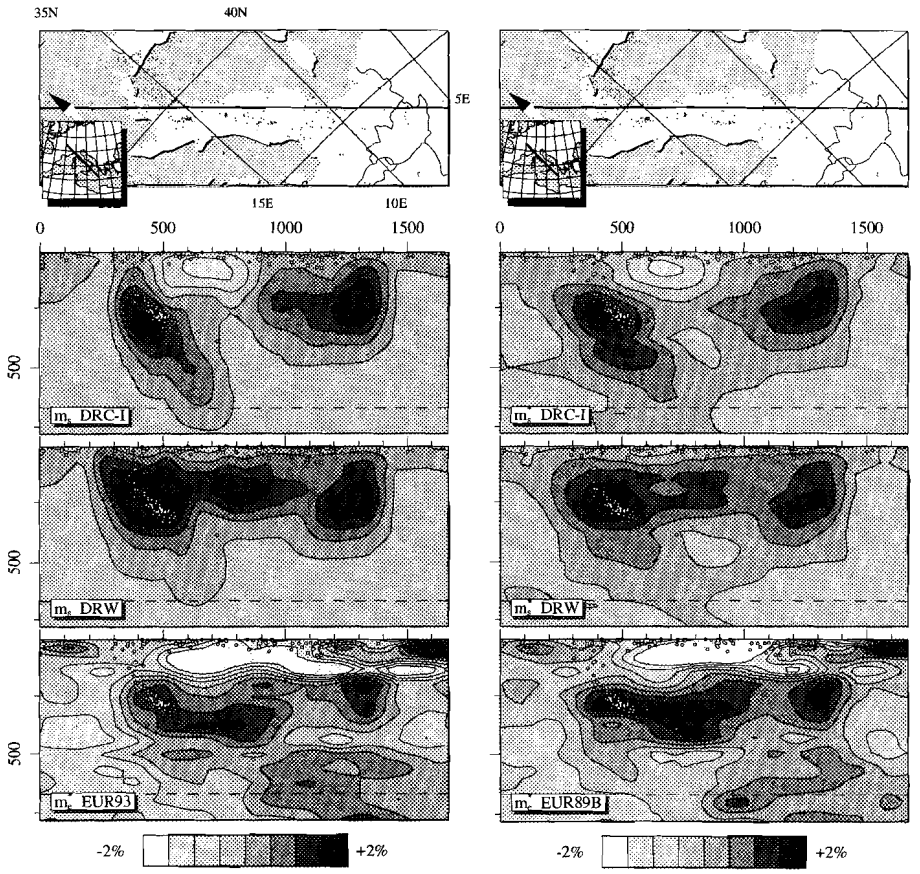

Figure 25. Comparison of the same two forward models (DRC-I and DRW) as shown in Figure 24 in a section along the Apennines.

Figure 25 shows an alternative section through the two models, running along the Apennines. In this section the difference between the two forward models is obvious. The high velocity structure associated with subduction below the Apennines is large and continuous for the DRW model, while that predicted in the DRC-I model is smaller and discontinuous. Comparison with the tomographic results EUR89B and EUR93, shown in the bottom two panels of Figure 25 indicates that the tectonic evolution represented in the DRW model explains the present mantle structure better. The overlying low-velocity layer associated with the back-arc extension may be more accurately predicted in the DRC-I model, but the difference between the two tectonic reconstructions is not very large in this respect.

Both reconstructions result in a mantle structure that shows a clear high velocity region below Italy, which is also found in the tomographic inversion result of real delay times. This implies that westward subduction below the Apennines is indeed likely to have occurred during the second half of the Tertiary.

Comparison of DRC-I and DRC-III. The model DRC-III [De Jonge et al., 1993] is an extension of DRC-I. For this model, the tectonic development of the Alpine-Carpathian mountain belt as described by Dercourt et al. [1990] is adopted. An important difference between this tectonic scenario and the one used for DRC-I consists of a longer phase of sea-floor spreading (starting in the early Jurassic), and consequently a larger width of the oceanic basins consumed in the Africa-Europe collision. The effect of this difference is illustrated in Figure 26, where an along-strike section is shown for the Alpine-Carpathian chains. We observe in the image of the DRC-III model a slightly more pronounced anomaly below the Western Alps, and a substantially more pronounced high-velocity anomaly below the Carpathians. This distribution of high-velocity material corresponds to what we find in the tomographic inversion results, albeit that in these sections the high velocity anomaly has sunk further into the mantle than the plate motion at the surface implies (bottom two panels of Figure 26). Furthermore, the low-velocity feature associated with asthenospheric upwelling below the extending Pannonian basin is better with the DRC-III scenario.

Note that, although the model DRC-III gives a better prediction of the mantle below the Eastern Alps, neither of the tested tectonic reconstructions produces the low-amplitude high-velocity structure at 670 km below the Western Alps shown in the tomographic results. Dercourt et al. [1990] already noted that the westernmost part of the Alps was possibly inaccurately described in their reconstruction, which is confirmed by our model results. The absence of this structure in the predicted models is a type-1 error, common to all tested reconstructions.

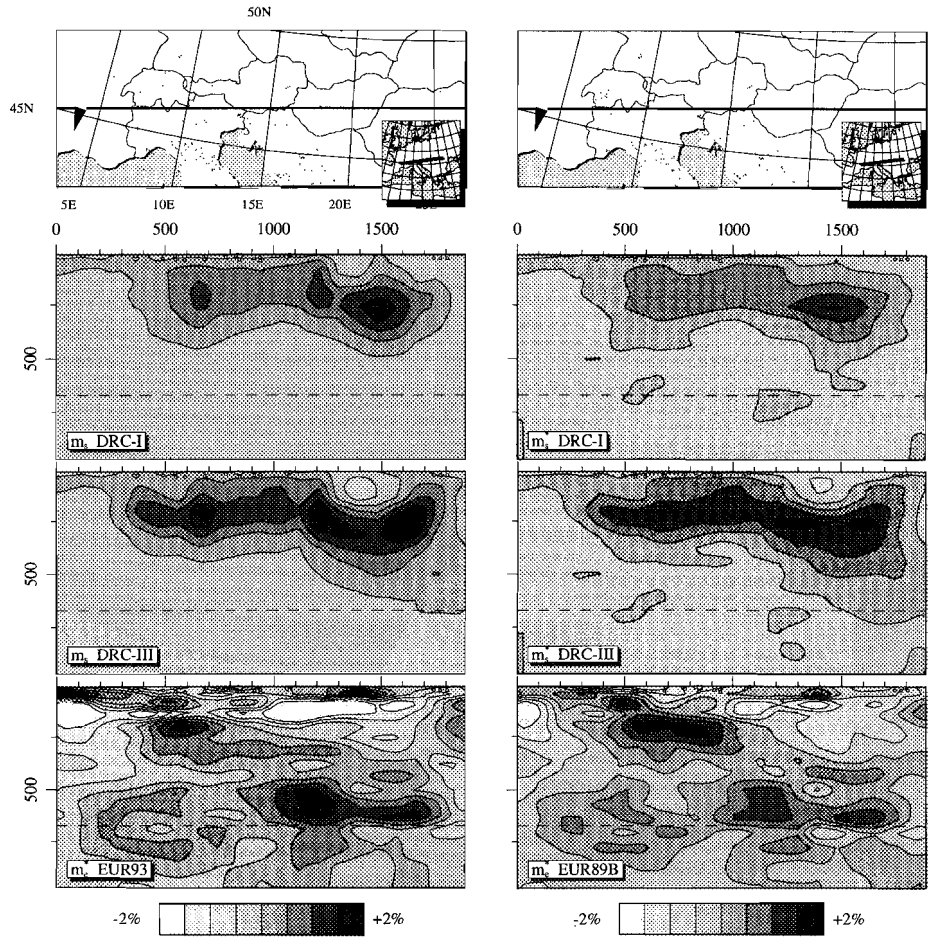

Figure26. Comparison of two forward models (DRC-I and DRC-III) in the indicative region (Alps and Carpathians) and the inversion results of real seismic data (EUR89B and EUR93).

4.6 Discussion and Conclusions

The primary aim of this study was to determine which tectonic reconstruction of the Alpine-Mediterranean region provides the best description of the actual evolution. We assume that this tectonic reconstruction results, through the forward modelling approach, in the best prediction of the seismic velocity structure of the mantle. To study the quality of the predicted structure we needed to determine the quality of the tomographic images of the mantle velocity structure. We, therefore, first established the imaging properties of the tomographic method (bottom path of figure 5). Secondly, we compared images

of different predicted models with tomographic images of the actual mantle to study the quality of the predictions, to draw conclusions on the causes of the imaged mantle structure, and to draw inferences on the nature of mantle processes in the region (right- and left-hand paths of Figure 5).

Quality of models

We conclude from sensitivity tests performed by Spakman et al. [1991] and from dedicated resolution tests in of this paper that the tomographic method employed (i.e. data, rays, and inversion method) has the potential to yield a realistic image of the actual mantle structure, within the limitations of linearized tomography. With the present seismic data set, this method shows considerable detail of the mantle structure, although some parts of the mantle may be less well imaged because of low ray-path coverage. The tomographic models EUR89B [Spakman et al., 1993] and EUR93 [Remkes and Spakman, 1993] therefore give a good description of actual mantle structure. With the information on the quality of the tomographic models and the importance of type-3 misfit we could study the quality of various mantle predictions.

In the second part of this study we started by studied properties that the predicted models all had in common. We found that an important part of the amplitude and spatial distribution discrepancies noted by de Jonge et al. [1994] reflect imperfect imaging of the real mantle structure (type-3 errors). Furthermore, we conclude that the forward modelling assumptions on the nature of mantle processes made by De Jonge and Wortel [1990] and de Jonge et al. [1993, 1994] are corroborated by comparing their model results with tomographic results obtained by Spakman et al. [1993] and Remkes and Spakman[1993]. Therefore, we have found a confirmation of the importance of the modelled mantle processes for the present seismic velocity structure. However, the most important mismatch between predicted and tomographic models - the low-velocity regions at shallow levels of the mantle in the latter - is a feature of the mantle that is not modelled in the forward modelling approach. We identified this as a type-2 error, which in principle could be resolved by including information from the study of slab-detachment processes by Yoshioka and Wortel [1995]. This error does not distract from the conclusion that normal subduction processes of oceanic lithosphere modelled as conductively cooling of plate-like bodies descending into a homogeneous mantle, provide an important part of the explanation of the observed mantle structure.

The general pattern of minor discrepancies between predicted and tomographically determined anomaly amplitudes observed in Figure 21 may provide important information on the material properties employed in the forward modelling. For an analytical model of the internal structure of subducted slabs, similar considerations have recently been put forward by Deal et al. [1994].

Quality of tectonic reconstructions

With respect to the various tectonic reconstructions, we conclude that the complicated tectonic evolution of the Alpine-Mediterranean region is reflected in an equally complicated (and long-lived) structure of the underlying mantle. The major features of this structure can be related to the tectonic history inferred from surface observations. In general, convergence between different tectonic domains is best described by interpreting it as the surface expression of subduction processes. Divergence between different domains can be considered as the expression of intra-plate extension, which - at the scale considered - can in turn be adequately modelled with a pure shear approximation. The real present-day seismic velocity structure of the mantle is described to considerable detail and accuracy by mantle models based on these assumptions. The verification of these assumptions by the good fit between predicted and actual mantle structure means we have obtained a better understanding of the lithosphere and mantle processes involved in the tectonic evolution.

We subsequently used some discerning characteristics of the different forward models to achieve the primary aim of this study: to determine the most likely tectonic evolution of the Alpine-Mediterranean region. We conclude from our tests that none of the reconstructions provide a completely accurate description of the actual tectonic evolution. However, the models have their relative merits:

- The evolution of the Aegean region is described to great detail by the tectonic reconstruction of Dercourt et al. [1986] albeit that the interpretation of this reconstruction needs to incorporate a long period of subduction in the Tertiary (a point not explicitly made by Dercourt et al. [1986], but suggested from tomographic results by Spakman et al. [1988] and required from geometric consistency considerations for the DRC-I model given by De Jonge et al. [1994]). Because both the predicted (DRC-I model) amplitude and the predicted spatial extent of the high velocity structure associated with subduction of the African plate below Europe correspond closely to the tomographic results.
- Below the Pontide and Tauride chains (Turkey) the predicted structure appears to be less accurate, but this discrepancy is largely a result of the lower signal recovery of the tomographic imaging in this region (type-3 misfit).
- The most likely interpretation of the convergence between Iberia and Africa during the middle and late Tertiary is also given by the DRC-I model, which implies that the bulk of convergence has been accommodated along a single (northward sloping) subduction zone in the Alboran region. The alternative interpretation we have tested with the DRC-II model, where the double mountain belt corresponds to a double subduction complex, explains the observed structure less well.
- The development of the Tyrrhenian Sea given by Dercourt et al. [1986] (DRC-I) and the one given by Dewey et al. [1989] (DRW) result in forward models that are equally good for the Calabrian Arc region. However, the DRW

model provides better information on the relative magnitude of convergence in the adjacent Apennine and North African mountain belts. We conclude this from the better prediction of mantle velocity structure in these regions obtained when using the kinematics of Dewey et al. [1989].
- The scenario for the evolution of the Northern margin of the Tethys given by Dercourt et al. [1990] (DRC-III) results in a better correspondence with the tomographic results below the Eastern Alps and the Carpathians than the DRC-I model. On the other hand neither DRC-I nor DRC-III show the deep high velocity anomaly observed below the Western Alps. For this particular part of the studied region, a reliable reconstruction of the Mesozoic and early Tertiary plate tectonic evolution has not been found.

In summary we can state that the three studied recent reconstructions provide a good description of the tectonic evolution in the Alpine-Mediterranean region. The differences between various forward model results and tomographic images suggest, however, that a combined scenario could give an even better prediction of the present mantle structure. This scenario should include elements of all three tectonic reconstructions:
1. The kinematics by Dercourt et al. [1986] for the tectonic evolution of the Aegean and Turkey, supplemented with the interpretation of the timing of the Hellenic arc development given by Spakman et al. [1988] and De Jonge et al. [1994].
2. The reconstruction by Dercourt et al. [1990] for the Carpathians and Eastern Alps.
3. The kinematics by Dewey et al. [1989] for the Tertiary development of the Apennines and the evolution of the North African margin.

In addition, a better description of the development of the Western Alps should be included in a model for the evolution of the whole region. Perhaps the Early Tertiary evolution recently proposed by Stampfli and Marchant [in press, 1995] can be used in this context.

In addition to the corroboration of the tested reconstructions, we conclude that we can now *explain* many aspects of the complex structure below the Alpine-Mediterranean region found by means of seismological studies: the mantle velocity structure is closely linked to the thermal effects associated with the tectonic evolution of the region. Finally, we have obtained new insight on mantle processes and properties that shaped the region throughout its history.

Acknowledgements. M. R. de Jonge is funded by NWO/AWON (Netherlands Organisation for Scientific Research, Earth Sciences branch), project 751-354-019. Part of this study is carried out in the framework of Pionier Project PGS 76-144 "Detailed Structure and Dynamics of the Upper Mantle", which is funded by NWO. Tomographic inversion were calculated at the NCF as part of project SC-245.
This is Geodynamic Research Institute (Utrecht University) contribution 95-###.

References:

Blanco, M. J., and W. Spakman, The P-wave velocity structure of the mantle below the Iberian peninsula: Evidence for subducted lithosphere below southern Spain, *Tectonophysics, 221*, 13-34, 1993.

De Jonge, M. R., and M. J. R. Wortel, The thermal structure of the Mediterranean upper mantle: A forward modelling approach, *Terra Nova, 2*, 609-616, 1990.

De Jonge, M. R., M. J. R. Wortel, and W. Spakman, From tectonic evolution to upper mantle model: an application to the Alpine-Mediterranean region, *Tectonophysics, 223*, 53-65, 1993.

De Jonge, M. R., M. J. R. Wortel, and W. Spakman, Regional scale tectonic evolution and the seismic velocity structure of the lithosphere and upper mantle: the Mediterranean region, *J. Geophys. Res., 99*, 12,091-12,108, 1994.

Deal, M., G. Nolet, and R. van der Hilst, Quantitative tomography, *EOS Trans. AGU (Abstract volume 1994 fall meeting), 75*, 424, 1994.

Dercourt, J., L. P. Zonenshain, L.-E. Ricou, V. G. Kazmin, X. Le Pichon, A. L. Knipper, C. Grandjacquet, I. M. Sbortshikov, J. Geyssant, C. Lepvrier, D. H. Perchersky, J. Boulin, J.-C. Sibuet, L. A. Savostin, O. Sorokhtin, M. Westphal, M. L. Bazhenov, J. P. Lauer, and B. Biju-Duval, Geological evolution of the Tethys from the Atlantic to the Pamirs since the Lias, in *Evolution of the Tethys*, edited by J. Auboin, X. Le Pichon, and A. S. Monin, *Tectonophysics, 123*, 241-315, 1986.

Dercourt, J., L. E. Ricou, S. Adamia, G. Császár, H. Funk, J. Lefeld, M. Rakús, M. Săndalescu, A. Tollman, and P. Tchoumachenko, Anisian to Oligocene paleogeography of the European margin of Tethys (Geneva to Baku), in *Evolution of the northern margin of the Tethys: the results of IGCP project 198, Mem. Soc. Géol. Fr., 154(III)*, 159-190, 1990.

Dewey, J. F., M. L. Helman, E. Turco, D. H. W. Hutton, and S. D. Knott, Kinematics of the western Mediterranean, in *Alpine Tectonics*, edited by M. P. Coward, D. Dietrich, and R. G. Park, *Spec. Publ. Geol. Soc. London, 45*, 265-283, 1989.

Humphreys, E. and R. W. Clayton, Adaptation of back-projection tomography to seismic travel time problems, *J. Geophys. Res., 93*, 1073-1085, 1988.

Jeffreys, H. and K. E. Bullen, *Seismological Tables*, British Assoc. for Adv. Sc., London, 1940.

Kennett, B. L. N., and E. R. Engdahl, Travel times for global earthquake location and phase identification, *Geophys. J. Int., 105*, 429-466, 1991.

Lévêque, J.-J., L. Rivera, and G. Wittlinger, On the use of the checker-board test to assess the resolution of tomographic inversions, *Geophys. J. Int., 115*, 313-318, 1993.

Paige, C. C., and M. A. Saunders, LSQR: an algorithm for sparse linear equations and sparse least squares, *ACM Trans. Math. Soft., 8*, 43-71 & 195-209, 1982.

Platt, J. P., and R. L. M. Vissers, Extensional collapse of thickened continental lithosphere: a working hypothesis for the Alboran Sea and the Gibraltar arc, *Geology, 17*, 540-543, 1989.

Remkes, M. and W. Spakman, Joint inversion of regional geoid and seismic delay time data for the European mantle structure, *Terra Abstracts EUG, 5*, 124, 1993.

Richards, M. A., and D. C. Engebretson, Large-scale mantle convection and the history of subduction, *Nature, 355*, 437-440, 1992.

Spakman W., Tomographic images of the upper mantle below central Europe and the Mediterranean, *Terra Nova, 2*, 542-553, 1990.

Spakman W., Delay-time tomography of the upper mantle below Europe, the Mediterranean, and Asia Minor, *Geophys. J. Int., 107*, 309-332, 1991.

Spakman, W., and G. Nolet, Imaging algorithms, accuracy, and resolution in delay-time tomography, In: *Mathematical Geophysics*, edited by N. J. Vlaar, G. Nolet, M. J. R. Wortel, and S. A. P. L. Cloetingh, Reidel, Dordrecht, 155-188, 1988.

Spakman, W., M. J. R. Wortel, and N. J. Vlaar, The Hellenic subduction zone: A

tomographic image and its geodynamic implications, *Geophys. Res. Lett., 15*, 60-63, 1988.

Spakman, W., S. Stein, R. D. van der Hilst, and M. J. R. Wortel, Resolution experiments for NW Pacific subduction zone tomography, *Geophys. Res. Lett., 16*, 1097-1100, 1989.

Spakman, W., S. van der Lee, R. D. van der Hilst, Travel-time tomography of the European-Mediterranean mantle down to 1400 km, *Phys. Earth Plan. Int., 79*, 3-74, 1993.

Stampfli, G. M., and R. H. Marchant, Geodynamic evolution of the Tethyan margins of the Western Alps, in: *Deep structure of Switzerland-Results from NFP 20*, edited by P. Lehner, P. Heitzman, W. Frei, H. Horstmeyer, S. Mueller, A. Pfiffner, and A. Steck, Birkhäuser AG, Basel, <in press 1995>.

Van der Hilst, R. D., E. R. Engdahl, and W. Spakman, Tomographic inversion of P and pP data for aspherical mantle structure below the northwest Pacific region, *Geophys. J. Int., 114,* 264-302, 1993.

Van der Hilst, R. D., and W. Spakman, Importance of the reference model in linearized tomographic inversions: images of subduction below the Caribbean plate, *Geophys. Res. Lett., 16*, 1093-1097, 1989.

Wortel, M. J. R., and W. Spakman, Structure and dynamics of subducted lithosphere in the Mediterranean region, *Proc. Kon. N. Akad. Wet., 95*, 325-347, 1992.

Wortel, M. J. R., and W. Spakman, The dynamic evolution of the Apenninic-Calabrian, Hellenic, and Carpathian arcs: a unifying approach, *Terra Abstracts EUG, 5*, 97, 1993.

Yoshioka, S. and M. J. R. Wortel, Three-dimensional numerical modelling of detachment of subducted lithosphere, *J. Geophys. Res.*, , <in press>, 1995.

Appendix 2

Verification of $\partial V_p/\partial T$

In this study the conversion of model temperature to P-wave velocity structure is performed with a $\partial V_p/\partial T$ relation estimated from laboratory experiments on olivine. Since the experiments need to be done under difficult circumstances (high pressure and temperature), there is a large margin of error in the measurements of elastic properties (resulting in the uncertainty range shown in Figure 4 of chapter 3).

Under the assumption that both the tomographic result (EUR93) and the temperature structure of the forward model (DRC-III) are essentially correct, it is possible to estimate a seismologically consistent effect of the thermal structure, that is, the best (in a least squares sense) relation between T and $\Delta V_p/V_p$. For the determination I assume that the signal recovery found with the synthetic tests (TEST-2 of chapter 4) gives an indication of the recovery of the real mantle structure. Therefore the anomalies of EUR93 are first divided by the recovery found for the well covered cells to produce $\Delta V_p/V_p^*$. Then the best fitting straight line (of $\Delta V_p/V_p^*$ against T) is determined for every horizontal layer in the tomographic model. This yields an estimate for the temperature dependence of ΔV_p for different depths that yields the highest average consistency between forward temperature model and tomographic result.

Figure 1 shows the resulting $\partial V_p/\partial T$ relation, and for comparison also the relation used in this study. The temperature dependence of V_p, found assuming that both temperature and tomographic models are correct, lies within the uncertainty range of the laboratory data. It is also clear that the heuristic relation differs strongly from a simple average of laboratory data. It is unclear how strongly this result is influenced by systematic errors in the tomographic inversion, but if these errors are also present in the synthetic tests, they should be compensated for by the scaling of ΔV_p with the signal recovery. In the top levels of Figure 1 the grey line denotes the same parameter, estimated using only the low-velocity/high-temperature cells. This new temperature dependence of V_p can be used to scale the thermal structure to velocity anomalies, to produce a P-wave velocity model that resembles the tomographic results more than the previous result as illustrated in Figure 2 (although in fact the predicted mantle temperature structure is the same). If the variation of $\partial V_p/\partial T$ found here can also be observed in independent cases, it holds important implications for the in-situ mantle properties. The relation shown in Figure 1 should not be used in determining synthetic velocity models directly, because it depends entirely on the assumption that both temperatures and tomographic results are correct, which is exactly what we intended to study. On the other hand, the fact that the best-fit $\partial V_p/\partial T$ lies within the range determined from laboratory data does reinforce both the forward modelling approach and the tomographic inversion results.

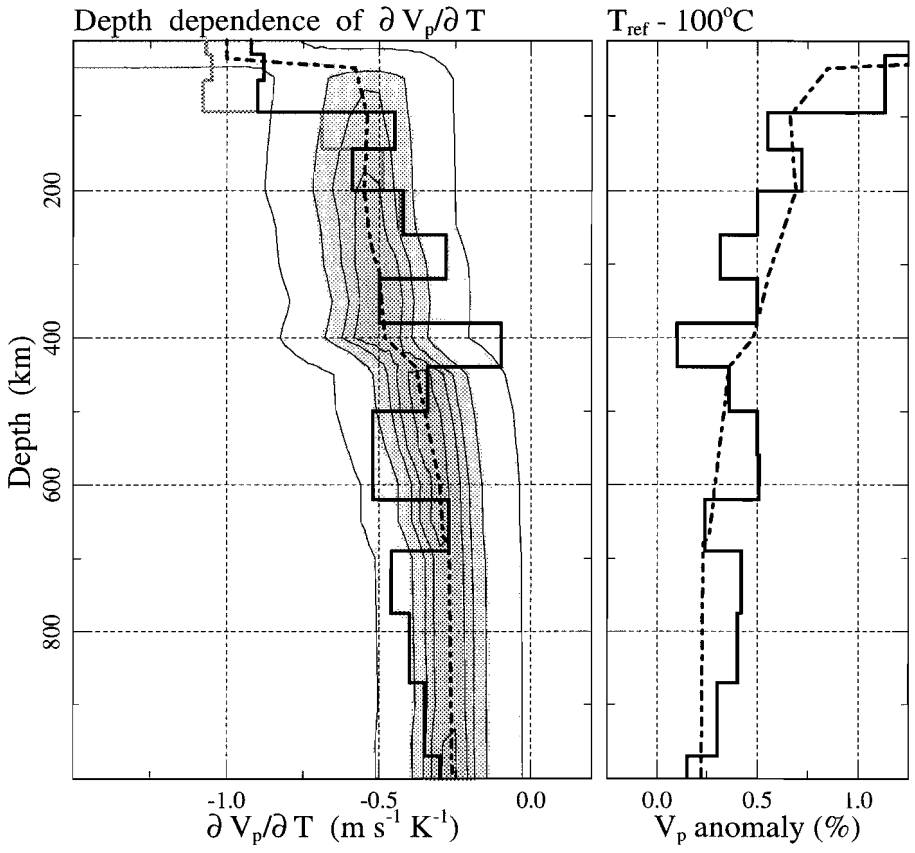

Figure 1. $\partial V_p/\partial T$ relation with best fit between calculated temperatures and tomographic results (thick line) and the estimate from laboratory data (dashed line).

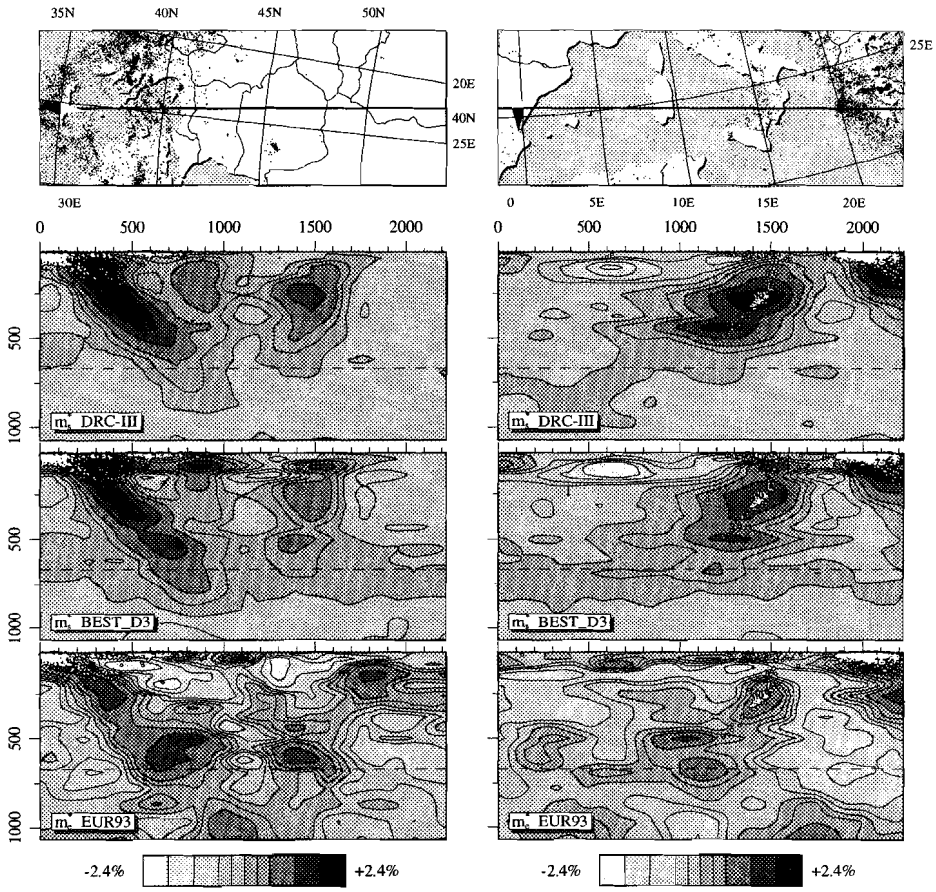

Figure 2. From top to bottom: Tomographic image of a forward model (DRC-III) scaled with laboratory estimate of $\partial V_p/\partial T$, the same with the new relation described in this section, and the tomographic result EUR93.

Epilogue

Crafty men contemn studies, simple men admire them, and wise men use them; for they teach not their own use; but that is a wisdom without them, and above them, won by observation.
Francis Bacon, The Essays, 1601

The onset of this study was a seemingly innocuous question: how well do the various descriptions of the tectonic evolution of the Alpine-Mediterranean region describe the actual processes? In addressing this problem it became rapidly clear that, also in this case, combining geophysical and geological interpretations was by no means simple. Much of the work of this thesis was dedicated to translating geology into numbers. In fact, both the qualitative geological methods used for deriving the reconstructions and the numerical methods used for calculating the temperature are well established. However, the rigorous application of one to the other and the interpretation of modelling results in terms of properties of the Earth has opened up a wealth of new opportunities for further research (or: has caused a multitude of new questions). In this thesis the main point of attention has been the implications of simple plate-tectonic concepts and geological observations for the seismic velocity structure of the lower lithosphere and upper mantle. In chapter 3 and in De Jonge et al. [1993] other results - in the form of predicted basin subsidence history - are briefly mentioned. The heat-flow can also be determined directly from the modelling. This is a very important parameter for the formation and maturation of hydrocarbons in sedimentary basins, and the thermal modelling approach gives an independently verifiable quantitative description of its past development for a large region.

Other topics that can be studied quantitatively using this approach are for example:
- The relation between tectonics (and its associated thermal evolution) and deep metamorphic processes.
- The relation between seismicity and internal slab structure and thereby the relation between seismicity and temperature at mantle pressures.
- The temperature dependence of elastic properties for in-situ mantle materials through the combination of V_p, the depth-dependent $\partial V / \partial T$, and the temperature.
- The depth-dependence of anelastic properties through the comparison of slab detachment processes and temperature dependent density.

In short, the forward models give a time-dependent description of one of the most important parameters for geological processes: the temperature. The added benefit of the modelling of seismic velocity anomalies is that this

description can be verified by independent means. From the comparison of forward models and tomographic results we have obtained understanding on the nature and causes of the mantle velocity structure, but in many ways this study is only the start of the exploration of the possibilities of the combined forward and inverse modelling approaches.

Samenvatting

In de plaattektoniek worden geologische processen beschouwd in de context van starre lithosfeerplaten die over de aarde bewegen. In hoofdstuk 1 wordt een overzicht gegeven van een aantal actuele plaattektonische beschrijvingen van de ontwikkeling van het Middellandse Zeegebied. De correctheid van zulke reconstructies is niet altijd eenvoudig vast te stellen, omdat een belangrijk deel van de aardkorst, die de benodigde geologische gegevens moet leveren, niet langer aanwezig is (oude oceanen zijn bijvoorbeeld vaak gedurende gebergtevorming weer verdwenen). Het hoofddoel van deze studie is een methode te ontwikkelen en toe te passen waarmee toch uitspraken over de betrouwbaarheid van incomplete tektonische reconstructies gedaan kunnen worden.

Uitgaande van de bestaande geologische reconstructies is een computermodel ontwikkeld dat naast de plaatbewgingenover het oppervlak van de aarde ook de derde dimensie (in de diepte) omvat. Dit model wordt gebruikt om de temperatuurverdeling in het inwendige van de aarde te berekenen uitgaande van reconstructies van de geologische ontwikkeling. Met verschillende reconstructies kunnen zo verschillende voorspellingen van de huidige thermische structuur van de lithosfeer en mantle gemaakt worden.

De temperatuurverdeling in de aarde heeft gevolgen voor allerlei andere fysische grootheden zoal de snelheid waarmee seismische golven zich door het inwendige voortplanten, de warmtestroom dichtheid, en de daling van sedimenaite bekkens. Met behulp van het computermodel leveren reconstructies van de geologische ontwikkeling daarom verschillende voorspellingen voor direct of indirect meetbare eigenschappen van de aarde. Hoofdtuk 2 behandeld de details van de modellering van de temperatuur en de daaraan verbonden fysische eigenschappen van de mantel. De belangrijkste grootheid waaraan getoetst wordt is de huidige verdeling van seismische snelheden in de mantel, zoals die afgebeeld wordt in tomografische studies. Ook wordt kort ingegaan op twee andere, van de temperatuurontwikkeling afgeleide, grootheden die geschikt zijn om bij uitstek de modellering van relatief ondiepe processen in een niet te ver verleden te toetsen: de warmtestroomdichtheid en de bekkendaling van sedimentaire bekkens.

In hoofdstuk 3 wordt de mehode toegepast op een aantal recente hypothesen over de geologische ontwikkeling van het Middellandse Zeegebied, en een eerste vergelijking met resultaten van tomografisch onderzoek van de mantel en geofysische observaties van de mantel wordt gemaakt

Om de verschillende modellen goed te kunnen vergelijken en om goed te kunnen bepalen welke geologische reconstructie de beste voordpelling oplevert wordt in hoofdstuk 4 bovendien in detail gekeken naar de oorzaken van diverse verschillen tussen de thermische en de tomografische modellen. Hierdoor wordt extra informatie verkregen over de aard van fysische processen die aktief zijn

geweest gedurende de geologische ontwikkeling en over de eigenschappen van de mantel van de aarde.

Dankwoord

Ik wil iedereen bedanken die behulpzaam is geweest bij de totstandkoming van dit proefschrift. In de eerste plaats Rinus Wortel voor de vruchtbare ideeen over de modellering van mantelprocessen en Wim Spakman voor de nauwgezette steun bij de tomografische analyse. Ik ben Johan Meulenkamp erkentelijk voor zijn enthousiast propageren van de 'grote lijn' in de geologie, dat heeft mij als geoloog de juiste grondhouding voor dit onderzoek geleverd. Verder is de samenwerking met mijn collega promovendi altijd zeer nuttig en plezierig geweest, zowel voor de geofysische theorie als voor de technische uitvoering van het onderzoek. Vooral de niet aflatende inspanningen van Maarten Remkes en Rob Govers om de computer nòg handiger te gebruiken heeft veel geholpen.

Ik dank familie en vrienden, en in het bijzonder Rian voor het geduld dat ze wisten op te brengen voor deze 'eeuwige promovendus'.

Curriculum Vitæ

De schrijver van dit proefschrift behaalde in 1980 het diploma ongedeeld VWO aan de rijksscholengemeenschap te Oud-Beijerland. In 1980 werd begonnen met de studie Natuurkunde aan de Universiteit Utrecht en in 1985 aan Geologie. In 1989 werd het doctoraalexamen geologie behaald. Van 1990 tot 1994 is hij werkzaam geweest als OIO bij de vakgroep geofysica van het instituut voor aardwetenschappen en sinds 1995 als postdoctoraal onderzoeker.